Eur. Phys. J. C (2018) 78:708
https://doi.org/10.1140/epjc/s10052-018-6146-9

THE EUROPEAN PHYSICAL JOURNAL C

Regular Article - Experimental Physics

Measurement of the $Z/\gamma^* \to \tau\tau$ cross section in pp collisions at $\sqrt{s} = 13$ TeV and validation of τ lepton analysis techniques

CMS Collaboration*

CERN, 1211 Geneva 23, Switzerland

Received: 10 January 2018 / Accepted: 10 August 2018

Abstract A measurement is presented of the $Z/\gamma^* \to \tau\tau$ cross section in pp collisions at $\sqrt{s} = 13$ TeV, using data recorded by the CMS experiment at the LHC, corresponding to an integrated luminosity of 2.3 fb^{-1}. The product of the inclusive cross section and branching fraction is measured to be $\sigma(\mathrm{pp} \to Z/\gamma^*\mathrm{+X})\,\mathcal{B}(Z/\gamma^* \to \tau\tau) = 1848 \pm 12\,(\mathrm{stat}) \pm 67\,(\mathrm{syst} + \mathrm{lumi})$ pb, in agreement with the standard model expectation, computed at next-to-next-to-leading order accuracy in perturbative quantum chromodynamics. The measurement is used to validate new analysis techniques relevant for future measurements of τ lepton production. The measurement also provides the reconstruction efficiency and energy scale for τ decays to hadrons + ν_τ final states, determined with respective relative uncertainties of 2.2 and 0.9%.

1 Introduction

Final states with τ leptons are important experimental signatures at the CERN LHC. In particular, the recently reported observation of decays of standard model (SM) Higgs bosons (H) [1–3] into pairs of τ leptons [4] suggests additional searches in the context of new charged [5–8] and neutral [9–17] Higgs bosons, lepton-flavor violation [18–20], supersymmetry [21–28], leptoquarks [29,30], extra spatial dimensions [31,32], and massive gauge bosons [33–35].

With a lifetime of 2.9×10^{-13} s, the τ lepton usually decays before reaching the innermost detector. Approximately two thirds of τ leptons decay into a hadronic system and a τ neutrino. Constrained by the τ lepton mass of 1.777 GeV, the hadronic system is characterized by low particle multiplicities, typically consisting of either one or three charged pions or kaons, and up to two neutral pions. The hadrons produced in τ decays therefore also tend to be highly collimated. The τ lepton decays into an electron or muon and two neutrinos with a probability of 35%. We denote the electron and muon produced in $\tau \to e\nu\nu$ and $\tau \to \mu\nu\nu$ decays by τ_e and τ_μ, to distinguish them from prompt electrons and muons, respectively. The hadronic system produced in a $\tau \to$ hadrons + ν_τ decay is denoted by the symbol τ_h.

The Drell–Yan (DY) [36] production of τ lepton pairs ($q\bar{q} \to Z/\gamma^* \to \tau\tau$) is interesting for several reasons. First, the process $Z/\gamma^* \to \tau\tau$ represents a reference signal to study the efficiency to reconstruct and identify τ_h, as well as to measure the τ_h energy scale. Moreover, $Z/\gamma^* \to \tau\tau$ production constitutes the dominant irreducible background to analyses of SM H $\to \tau\tau$ events, and to searches for new resonances decaying to τ lepton pairs. The cross section for DY production exceeds the one for SM H production by about two orders of magnitude. Signals from new resonances are expected to be even more rare. It is therefore important to control with a precision reaching the sub-percent level the rate for $Z/\gamma^* \to \tau\tau$ production, as well as its distribution in kinematic observables. In addition, the reducible backgrounds relevant for the study of $Z/\gamma^* \to \tau\tau$ are also relevant for studies of SM H production and to searches for new resonances.

This paper reports a precision measurement of the inclusive pp $\to Z/\gamma^*\mathrm{+X} \to \tau\tau\mathrm{+X}$ cross section. The measurement demonstrates that $Z/\gamma^* \to \tau\tau$ production is well understood, and provides ways to validate techniques relevant in future analyses of τ lepton production. Most notably, a method based on control samples in data is introduced for determining background contributions arising from the misidentification of quark or gluon jets as τ_h. Measurements of the τ_h identification (ID) efficiency and of the τ_h energy scale [37] are obtained as byproducts of the analysis.

The cross section for DY production of τ lepton pairs was previously measured by the CMS and ATLAS experiments in proton-proton (pp) collisions at $\sqrt{s} = 7$ TeV at the LHC [38,39], and in proton–antiproton collisions at $\sqrt{s} = 1.96$ TeV by the CDF and D0 experiments at the Fermilab Tevatron [40–42]. In this study, we present the pp $\to Z/\gamma^*\mathrm{+X} \to \tau\tau\mathrm{+X}$ cross section measured at $\sqrt{s} = 13$ TeV, using data recorded by the CMS experiment, corresponding to an integrated luminosity of 2.3 fb^{-1}. Events

* e-mail: cms-publication-committee-chair@cern.ch

Published online: 03 September 2018

are selected in the $\tau_e\tau_h$, $\tau_\mu\tau_h$, $\tau_h\tau_h$, $\tau_e\tau_\mu$, and $\tau_\mu\tau_\mu$ decay channels. The $\tau_e\tau_e$ channel is not considered in this analysis, as it was studied previously in the context of the SM $H \to \tau\tau$ analysis, and found to be the least sensitive of these channels [43]. The $pp \to Z/\gamma^*+X \to \tau\tau+X$ cross section is obtained through a simultaneous fit of τ lepton pair mass distributions in all decay channels.

The paper is organized as follows. The CMS detector is described briefly in Sect. 2. Section 3 describes the data and the Monte Carlo (MC) simulations used in the analysis. The reconstruction of electrons, muons, τ_h, and jets, along with various kinematic quantities, is described in Sect. 4. Section 5 details the selection of events in the different decay channels, followed in Sect. 6 by a description of the procedures used to estimate background contributions. The systematic uncertainties relevant for the measurement of the $pp \to Z/\gamma^*+X \to \tau\tau+X$ cross section are described in Sect. 7, and the extraction of the signal is given in Sect. 8. The results are presented in Sect. 9, and the paper concludes with a summary in Sect. 10.

2 The CMS detector

The central feature of the CMS apparatus is a superconducting solenoid of 6 m internal diameter, providing a magnetic field of 3.8 T. A silicon pixel and strip tracker, a lead tungstate crystal electromagnetic calorimeter (ECAL), and a brass and scintillator hadron calorimeter (HCAL), each composed of a barrel and two endcap sections, are positioned within the solenoid volume. The silicon tracker measures charged particles within the pseudorapidity range $|\eta| < 2.5$. Trajectories of isolated muons with $p_T = 100$ GeV, emitted at $|\eta| < 1.4$, are reconstructed with an efficiency close to 100% and resolutions of 2.8% in p_T, and with uncertainties of 10 and 30 μm in their respective transverse and longitudinal impact parameters relative to their points of origin [44]. The ECAL is a fine-grained hermetic calorimeter with quasi-projective geometry, segmented in the barrel region of $|\eta| < 1.48$, as well as in the two endcaps that extend up to $|\eta| < 3.0$. Similarly, the HCAL barrel and endcaps cover the region $|\eta| < 3.0$. Forward calorimeters extend the coverage up to $|\eta| < 5.0$. Muons are measured and identified in the range $|\eta| < 2.4$ using gas-ionization detectors embedded in the steel flux-return yoke outside the solenoid. A two-level trigger system is used to reduce the rate of recorded events to a level suitable for data acquisition and storage. The first level (L1) of the CMS trigger system, composed of specialized hardware processors, uses information from the calorimeters and muon detectors to select the most interesting events in a fixed time interval of less than 4 μs. The high-level trigger processor farm decreases the event rate from around 100 kHz to less than 1 kHz before storage and subsequent analysis. Details of the CMS detector and its performance, together with a definition of the coordinate system and kinematic variables, can be found in Ref. [45].

3 Data and Monte Carlo simulation

The data were recorded in pp collisions at 25 ns bunch spacing and are required to satisfy standard data quality criteria. The analysed data correspond to an integrated luminosity of 2.3 fb^{-1}.

The $Z/\gamma^* \to \tau\tau$ signal and the $Z/\gamma^* \to ee$, $Z/\gamma^* \to \mu\mu$, W+jets, $t\bar{t}$, single top quark, and diboson (WW, WZ, and ZZ) background processes are modelled through samples of MC simulated events. Background contributions arising from multijet production via quantum chromodynamic interactions are determined from data. The $Z/\gamma^* \to \ell\ell$ (where ℓ refers to e, μ, or τ) and W+jets events are generated using leading-order (LO) matrix elements (ME) in quantum chromodynamics, implemented in the program MADGRAPH5_aMC@NLO 2.2.2 [46], and $t\bar{t}$ and single top quark events are generated using the next-to-leading order (NLO) program POWHEG v2 [47–51]. The diboson events are modelled using the NLO ME program implemented in MADGRAPH5_aMC@NLO. The background events are complemented with SM $H \to \tau\tau$ events, generated for an H mass of $m_H = 125$ GeV, using the implementation of the gluon-gluon and vector boson fusion processes in POWHEG [52,53]. All events are generated using the NNPDF3.0 [54–56] set of parton distribution functions (PDF). Parton showers and parton hadronization are modelled using PYTHIA 8.212 [57] and the CUETP8M1 underlying-event tune [58], which is based on the Monash tune [59]. The decays of τ leptons, including polarization effects, are modelled through PYTHIA. The $Z/\gamma^* \to \ell\ell$, W+jets, and $t\bar{t}$ events are normalized to cross sections computed at next-to-next-to-leading order (NNLO) accuracy [60,61]. A reweighting is applied to MC-generated $t\bar{t}$ and $Z/\gamma^* \to \ell\ell$ events to improve the respective modelling of the p_T spectrum of the top quarks [62,63] and the dilepton mass and p_T spectra relative to data. The weights applied to simulated $Z/\gamma^* \to \ell\ell$ events are obtained from studies of the distributions in dilepton mass and p_T in $Z/\gamma^* \to \mu\mu$ events. The cross sections for single top quark [64–66] and diboson [67] production are computed at NLO accuracy.

Minimum bias events generated with PYTHIA are overlaid on all simulated events to account for the presence of additional inelastic pp interactions, referred to as pileup (PU), which take place in the same, previous, or subsequent bunch crossings as the hard-scattering interaction. The pileup distribution in simulated events matches that in data, amounting to, on average, ≈ 12 inelastic pp interactions per bunch crossing. All generated events are passed through a detailed simulation of the CMS apparatus, based on GEANT4 [68],

and reconstructed using the same version of the CMS reconstruction software as used for data.

4 Event reconstruction

The information provided by all CMS subdetectors is employed in a particle-flow (PF) algorithm [69] to identify and reconstruct individual particles in the event, namely muons, electrons, photons, charged and neutral hadrons. These particles are then used to reconstruct jets, τ_{h} candidates and the vector imbalance in missing transverse momentum in the event, referred to as $\vec{p}_{\mathrm{T}}^{\,\mathrm{miss}}$, as well as to quantify the isolation of leptons.

Electrons are reconstructed using an algorithm [70] that matches trajectories in the silicon tracker to energy depositions in the ECAL. Trajectories of electron candidates are reconstructed using a dedicated algorithm that accounts for the emission of bremsstrahlung photons. The energy loss due to bremsstrahlung is determined by searching for energy depositions in the ECAL emitted tangentially to the track. A multivariate (MVA) approach based on boosted decision trees (BDT) [71] is employed to distinguish electrons from hadrons that mimic electron signatures. Observables that quantify the quality of the electron track, the compactness of the electron cluster in directions transverse and longitudinal relative to the electron motion, and the matching of the track momentum and direction to the sum and positions of energy depositions in the ECAL are used as inputs to the BDT. The BDT is trained on samples of genuine and false electrons, produced in MC simulation. Additional requirements are applied to remove electrons originating from photon conversions.

The identification of muons is based on linking track segments reconstructed in the silicon tracking detector and in the muon system [72]. The matching is done both by starting from a track in the muon system and starting from a track in the inner detector. When a link is established, the track parameters are refitted using the combination of hits in the inner and outer detectors, and the reconstructed trajectory is referred to as a global muon track. Quality criteria are applied on the multiplicity of hits, the number of matched segments, and the quality of the fit to a global muon track, the latter being quantified through a χ^2 criterion.

Electrons and muons in signal events are expected to be isolated, while leptons from heavy flavour (charm and bottom quark) decays, as well as from in-flight decays of pions and kaons, are often reconstructed within jets. Isolated leptons are distinguished from leptons in jets through a sum, denoted by the symbol I_ℓ, of the scalar p_{T} values of additional charged particles, neutral hadrons, and photons reconstructed using the PF algorithm within a cone in η and azimuth ϕ (in radians) of size $\Delta R = \sqrt{(\Delta\eta)^2 + (\Delta\phi)^2} = 0.3$, centred around the lepton direction. Neutral hadrons and photons within the innermost region of the cone, $\Delta R < 0.01$, are excluded from the isolation sum for muons to prevent the footprint of the muon in ECAL and HCAL from causing the muon to fail isolation criteria. When computing the isolation of electrons reconstructed in the ECAL endcap region, we exclude photons within $\Delta R < 0.08$ and charged particles within $\Delta R < 0.015$ of the direction of the electron, to avoid counting photons emitted in bremsstrahlung and tracks originating from the conversion of such photons. As the amount of material that electrons traverse in the barrel region before reaching the ECAL is smaller, the resulting probability for bremsstrahlung emission and photon conversion is sufficiently reduced so as not to require exclusion of particles in the innermost cone from the isolation sum. Efficiency loss due to pileup is kept minimal by considering only charged particles originating from the lepton production vertex ("charged from PV"). The contribution from the neutral component of pileup to the isolation of the lepton is taken into account by means of $\Delta\beta$ corrections [69], which enter the computation of the isolation I_ℓ, as follows:

$$I_\ell = \sum_{\substack{\text{charged}\\ \text{from PV}}} p_{\mathrm{T}} + \max\left\{0, \sum_{\text{neutrals}} p_{\mathrm{T}} - \Delta\beta\right\}, \tag{1}$$

where ℓ corresponds to either e or μ, and the sums extend over, respectively, the charged particles that originate from the lepton production vertex and the neutral particles. The "max" function represents taking the largest of the two values within the brackets. The $\Delta\beta$ corrections are computed by summing the scalar p_{T} of charged particles that are within a cone of size $\Delta R = 0.3$ around the lepton direction, but do not originate from the lepton production vertex, ("charged from PU") and scaling that sum by a factor of one-half:

$$\Delta\beta = 0.5 \sum_{\substack{\text{charged}\\ \text{from PU}}} p_{\mathrm{T}}. \tag{2}$$

The factor of 0.5 approximates the phenomenological ratio of neutral-to-charged hadron production in the hadronization of inelastic pp collisions.

Collision vertices are reconstructed using a deterministic annealing algorithm [73,74], with the reconstructed vertex position required to be compatible with the location of the LHC beam in the x–y plane. The primary collision vertex (PV) is taken to be the vertex that has the maximum $\sum p_{\mathrm{T}}^2$ of tracks associated to it. Electrons, muons, and τ_{h} candidates are required to be compatible with originating from the PV.

Hadronic τ decays are reconstructed using the "hadrons+strips" (HPS) algorithm [37], which is used to separate the individual decay modes of the τ into $\tau^- \to \mathrm{h}^-\nu_\tau$, $\tau^- \to \mathrm{h}^-\pi^0\nu_\tau$, $\tau^- \to \mathrm{h}^-\pi^0\pi^0\nu_\tau$, and $\tau^- \to \mathrm{h}^-\mathrm{h}^+\mathrm{h}^-\nu_\tau$,

where $h^{\pm}$ denotes either a charged pion or kaon (the decay modes of τ^+ are assumed to be identical to their partner τ^- modes through charge conjugation invariance). The τ_h candidates are constructed by combining the charged PF hadrons with neutral pions. The neutral pions are reconstructed by clustering the PF photons within rectangular strips, narrow in the η, but wide in the ϕ directions, to account for the non-negligible probability for photons produced in $\pi^0 \to \gamma\gamma$ decays to convert into electron-positron pairs when traversing the all-silicon tracking detector of CMS and the broadening of energy depositions in the ECAL that occurs when this happens. For the same reason, electrons and positrons reconstructed through the PF algorithm are considered in the reconstruction of the neutral pions besides photons. The momentum of the τ_h candidate is taken as the vector sum over the momenta of the charged hadrons and neutral pions used in reconstructing the τ_h decay mode, assuming the pion-mass hypotheses. We do not use the strips of 0.20×0.05 size in the η–ϕ plane, used in previous analyses [5–7,9–13,18,21–23,29–31,33,34,38,43], but an improved version of the strip reconstruction developed during the $\sqrt{s} = 13$ TeV run. In the improved version, the size of the strip is adjusted as function of p_T, taking into consideration the bending of charged particles in the magnetic field increasing inversely with p_T. More details on strip reconstruction and validation of the algorithm with data are given in Ref. [75]. The main handle for distinguishing τ_h from the large background of quark and gluon jets relies on the use of tight isolation requirements. The sums of scalar p_T values from photons and from charged particles originating from the PV within a cone of $\Delta R = 0.5$ centred around the τ_h direction, are used as input to an MVA-based τ_h ID discriminant. The set of input variables is complemented with the scalar p_T sum of charged particles not originating from the PV, by the τ_h decay mode, and by observables that are sensitive to the lifetime of the τ. The transverse impact parameter of the "leading" (highest p_T) track of each τ_h candidate relative to the PV is used for τ_h candidates reconstructed in any decay mode. For τ_h candidates reconstructed in the $\tau^- \to h^-h^+h^-\nu_\tau$ decay mode, a fit of the three tracks to a common secondary vertex (SV) is attempted, and the distance between SV and PV is used as additional input to the MVA. The MVA is trained on genuine τ_h and jets generated in MC simulation. Four working points (WP), referred to as barely, minimally, moderately, and tightly constrained, are defined through changes made in the selections on the MVA output. The thresholds are adjusted as functions of the p_T of the τ_h candidate, such that the τ_h identification efficiency for each WP is independent of p_T. The moderate and tight WP used to select events in different channels provide efficiencies of 55 and 45%, and misidentification rates for jets of typically 1 and 0.5%, depending on the p_T of the jet [75]. Additional discriminants are employed to separate τ_h from electrons and muons. The separation of τ_h from electrons is performed via another MVA-based discriminant [75] that utilizes input observables that quantify the matching between the sum of energy depositions in the ECAL and the momentum of the leading track of the τ_h candidate, as well as variables that distinguish electromagnetic from hadronic showers. The cutoff-based discriminant described in Ref. [37] is used to separate τ_h from muons. It is based on matching the leading track of the τ_h candidate with energy depositions in the ECAL and HCAL, as well as with track segments in the muon detectors.

Jets within the range $|\eta| < 4.7$ are reconstructed using the anti-k_t algorithm [76,77] with a distance parameter $R = 0.4$. Reconstructed jets are required not to overlap with identified electrons, muons, or τ_h candidates within $\Delta R < 0.5$, and to pass a set of minimal identification criteria that aim to reject jets arising from calorimeter noise [78]. The energy of reconstructed jets is calibrated as function of jet p_T and η [79]. Average energy density corrections calculated using the FastJet algorithm [80,81] are applied to compensate pileup effects. Jets originating from the hadronization of b quarks are identified using the "combined secondary vertex" (CSV) algorithm [82], which exploits observables related to the long lifetime of b hadrons and the higher particle multiplicity and mass of b jets compared to light-quark and gluon jets.

The vector $\vec{p}_T^{\,\text{miss}}$, with its magnitude referred to as E_T^{miss}, is reconstructed using an MVA regression algorithm [83]. To reduce the impact of pileup on the resolution in E_T^{miss}, the algorithm utilizes the fact that pileup produces jets predominantly of low p_T, while leptons and high-p_T jets are almost exclusively produced through hard scattering processes.

The $Z/\gamma^* \to \tau\tau$ signal is distinguished from backgrounds by means of the mass of the τ lepton pair. The mass, denoted by the symbol $m_{\tau\tau}$, is reconstructed using the SVFit algorithm [84]. The algorithm is based on a likelihood approach and uses as inputs the measured momenta of the visible decay products of both τ leptons, the reconstructed E_T^{miss}, and an event-by-event estimate of the E_T^{miss} resolution. The latter is computed as described in Refs. [83,85]. The inputs are combined with a probabilistic model for leptonic and hadronic τ decays to estimate the momenta of the neutrinos produced in these decays. The algorithm achieves a resolution in $m_{\tau\tau}$ of $\approx 15\%$ relative to the mass of the τ lepton pairs at the generator level.

5 Event selection

The events selected in the $\tau_e\tau_h$, $\tau_\mu\tau_h$, $\tau_h\tau_h$, $\tau_e\tau_\mu$, and $\tau_\mu\tau_\mu$ channels are recorded by combining single-electron and single-muon triggers, triggers that are based on the presence of two τ_h candidates in the event, and triggers based on the presence of both an electron and a muon.

The $\tau_e\tau_h$ and $\tau_\mu\tau_h$ channels utilize single-electron and -muon triggers with p_T thresholds of 23 and 18 GeV, respectively. Selected events are required to contain an electron of $p_T > 24$ GeV or a muon of $p_T > 19$ GeV, both with $|\eta| < 2.1$, and a τ_h candidate with $p_T > 20$ GeV and $|\eta| < 2.3$. The electron or muon is required to pass an isolation requirement of $I_\ell < 0.10\, p_T^\ell$, computed according to Eq. (1). The τ_h candidate is required to pass the moderate WP of the MVA-based τ_h ID discriminant, and to have a charge opposite to that of the electron or muon. The τ_h candidate is further required to pass a tight or minimal requirement on the discriminant that separates hadronic τ decays from electrons, and a minimal or tight selection on the discriminant that separates τ_h from muons. Background arising from W+jets and $t\bar{t}$ production is reduced by requiring the transverse mass of electron or muon and $\vec{p}_T^{\,\text{miss}}$ to satisfy $m_T < 40$ GeV. The transverse mass is defined by:

$$m_T = \sqrt{2\, p_T^\ell\, E_T^{\text{miss}}\, (1 - \cos\Delta\phi)}, \tag{3}$$

where the symbol ℓ refers to the electron or muon, and $\Delta\phi$ denotes the angle in the transverse plane between the lepton momentum and the $\vec{p}_T^{\,\text{miss}}$ vector. Events containing additional electrons with $p_T > 10$ GeV and $|\eta| < 2.5$, or muons with $p_T > 10$ GeV and $|\eta| < 2.4$, passing minimal identification and isolation criteria, are rejected to reduce backgrounds from $Z/\gamma^* \to ee$ and $\mu\mu$ events, and from diboson production.

A trigger based on the presence of two τ_h candidates is used to record events in the $\tau_h\tau_h$ channel. The trigger selects events containing two isolated calorimeter energy deposits at the L1 trigger stage, which are subsequently required to pass a simplified version of the PF-based offline τ_h reconstruction at the high-level trigger stage. The latter applies additional isolation criteria. The p_T threshold for both τ_h candidates is 35 GeV. The trigger efficiency increases with p_T of the τ_h, because different algorithms are used to reconstruct the p_T at the L1 trigger stage and in the offline reconstruction. The trigger reaches an efficiency plateau of $\approx 80\%$ for events in which both τ_h candidates have $p_T > 60$ GeV. Selected events are required to contain two τ_h candidates with $p_T > 40$ GeV and $|\eta| < 2.1$ that have opposite charge and satisfy the tight WP of the MVA-based τ_h ID discriminant, as well as the minimal criteria on the discriminants used to separate τ_h from electrons and muons. Events containing electrons with $p_T > 10$ GeV and $|\eta| < 2.5$ or muons with $p_T > 10$ GeV and $|\eta| < 2.4$, passing minimal identification and isolation criteria, are rejected to avoid overlap with the $\tau_e\tau_h$ and $\tau_\mu\tau_h$ channels.

Events in the $\tau_e\tau_\mu$ channel are recorded with the triggers based on the presence of an electron and a muon. The acceptance for the $Z/\gamma^* \to \tau\tau$ signal is increased by using two complementary triggers. The first trigger selects events that contain an electron with $p_T > 12$ GeV and a muon with $p_T > 17$ GeV, while events containing an electron with $p_T > 17$ GeV and a muon with $p_T > 8$ GeV are recorded through the second trigger. The offline event selection demands the presence of an electron with $p_T > 13$ GeV and $|\eta| < 2.5$, in conjunction with a muon of $p_T > 10$ GeV and $|\eta| < 2.4$. Either the electron or the muon is required to pass a threshold of $p_T > 18$ GeV, to ensure that at least one of the two triggers is fully efficient. Electrons and muons are further required to satisfy isolation criteria of $I_\ell < 0.15\, p_T^\ell$, and to have opposite charge. Background from $t\bar{t}$ production is reduced through a cutoff on a topological discriminant [86] based on the projections:

$$P_\zeta^{\text{miss}} = \vec{p}_T^{\,\text{miss}} \cdot \hat{\zeta} \quad \text{and} \quad P_\zeta^{\text{vis}} = \left(\vec{p}_T^{\,e} + \vec{p}_T^{\,\mu}\right) \cdot \hat{\zeta}, \tag{4}$$

where the symbol $\hat{\zeta}$ denotes a unit vector in the direction of the bisector of the electron and muon $\vec{p}_T$ vectors. The discriminator takes advantage of the fact that the angle between the neutrinos and the visible τ lepton decay products is typically small, causing the $\vec{p}_T^{\,\text{miss}}$ vector in signal events to point in the direction of the visible τ decay products, which is often not true for $t\bar{t}$ background. Selected events are required to satisfy the condition $P_\zeta^{\text{miss}} - 0.85\, P_\zeta^{\text{vis}} > -20$ GeV. The reconstruction of the projections P_ζ^{miss} and P_ζ^{vis} is illustrated in Fig. 1. The figure also shows the distribution in the observable $P_\zeta^{\text{miss}} - 0.85\, P_\zeta^{\text{vis}}$ for events selected in the $\tau_e\tau_\mu$ channel before that condition is applied.

The events selected in the $\tau_\mu\tau_\mu$ channel are recorded using a single-muon trigger with a p_T threshold of 18 GeV. The two muons are required to be within the acceptance of $|\eta| < 2.4$, and to have opposite charge. The muons of higher and lower p_T are required to satisfy the conditions of $p_T > 20$ and > 10 GeV, respectively. Both muons are required to pass an isolation criterion of $I_\mu < 0.15\, p_T^\mu$. The large background arising from DY production of μ pairs is reduced by requiring the mass of the two muons to satisfy $m_{\mu\mu} < 80$ GeV, and through the application of a cutoff on the output of a BDT trained to separate the $Z/\gamma^* \to \tau\tau$ signal from the $Z/\gamma^* \to \mu\mu$ background. The following observables are used as BDT inputs: the ratio of the p_T of the dimuon system to the scalar p_T sum of the two muons ($p_T^{\mu\mu} / \sum p_T^\mu$), the pseudorapidity of the dimuon system ($\eta_{\mu\mu}$), the E_T^{miss}, the topological discriminant P_ζ, computed according to Eq. (4), and the azimuthal angle between the muon of positive charge and the $\vec{p}_T^{\,\text{miss}}$ vector, denoted by the symbol $\Delta\phi(\mu^+, \vec{p}_T^{\,\text{miss}})$. The angle between the muon of negative charge and the $\vec{p}_T^{\,\text{miss}}$ vector, $\Delta\phi(\mu^-, \vec{p}_T^{\,\text{miss}})$, is not used as BDT input, as it is strongly anticorrelated with $\Delta\phi(\mu^+, \vec{p}_T^{\,\text{miss}})$.

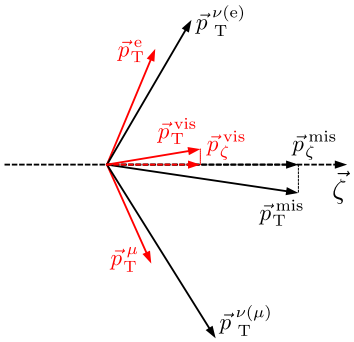

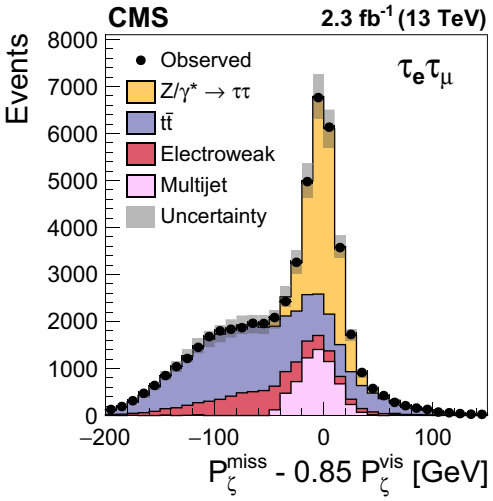

Fig. 1 (Left) Construction of the projections $P_{\zeta}^{\mathrm{miss}}$ and P_{ζ}^{vis}, and (right) the distribution in the observable $P_{\zeta}^{\mathrm{miss}} - 0.85\,P_{\zeta}^{\mathrm{vis}}$ for events selected in the $\tau_{\mathrm{e}}\tau_{\mu}$ channel, before imposing the condition $P_{\zeta}^{\mathrm{miss}} - 0.85\,P_{\zeta}^{\mathrm{vis}} > -20\,\mathrm{GeV}$. Also indicated is the separation of the background into its main components. The sum of background contributions from W+jets, single top quark, and diboson production is referred to as "electroweak" background. The symbols $\vec{p}_{\mathrm{T}}^{\,\nu(\mathrm{e})}$ and $\vec{p}_{\mathrm{T}}^{\,\nu(\mu)}$ refer to the vectorial sum of transverse momenta of the two neutrinos produced in the respective $\tau \to \mathrm{e}\nu\nu$ and $\tau \to \mu\nu\nu$ decays

We refer to the events passing the selection criteria detailed in this Section as belonging to the "signal region" (SR) of the analysis.

6 Background estimation

The accuracy of the background estimate is improved by determining from data the contributions from the main backgrounds, as well as from backgrounds that are difficult to model through MC simulation. In particular, the background from multijet production falls into the latter category. In the $\tau_{\mathrm{e}}\tau_{\mathrm{h}}$, $\tau_{\mu}\tau_{\mathrm{h}}$, and $\tau_{\mathrm{h}}\tau_{\mathrm{h}}$ channels, the dominant background is from events in which a quark or gluon jet is misidentified as τ_{h}. The estimation of background from these "false" τ_{h} sources is discussed in Sect. 6.1. It predominantly arises from multijet production in the $\tau_{\mathrm{h}}\tau_{\mathrm{h}}$ channel and from W+jets events, as well as from multijet production in the $\tau_{\mathrm{e}}\tau_{\mathrm{h}}$ and $\tau_{\mu}\tau_{\mathrm{h}}$ channels. A small additional background contribution in the $\tau_{\mathrm{e}}\tau_{\mathrm{h}}$, $\tau_{\mu}\tau_{\mathrm{h}}$, and $\tau_{\mathrm{h}}\tau_{\mathrm{h}}$ channels arises from $\mathrm{t\bar{t}}$ events with quark or gluon jets misidentified as τ_{h}. The multijet background is also relevant in the $\tau_{\mathrm{e}}\tau_{\mu}$ and $\tau_{\mu}\tau_{\mu}$ channels. The estimation of the multijet background in these channels is described in Sect. 6.2. The contribution to the SR from the $\tau_{\mathrm{e}}\tau_{\mu}$ and $\tau_{\mu}\tau_{\mu}$ channels arising from backgrounds with misidentified leptons other than multijet production is small and not distinguished from background contributions with genuine leptons. Significant background contributions arise from $\mathrm{t\bar{t}}$ production in the $\tau_{\mathrm{e}}\tau_{\mu}$ channel and from the DY production of muon pairs in the $\tau_{\mu}\tau_{\mu}$ channel. The normalization of the $\mathrm{t\bar{t}}$ background in the $\tau_{\mathrm{e}}\tau_{\mu}$ and $\tau_{\mu}\tau_{\mu}$ channels is determined from data, using a control region that contains events with one electron, one muon, and one or more b-tagged jets. Details of the procedure are given in Sect. 6.3. The $\mathrm{t\bar{t}}$ normalization factor obtained from this control region is also applied to the $\mathrm{t\bar{t}}$ background events selected in the $\tau_{\mathrm{e}}\tau_{\mathrm{h}}$, $\tau_{\mu}\tau_{\mathrm{h}}$, and $\tau_{\mathrm{h}}\tau_{\mathrm{h}}$ channels, in which the reconstructed τ_{h} is either due to a genuine τ_{h} or due to the misidentification of an electron or muon. The background rate from $\mathrm{Z}/\gamma^{*} \to \mathrm{ee}$ and $\mathrm{Z}/\gamma^{*} \to \mu\mu$ production is determined from the data through a maximum-likelihood (ML) fit of the $m_{\tau\tau}$ distributions in the SR, described in Sect. 8. The contributions of minor backgrounds from single top quark and diboson production, as well as a small contribution from W+jets background in the $\tau_{\mathrm{e}}\tau_{\mu}$ and $\tau_{\mu}\tau_{\mu}$ channels, are obtained from MC simulation. The sum of these minor backgrounds is referred to as "electroweak" background. A Higgs boson with a mass of $m_{\mathrm{H}} = 125\,\mathrm{GeV}$, produced at the rate and with branching fractions predicted in the SM, is considered as background. Nevertheless, this contribution is found to be negligible.

The background estimates are summarized in Table 1. The quoted uncertainties represent the quadratic sum of statistical and systematic sources.

In preparation for future analyses of τ lepton production, the validity of the background-estimation procedures described in this section is further tested in event categories that are relevant to the SM $\mathrm{H} \to \tau\tau$ analysis, as well as in searches for new physical phenomena. Event categories based on jet multiplicity, p_{T} of the τ lepton pair, and on the multiplicity of b jets in the event are used in $\mathrm{H} \to \tau\tau$ analy-

Table 1 Expected number of background events in the $\tau_e\tau_h$, $\tau_\mu\tau_h$, $\tau_h\tau_h$, $\tau_e\tau_\mu$, and $\tau_\mu\tau_\mu$ channels in data, corresponding to an integrated luminosity of 2.3 fb^{-1}. The uncertainties are rounded to two significant digits, except when they are < 10, in which case they are rounded to one significant digit, and the event yields are rounded to match the precision in the uncertainties

Process	$\tau_e\tau_h$	$\tau_\mu\tau_h$	$\tau_h\tau_h$
Jets misidentified as τ_h	5400 ± 880	$10{,}200 \pm 1300$	680 ± 210
$t\bar{t}$	365 ± 35	651 ± 60	19 ± 3
$Z/\gamma^* \to$ ee, $\mu\mu$ (e or μ misidentified as τ_h)	940 ± 250	780 ± 210	–
Electroweak	96 ± 15	185 ± 29	43 ± 8
SM H	48 ± 10	100 ± 21	13 ± 3
Total expected background	6850 ± 910	$11{,}900 \pm 1300$	750 ± 210
Process	$\tau_e\tau_\mu$		$\tau_\mu\tau_\mu$
Multijet	4530 ± 670		740 ± 140
$Z/\gamma^* \to \mu\mu$	–		7650 ± 300
$t\bar{t}$	3650 ± 310		1370 ± 110
Electroweak	1180 ± 120		312 ± 34
SM H	57 ± 12		18 ± 4
Total expected background	9400 ± 760		$10{,}100 \pm 390$

ses performed by CMS in the context of the SM [43] and of its minimal supersymmetric extension [9–11], as well as in the context of searches for Higgs boson pair production [87]. The validation of the background-estimation procedures in these event categories is detailed in the Appendix.

6.1 Estimation of false-τ_h background in $\tau_e\tau_h$, $\tau_\mu\tau_h$, and $\tau_h\tau_h$ channels

The background arising from events in which a quark or gluon jet is misidentified as τ_h in the $\tau_e\tau_h$, $\tau_\mu\tau_h$, and $\tau_h\tau_h$ channels is estimated via the "fake factor" (F_F) method. The method is based on selecting events that pass altered τ_h ID criteria, and weighting the events through suitably chosen extrapolation factors (the F_F). The events passing the altered τ_h ID criteria are referred to as belonging to the "application region" (AR) of the F_F method. Except for modifying the τ_h ID criteria, the same selections are applied to events in the AR and in the SR. The F_F are measured in dedicated control regions in data. These are referred to as "determination regions" (DR) of the F_F method, and are chosen such that they neither overlap with the SR nor with the AR.

The F_F are determined in bins of decay mode and p_T of the τ_h candidate, and as a function of jet multiplicity. In each such bin, the F_F is given by the ratio:

$$F_F = \frac{N_{\text{nominal}}}{N_{\text{altered}}}, \tag{5}$$

where N_{nominal} corresponds to the number of events with τ_h candidates that pass the nominal WP of the MVA-based τ_h ID discriminant in a given channel, and N_{altered} is the number of events with τ_h candidates that satisfy the altered τ_h ID criteria. To satisfy the altered τ_h ID criteria, τ_h candidates must satisfy the barely constrained WP, but fail the nominal WP. The multiplicity of jets that is used to parametrize the F_F is denoted by N_{jet}, and is defined by the jets that satisfy the conditions $p_T > 20$ GeV and $|\eta| < 4.7$, and do not overlap with τ_h candidates passing the barely constrained WP of the MVA-based τ_h ID discriminant, nor with electrons or muons within $\Delta R < 0.5$. In each bin, the contribution from processes with genuine τ_h, and with electrons or muons misidentified as τ_h, are estimated through MC simulation, and subtracted from the numerator as well as from the denominator in Eq. (5).

As the probabilities for jets to be misidentified as τ_h depend on the τ_h ID criteria, and the latter differ in different channels, the F_F are measured separately in each one of them. Moreover, the misidentification rates differ for multijet, W+jets, and $t\bar{t}$ events, necessitating a measurement of the F_F in the DR enriched in contributions from multijet, W+jets, and $t\bar{t}$ backgrounds. The relative fractions of multijet, W+jets, and $t\bar{t}$ background processes in the AR, denoted by R_p, are determined through a fit to the distribution in m_T, and are used to weight the F_F determined in the DR when computing the estimate of the false-τ_h background in the SR. The procedure is illustrated in Fig. 2.

The τ_h ID criteria applied in the AR are identical to the τ_h ID criteria applied in the denominator of Eq. (5). More specifically, the criteria on p_T and η, as well as the requirements on the discriminators that distinguish τ_h from electrons and muons, are the same as in the SR. The τ_h candidates selected in the $\tau_e\tau_h$ and $\tau_\mu\tau_h$ channels are required to pass the barely constrained, but fail the moderately constrained WP of the MVA-based τ_h ID discriminant. In the $\tau_h\tau_h$ channel, one of the two τ_h candidates must pass the tight WP, while the other τ_h candidate is required to pass the barely constrained, but fail the tight WP, precluding overlap of the AR with the SR.

The DR enriched in contributions from multijet, W+jets, and $t\bar{t}$ backgrounds contain specific mixtures of gluon, light-

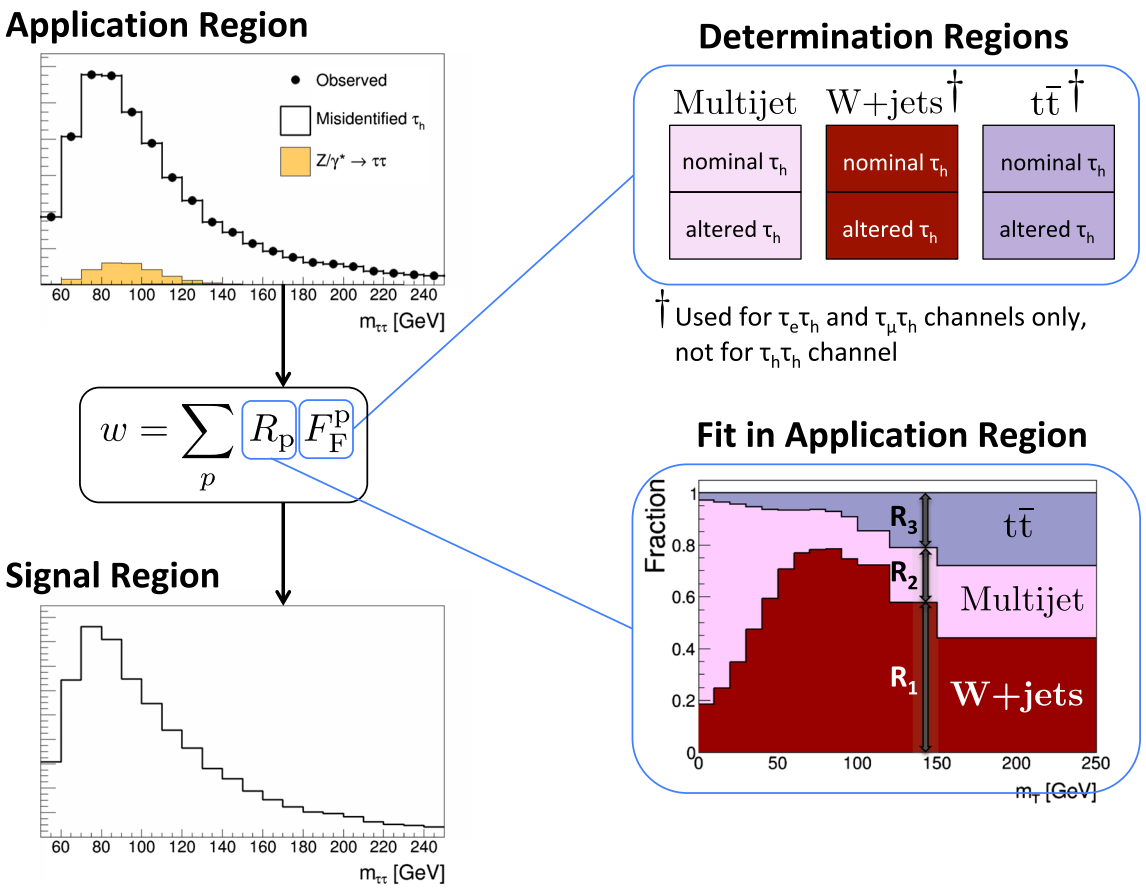

Fig. 2 Schematic illustration of the F_F method, used to estimate the false-τ_h background in the $\tau_e\tau_h$, $\tau_\mu\tau_h$, and $\tau_h\tau_h$ channels. An event sample enriched in multijet, W+jets, and $t\bar{t}$ backgrounds is selected in the AR (top left). The weights w, given by the product of the F_F measured in the DR (top right) and the relative fractions R_p of different background processes p in the AR, are applied to the events selected in the AR to yield the estimate of the false-τ_h background in the SR (bottom left). The superscript p on the symbol F_F^p indicates that the F_F depend on the background process p, where p refers to either multijet, W+jets, or $t\bar{t}$ background. The contribution of the $Z/\gamma^* \to \tau\tau$ signal in the AR is subtracted, based on MC simulation. The fractions R_p are determined by a fit of the m_T distribution in the AR (bottom right), described in more detail in Sect. 6.1.2. The fraction R_1 includes a small contribution from DY events in which the reconstructed τ_h is due to the misidentification of a quark or a gluon jet

quark (u, d, s), and heavy-flavour (c, b) quark jets, with different probabilities for misidentification as τ_h, as illustrated for simulated events in Fig. 3. The misidentification rates are shown for jets passing $p_T > 20$ GeV and $|\eta| < 2.3$, and for jets satisfying in addition the barely constrained WP of the MVA-based τ_h ID discriminant. In general, the misidentification rates are higher in quark jets compared to gluon jets, as the former typically have lower particle multiplicity and are more collimated than the latter, thereby increasing their probability to be misidentified as τ_h. As it can be seen in the figure, the requirement for jets to pass minimal τ_h selection criteria significantly reduce the flavour dependence of the misidentification rates. This in turn lowers the systematic uncertainty that arises from the limited knowledge of the flavour composition in the AR. Residual flavour dependence of the F_F is taken into account by measuring separate sets of F_F in each DR, and determining the relative fraction R_p of multijet, W+jets, and $t\bar{t}$ backgrounds in the AR of the respective channel. Given the F_F and the fractions R_p, the estimate of the background from misidentified τ_h in the SR is obtained by applying the weights

$$w = \sum_p R_p F_F^p \tag{6}$$

to events selected in the AR, where the sum extends over the above three background processes p. The F_F refer, as usual, to Eq. (5). The symbol F_F^p indicates that, in addition to their dependence on τ_h decay mode, τ_h candidate p_T, and jet multiplicity, the F_F depend on the background process p, where the superscript p refers to either multijet, W+jets, or $t\bar{t}$ background. In the $\tau_h\tau_h$ channel, the F_F^p is determined by the decay mode and p_T of the τ_h candidate that passes the barely constrained, but fails the tight WP of the MVA-based τ_h ID discriminant. The τ_h candidate that passes the tight WP does not enter the computation of the weight w.

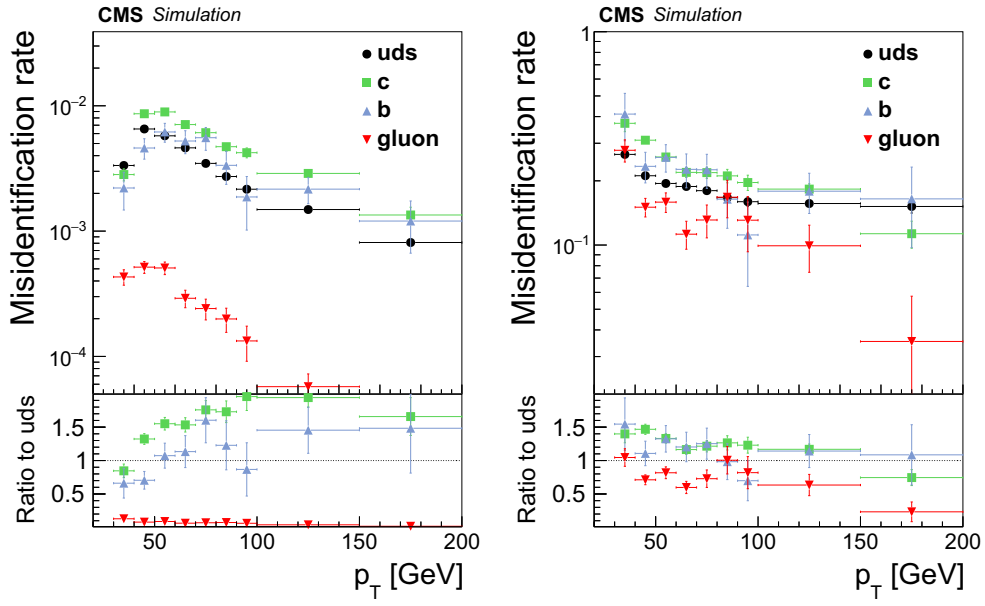

Fig. 3 Probabilities for gluon and quark jets, of different flavour in simulated multijet events, to pass the moderate WP of the MVA-based τ_h ID discriminant, as a function of jet p_T, for jets passing $p_T > 20\,\text{GeV}$ and $|\eta| < 2.3$ (left), and for jets passing in addition the barely constrained WP of the MVA-based τ_h ID discriminant (right)

The underlying assumption in the F_F method is that the ratio of the number of events from background process p in the SR to the number of events from the same background in the AR is equal to the ratio $N_{\text{nominal}}/N_{\text{altered}}$ that is measured in the background-specific DR.

The measurement of the F_F is detailed in Sect. 6.1.1, while the fractions R_p are discussed in Sect. 6.1.2. The estimate of the false-τ_h background obtained from the F_F method is validated in control regions devoid of $Z/\gamma^* \to \tau\tau$ signal. The result of this validation is presented in Sect. 6.1.3.

6.1.1 Measurement of F_F

The F_F are measured in DR chosen such that one particular background process is enhanced in each DR. The selection criteria applied in the DR are similar to those applied in the SR. In the following, we describe only the differences relative to the SR.

In the $\tau_e\tau_h$ and $\tau_\mu\tau_h$ channels, three different DR are used to measure the F_F for multijet, W+jets, and $t\bar{t}$ backgrounds. The DR dominated by multijet background contains events in which the charges of the τ_h candidate and of the light lepton candidates are the same, and the electron or muon satisfies a modified isolation criterion of $0.05 < I_\ell/p_T^\ell < 0.15$. Depending on whether the τ_h candidate passes or fails the moderate WP of the MVA-based τ_h ID discriminant, the event contributes either to the numerator or to the denominator of Eq. (5). The DR dominated by W+jets background is defined by modifying the requirement for the transverse mass of lepton and $\vec{p}_T^{\,\text{miss}}$ to $m_T > 70\,\text{GeV}$. The contamination arising from $t\bar{t}$ background is reduced by vetoing events containing jets that pass the b tagging criteria described in Sect. 4. A common $t\bar{t}$ DR is used for the $\tau_e\tau_h$ and $\tau_\mu\tau_h$ channels. The events are required to contain an electron, a muon, at least one τ_h candidate, and pass triggers based on the presence of an electron or a muon. The offline event selection demands that the electron satisfy the conditions $p_T > 13\,\text{GeV}$ and $|\eta| < 2.5$, the muon $p_T > 10\,\text{GeV}$ and $|\eta| < 2.4$, and that both pass an isolation criterion of $I_\ell < 0.10\,p_T^\ell$. The event is furthermore required to contain at least one jet that passes the b tagging criteria described in Sect. 4. In case events contain multiple τ_h candidates, the candidate used for the F_F measurement is chosen at random.

In the $\tau_h\tau_h$ channel, a single DR is used, which selects a high purity sample of multijet events, the dominant background in this channel. The multijet DR is identical to the SR of the $\tau_h\tau_h$ channel, except that the two τ_h candidates are required to have the same rather than opposite charge. One of the jets is chosen to be the "tag" jet, and required to pass the tight WP of the MVA-based τ_h ID discriminant, while the measurement of the F_F is performed on the other jet, referred to as the "probe" jet. The tag jet is chosen at random. The W+jets and $t\bar{t}$ backgrounds are small in the $\tau_h\tau_h$ channel, making it difficult to define a DR that is dominated by these backgrounds, or that provides sufficient statistical information for the F_F measurement. The F_F in the multijet DR of the $\tau_h\tau_h$ channel are therefore used to weight all events selected in the AR of the $\tau_h\tau_h$ channel. Differences in the F_F between

W+jets, $\mathrm{t\bar{t}}$, and multijet events are accounted for by adding a systematic uncertainty of 30% on the part of the background from misidentified τ_h expected from the contribution of W+jets and $\mathrm{t\bar{t}}$ background processes. This contribution is estimated using MC simulation, and the magnitude of the systematic uncertainty is motivated by the difference found in the F_F measured in multijet, W+jets, and $\mathrm{t\bar{t}}$ DR in the $\tau_\mathrm{e}\tau_\mathrm{h}$ and $\tau_\mu\tau_\mathrm{h}$ channels.

The F_F determined in the various DR are shown in Figs. 4 and 5. The decay modes $\tau^- \to \mathrm{h}^-\nu_\tau$, $\tau^- \to \mathrm{h}^-\pi^0\nu_\tau$, and $\tau^- \to \mathrm{h}^-\pi^0\pi^0\nu_\tau$ are referred to as "one-prong" decays and the mode $\tau^- \to \mathrm{h}^-\mathrm{h}^+\mathrm{h}^-\nu_\tau$ as "three-prong" decays. The measured F_F are corrected for differences in the τ_h misidentification rates between DR and AR. The magnitude of these relative corrections is $\approx 10\%$, as discussed below.

For the multijet DR in the $\tau_\mathrm{e}\tau_\mathrm{h}$ and $\tau_\mu\tau_\mathrm{h}$ channels, correlations between the F_F and the charge of the electron or muon and the τ_h candidate, and between F_F and the isolation of the electron or muon, are studied in data and taken into account as follows. A correction for the extrapolation from events in which the charges of lepton and τ_h candidate have the same sign (SS) to events in which they have opposite sign (OS) is obtained by comparing F_F in the SS and OS events containing electrons or muons that pass an inverted isolation criterion of $0.1 < I_\ell/p_\mathrm{T}^\ell < 0.2$. The dependence of the F_F on the isolation of the electron or muon is studied using an event sample selected with no isolation condition applied to the lepton. The results of this study are used to extrapolate the F_F obtained in the multijet DR ($0.05 < I_\ell/p_\mathrm{T}^\ell < 0.15$) to the SR ($I_\ell < 0.10\, p_\mathrm{T}^\ell$).

For the DR dominated by W+jets background in the $\tau_\mathrm{e}\tau_\mathrm{h}$ and $\tau_\mu\tau_\mathrm{h}$ channels, closure tests of the F_F method reveal a dependence of the F_F on m_T, which is not accounted for by the chosen parametrization of the F_F as functions of jet multiplicity, τ_h decay mode, and p_T. The dependence on m_T is studied using simulated W+jets events, and used to extrapolate the F_F measured in the W+jets DR ($m_\mathrm{T} > 70\,\mathrm{GeV}$) to the SR ($m_\mathrm{T} < 40\,\mathrm{GeV}$).

In the $\tau_\mathrm{h}\tau_\mathrm{h}$ channel, the F_F determined in the multijet DR are corrected for a dependence of the F_F on the relative charge of the two τ_h candidates. This is studied in events in which the tag jet (the jet on which the FF measurement is not performed) fails the tight WP of the MVA-based τ_h ID discriminant. The difference between the F_F in OS and SS events defines this correction.

6.1.2 Determination of R_p

In the $\tau_\mathrm{e}\tau_\mathrm{h}$ and $\tau_\mu\tau_\mathrm{h}$ channels, the relative fractions R_p of multijet, W+jets, and $\mathrm{t\bar{t}}$ backgrounds in the AR are determined through a fit to the distribution in m_T. The distribution in m_T ("template") used to represent the multijet background in the fit is obtained from a sample of events selected in data, in which the τ_h candidate and the electron or muon have same charge, and where at least one of the leptons satisfies a modified isolation criterion of $0.05 < I_\ell/p_\mathrm{T}^\ell < 0.15$. The contributions from other backgrounds to this control region are subtracted, based on MC simulation. The distribution representing the other backgrounds in the fit are also taken from simulation. The templates for $\mathrm{t\bar{t}}$, diboson, and DY events are split into three components: events in which the reconstructed τ_h is due to a genuine τ_h, events in which the τ_h is due to the misidentification of an electron or muon, and events in which a quark or gluon jet is misidentified as τ_h. The normalization of each component is determined independently in the fit. The relative fractions of the $\mathrm{Z}/\gamma^* \to \tau\tau$ signal and all individual background processes are left unconstrained in the fit. Finally, the fractions R_p are parametrized as function of m_T and are normalized such that the contribution of all processes p in which the reconstructed τ_h is due to a misidentified jet sums to unity, $\sum_\mathrm{p} R_\mathrm{p} = 1$.

In the $\tau_\mathrm{h}\tau_\mathrm{h}$ channel, the AR is dominated by multijet background. The contributions from the $\mathrm{Z}/\gamma^* \to \tau\tau$ signal and all background processes, except multijet production, are small and taken from simulation. The fraction of multijet background in the AR is determined by subtracting the sum of all processes modelled in the MC simulation from the data in the AR, without performing a fit in this channel.

A small fraction of events in the AR of the $\tau_\mathrm{e}\tau_\mathrm{h}$, $\tau_\mu\tau_\mathrm{h}$, and $\tau_\mathrm{h}\tau_\mathrm{h}$ channels arises from DY events in which quark or gluon jets are misidentified as τ_h candidates. These events are treated as background and are included in the false-τ_h estimate using the F_F method. As the analysed data do not provide a way of determining F_F in DY events with sufficient statistical accuracy, the F_F measured in W+jets events are used instead for the fraction of DY events with jets misidentified as τ_h in the $\tau_\mathrm{e}\tau_\mathrm{h}$ and $\tau_\mu\tau_\mathrm{h}$ channels. The validity of this procedure is justified by studies of F_F in simulated W+jets and DY events, which indicate that the flavour composition of jets and the F_F are very similar in these events. In the $\tau_\mathrm{h}\tau_\mathrm{h}$ channel, the F_F measured in multijet events are used and the systematic uncertainty on the DY background with misidentified τ_h is increased by 30%.

6.1.3 Validation of the false-τ_h background estimate in control regions

The modelling of the background from jets misidentified as τ_h in the $\tau_\mathrm{e}\tau_\mathrm{h}$, $\tau_\mu\tau_\mathrm{h}$, and $\tau_\mathrm{h}\tau_\mathrm{h}$ channels through the F_F method is validated by comparing the background estimates obtained in this method to the data in control regions containing events with SS $\mathrm{e}\tau_\mathrm{h}$, $\mu\tau_\mathrm{h}$, and $\tau_\mathrm{h}\tau_\mathrm{h}$ pairs. A dedicated set of F_F, without corrections for the extrapolation from OS to SS events, is determined for this validation. The selection of events in the multijet DR is also altered in this validation, to avoid overlap with the AR. The distributions in $m_{\tau\tau}$ in events con-

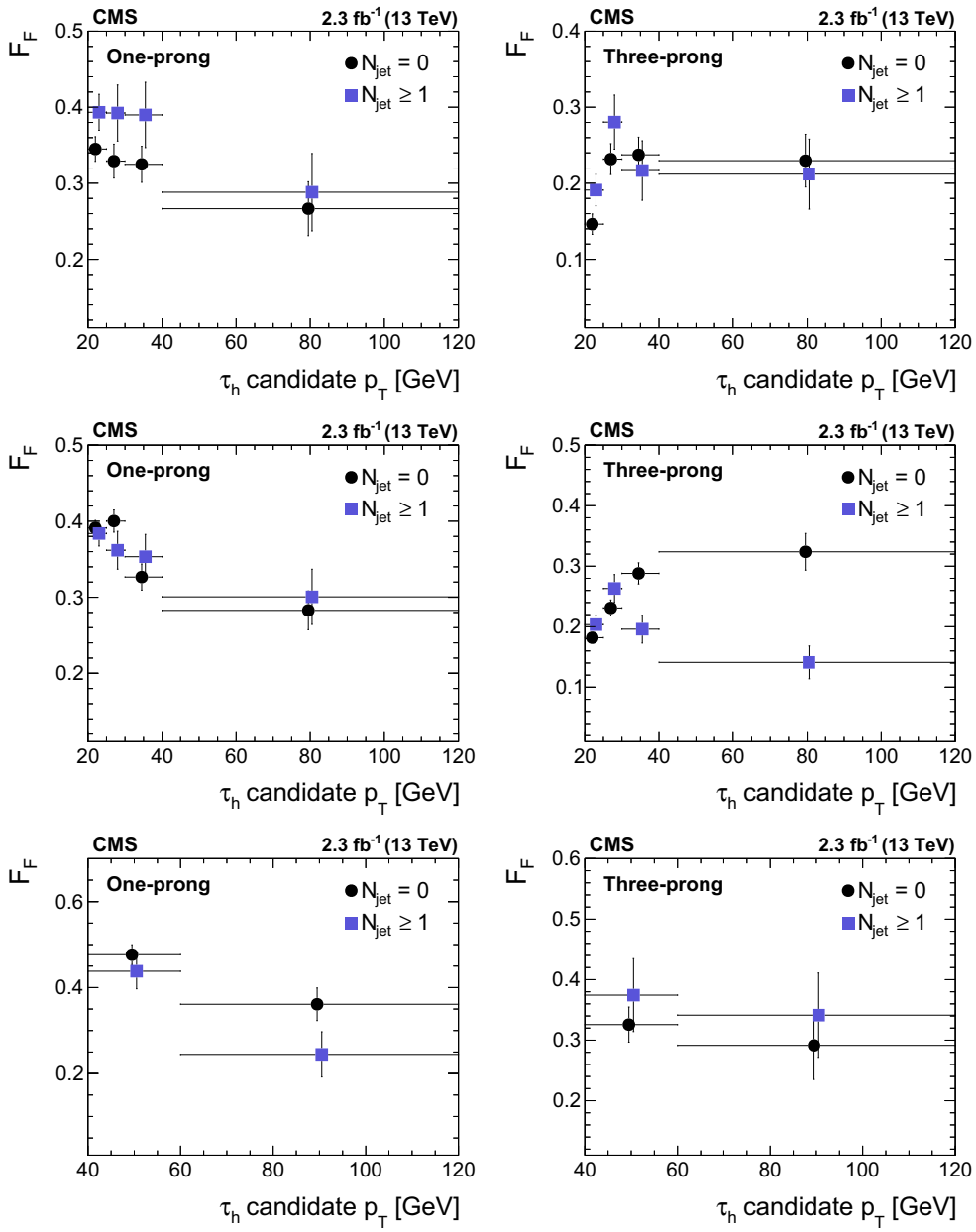

Fig. 4 The F_{F} values measured in multijet events in the $\tau_{\mathrm{e}}\tau_{\mathrm{h}}$ (upper), $\tau_{\mu}\tau_{\mathrm{h}}$ (center), and $\tau_{\mathrm{h}}\tau_{\mathrm{h}}$ (lower) channels, presented in bins of jet multiplicity and τ_{h} decay mode, as a function of τ_{h} p_{T}. The abscissae of the points are offset to distinguish the points with different jet multiplicities

taining SS $\mathrm{e}\tau_{\mathrm{h}}$, $\mu\tau_{\mathrm{h}}$, and $\tau_{\mathrm{h}}\tau_{\mathrm{h}}$ pairs are shown in Fig. 6. The data are compared to the sum of false-τ_{h} background and other backgrounds. The contribution of other backgrounds, in which the reconstructed τ_{h} is due either to a genuine τ_{h} or to the misidentification of an electron or muon, is obtained from the MC simulation. The event yield of the $\mathrm{Z}/\gamma^{*} \to \tau\tau$ signal in these control regions is small. The normalization of individual backgrounds and of the $\mathrm{Z}/\gamma^{*} \to \tau\tau$ signal is determined through a fit to the distributions in $m_{\tau\tau}$ in which the rate of each background is allowed to vary within its estimated systematic uncertainty. The good agreement observed between the data and the background prediction in the control regions of all three channels confirms the validity of false-τ_{h} background estimates obtained through the F_{F} method.

6.2 Estimation of multijet background in $\tau_{\mathrm{e}}\tau_{\mu}$ and $\tau_{\mu}\tau_{\mu}$ channels

The contributions from multijet background in the SR of the $\tau_{\mathrm{e}}\tau_{\mu}$ or $\tau_{\mu}\tau_{\mu}$ channels are estimated using control regions

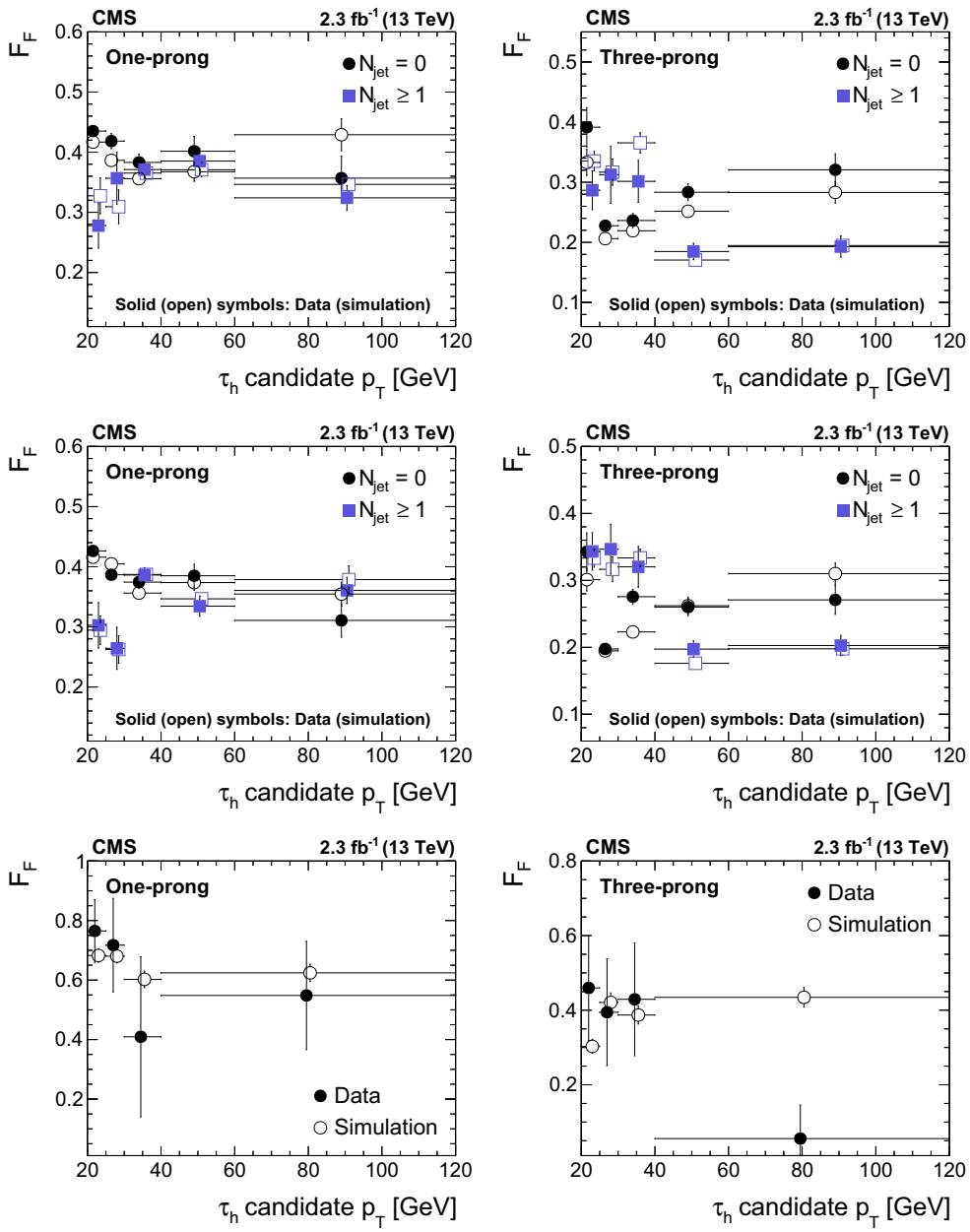

Fig. 5 The F_F values measured in W+jets events in the $\tau_e\tau_h$ (upper) and $\tau_\mu\tau_h$ (center) channels and in $t\bar{t}$ events (lower), presented in bins of jet multiplicity and τ_h decay mode, as a function of τ_h p_T. A common $t\bar{t}$ DR is used for the $\tau_e\tau_h$ and $\tau_\mu\tau_h$ channels. The abscissae of the points are offset to distinguish the points with different jet multiplicities

containing events with an electron and muon or two muons of same charge, respectively. An estimate for the contribution from multijet events in the SR is obtained by scaling the yield of the multijet background in the SS control region by a suitably chosen extrapolation factor, defined by the ratio of $e\mu$ or $\mu\mu$ pairs with opposite charge to those with same charge. The ratio is measured in events in which at least one lepton passes an inverted isolation criterion of $I_\ell > 0.15\ p_T^\ell$. We refer to this event sample as an isolation sideband region (SB). The requirement $I_\ell > 0.15\ p_T^\ell$ ensures that the SB does not overlap with the SR. A complication arises from the fact that the ratio of OS to SS pairs depends on the lepton kinematics and the isolation criterion used in the SB. The nominal OS/SS ratio is measured in an isolation sideband (SB1) defined by requiring both leptons to satisfy a relaxed isolation criterion of $I_\ell < 0.60\ p_T^\ell$, with at least one lepton passing the condition $I_\ell > 0.15\ p_T^\ell$. The systematic uncertainty in the OS/SS ratio that arises from the choice of the

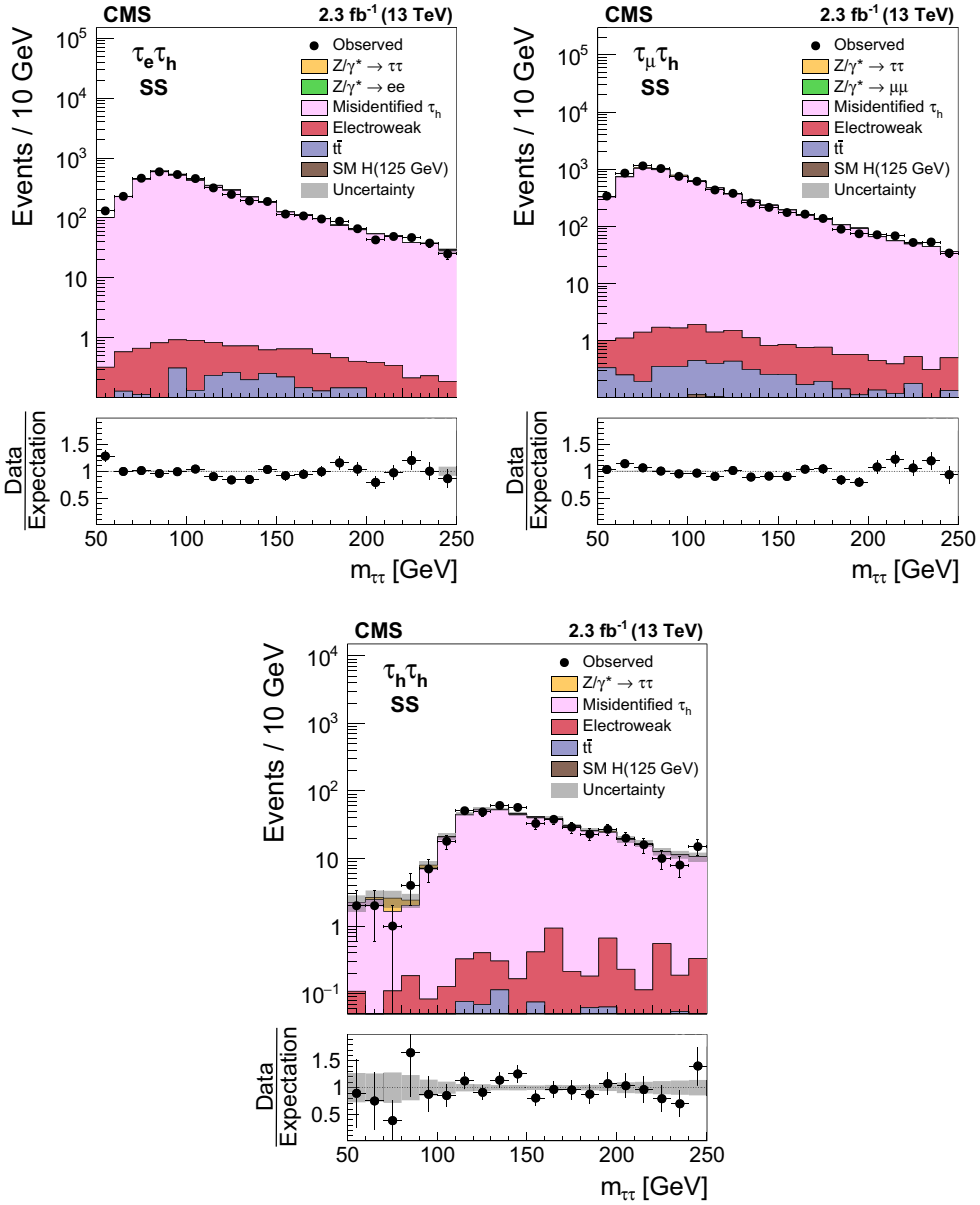

Fig. 6 Distributions in $m_{\tau\tau}$ for SS events containing (upper left) eτ_h, (upper right) $\mu\tau_h$, and (lower) $\tau_h\tau_h$ pairs, compared to expected background contributions

upper limit on I_ℓ applied in SB1 is estimated by taking the difference between the OS/SS ratio computed in SB1 and the ratio computed in a different isolation sideband region (SB2). The latter is defined by requiring at least one lepton to pass the condition $I_\ell > 0.60\, p_{\mathrm{T}}^{\ell}$, without setting an upper limit on I_ℓ in the SB2 region. The criteria to select events in the isolation sidebands are optimized to ensure high statistical accuracy in the measurement of the OS/SS extrapolation factor and at the same time the minimization of differences in lepton kinematic distributions between the SR and the SB. In both isolation sidebands, the OS/SS ratio is measured as function of p_{T} of the two leptons ℓ and ℓ' and of their separation $\Delta R(\ell, \ell') = \sqrt{(\eta_\ell - \eta_{\ell'})^2 + (\phi_\ell - \phi_{\ell'})^2}$ in the η-ϕ plane. The contributions to the SS control region, as well as to SB1 and SB2, from backgrounds other than multijet production are subtracted, based on results from MC simulation.

6.3 Estimation of $\mathrm{t\bar{t}}$ background

While the $m_{\tau\tau}$ distribution for $\mathrm{t\bar{t}}$ background is obtained from MC simulation, the event yield in the $\mathrm{t\bar{t}}$ background in the SR is determined from data, using a control region dominated by $\mathrm{t\bar{t}}$ background. Events in the $\mathrm{t\bar{t}}$ control region are required to satisfy selection criteria that are similar to the requirements

for the SR of the $\tau_e\tau_\mu$ channel, described in Sect. 5. The main differences are that the cutoff on $P_\zeta^{\text{miss}} - 0.85\, P_\zeta^{\text{vis}}$ is inverted to $P_\zeta^{\text{miss}} - 0.85\, P_\zeta^{\text{vis}} < -40$ GeV, and a condition $E_{\text{T}}^{\text{miss}} > 80$ GeV is added to the event selection in the $\bar{\text{t}}\text{t}$ control region. The $\bar{\text{t}}\text{t}$ event yield observed in the control region is a 1.01 ± 0.07 multiple of the expectation from the MC simulation. The ratio of the $\bar{\text{t}}\text{t}$ event yield measured in data to the MC prediction is applied as a scale factor to simulated $\bar{\text{t}}\text{t}$ events, to correct the $\bar{\text{t}}\text{t}$ background yield in the $\tau_e\tau_\mu$ and $\tau_\mu\tau_\mu$ channels, as well as to correct the part of the $\bar{\text{t}}\text{t}$ background in the $\tau_e\tau_h$, $\tau_\mu\tau_h$, and $\tau_h\tau_h$ channels that is either due to genuine τ_h or due to the misidentification of an electron or muon as τ_h. The latter is not included in the background estimate obtained through the F_F method, but modelled in the MC simulation.

7 Systematic uncertainties

Imprecisely measured or imperfectly simulated effects can alter the normalization and distribution of the $m_{\tau\tau}$ mass spectrum in $Z/\gamma^* \to \tau\tau$ signal or background processes. These systematic uncertainties can be categorized into theory-related and experimental sources. The latter can be further subdivided into those associated with the reconstruction of physical objects of interest and with estimated backgrounds. The uncertainties related to the reconstruction of physical objects apply to the $Z/\gamma^* \to \tau\tau$ signal and to backgrounds modelled in the MC simulation. The main background contributions are determined from data, as described in Sect. 6, and are largely unaffected by the accuracy achieved in modelling data in the MC simulation.

The main experimental uncertainties are related to the reconstruction and identification of electrons, muons, and τ_h, as follows. The efficiency to reconstruct and identify τ_h and the energy scale of τ_h (τ_h ES) is measured using $Z/\gamma^* \to \tau\tau \to \tau_\mu\tau_h$ events. The former is done by comparing the number of $Z/\gamma^* \to \tau\tau \to \tau_\mu\tau_h$ events with τ_h candidates passing and failing the τ_h ID criteria, and the latter by comparing the distributions in the τ_h candidate mass, as well as the visible mass of the muon and τ_h system in data and in MC simulation [75], measured with respective uncertainties of ≈ 6 and $\approx 1\%$. The events selected for the τ_h ID efficiency and τ_h ES measurements overlap with the events in the $\tau_\mu\tau_h$ channel. We account for the overlap by assigning a 3% uncertainty to τ_h ES. A 3% change in the τ_h ES affects the acceptance in $Z/\gamma^* \to \tau\tau$ signal by 3, 3, and 17% in the $\tau_e\tau_h$, $\tau_\mu\tau_h$, and $\tau_h\tau_h$ channels, respectively. The impact on the signal acceptance and on the distribution in $m_{\tau\tau}$ is illustrated in Fig. 7. It has been checked that the overlap and the choice in the τ_h ES uncertainty have little impact on the final results. The ML fit performed to measure the $Z/\gamma^* \to \tau\tau$ cross section, described in Sect. 8, reduces the uncertainties in the τ_h ID efficiency and in the τ_h ES to 2.2 and 0.9%, respectively. The efficiency of the τ_h trigger used in the $\tau_h\tau_h$ channel is measured in $Z/\gamma^* \to \tau\tau \to \tau_\mu\tau_h$ events with an uncertainty of $\approx 4.5\%$ per τ_h. The measurement is detailed in Ref. [88].

Electron and muon reconstruction, identification, isolation, and trigger efficiencies are measured using $Z/\gamma^* \to$ ee and $Z/\gamma^* \to \mu\mu$ events via the "tag-and-probe" method [89] at an accuracy of 2%. The energy scales for electrons and muons (e ES and μ ES) are calibrated using $J/\psi(1S) \to \ell\ell$, $\Upsilon \to \ell\ell$, and $Z/\gamma^* \to \ell\ell$ events (with ℓ referring to e and μ), and have an uncertainty of 1%. The e ES and μ ES uncertainties affect the acceptance in the $Z/\gamma^* \to \tau\tau$ signal in the $\tau_e\tau_h$, $\tau_\mu\tau_h$, $\tau_e\tau_\mu$, and $\tau_\mu\tau_\mu$ channels by less than 1%.

The $E_{\text{T}}^{\text{miss}}$ response and resolution are known within uncertainties of a few percent from studies performed in $Z/\gamma^* \to \mu\mu$, $Z/\gamma^* \to$ ee, and γ+jets events [90]. The impact of these uncertainties on the acceptance in the $Z/\gamma^* \to \tau\tau$ signal is small, amounting to less than 1%. In the $\tau_e\tau_h$ and $\tau_\mu\tau_h$ channels, the impact arises from the $m_{\text{T}} < 40$ GeV selection criterion. In the $\tau_e\tau_\mu$ and $\tau_\mu\tau_\mu$ channels, the impact is due to the $P_\zeta^{\text{miss}} - 0.85\, P_\zeta^{\text{vis}} > -20$ GeV requirement and the use of $E_{\text{T}}^{\text{miss}}$ and P_ζ as input variables in the BDT that separates the $Z/\gamma^* \to \tau\tau$ signal from the $Z/\gamma^* \to \mu\mu$ background, respectively. The effect of uncertainties related to the modelling of the $E_{\text{T}}^{\text{miss}}$ on the distribution in $m_{\tau\tau}$ is small.

The uncertainty in the integrated luminosity is 2.3% [91].

The backgrounds determined from data are also subject to uncertainties that alter the normalization and distribution ("shape") of the $m_{\tau\tau}$ mass spectrum. Background yields and their associated uncertainties are given in Table 1. The uncertainties in the backgrounds arising from the misidentification of quark and gluon jets as τ_h candidates in the $\tau_e\tau_h$, $\tau_\mu\tau_h$, and $\tau_h\tau_h$ channels are obtained by changing the F_F values as well as the relative fractions R_p of multijet, W+jets, and $\bar{\text{t}}\text{t}$ backgrounds within their uncertainties. The resulting uncertainties in the $m_{\tau\tau}$ distribution in the $\tau_e\tau_h$, $\tau_\mu\tau_h$, and $\tau_h\tau_h$ channels are illustrated in Fig. 8. The uncertainties in the size of the false-τ_h backgrounds are 8, 6, and 16% in the $\tau_e\tau_h$, $\tau_\mu\tau_h$, and $\tau_h\tau_h$ channels, respectively. In the $\tau_e\tau_\mu$ and $\tau_\mu\tau_\mu$ channels, the uncertainty in the size of the multijet background is $\approx 20\%$. The magnitude of the $\bar{\text{t}}\text{t}$ background is known to an accuracy of 7%. The uncertainty in the distribution of the $\bar{\text{t}}\text{t}$ background is estimated by changing the weights applied to the $\bar{\text{t}}\text{t}$ MC sample, to improve the modelling of the top quark p_{T} distribution (described in Sect. 3), between no reweighting and the reweighting applied twice.

The uncertainties in the yields of single top quark and diboson backgrounds, modelled using MC simulation, are each $\approx 15\%$. Besides constituting the dominant background in the $\tau_\mu\tau_\mu$ channel, the DY production of electron and

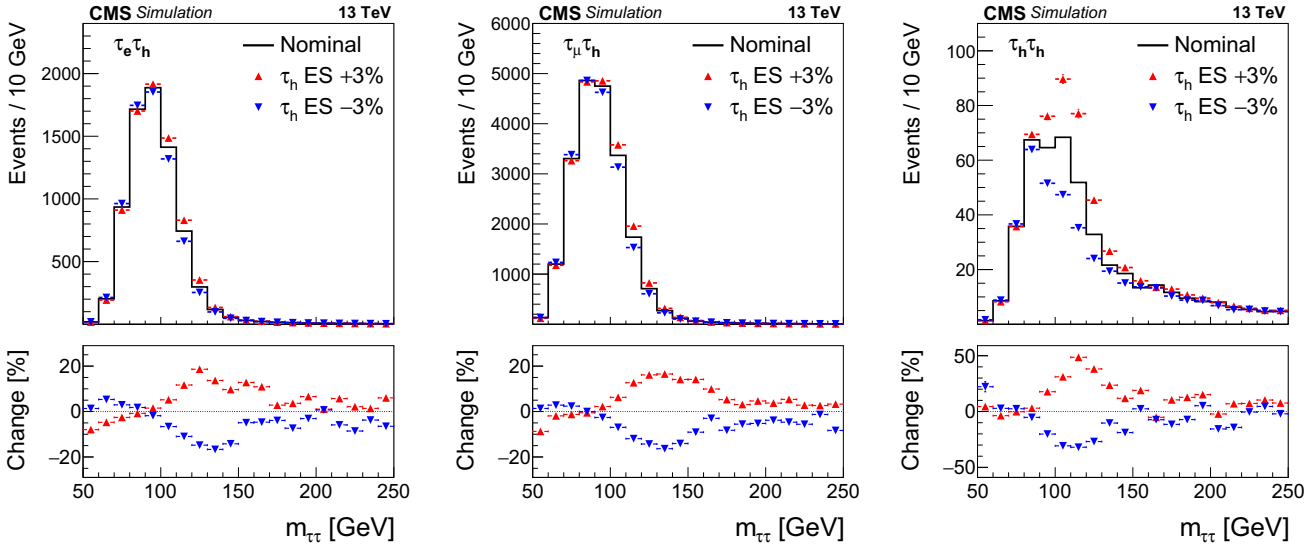

Fig. 7 Distributions expected in $m_{\tau\tau}$ for $Z/\gamma^* \rightarrow \tau\tau$ signal events in the (left) $\tau_e\tau_h$, (center) $\tau_\mu\tau_h$, and (right) $\tau_h\tau_h$ channels for the nominal value of the τ_h ES, and after implementing 3% systematic shift

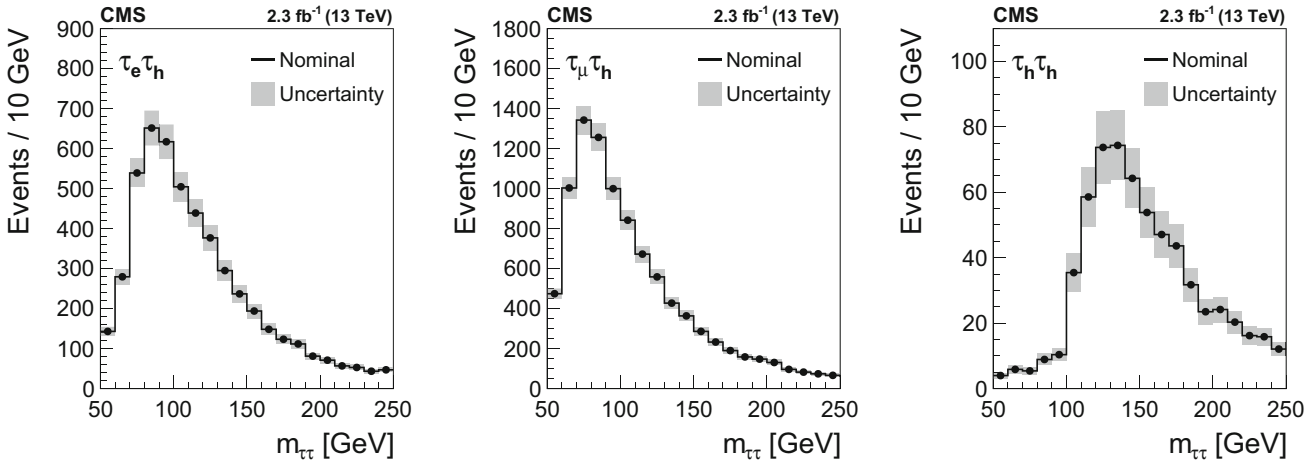

Fig. 8 Distributions in $m_{\tau\tau}$ expected for the background arising from quark or gluon jets misidentified as τ_h in the (left) $\tau_e\tau_h$, (center) $\tau_\mu\tau_h$, and (right) $\tau_h\tau_h$ channels, and the systematic uncertainty in the false-τ_h background estimate. The grey shaded band represents the quadratic sum of all systematic uncertainties related to the F_F method: uncertainties in the F_F measured in the multijet, W+jets, and $t\bar{t}$ DR; uncertainties in the relative fractions of multijet, W+jets, and $t\bar{t}$ backgrounds in the AR; and uncertainties in the non-closure corrections (described in Sect. 6.1)

muon pairs are relevant backgrounds in, respectively, the decay channels $\tau_e\tau_h$ and $\tau_\mu\tau_h$, because of the small but non-negligible rate at which electrons and muons are misidentified as τ_h. The probability for electrons and muons to pass the tight-electron or tight-muon removal criteria applied, respectively, in the $\tau_e\tau_h$ and $\tau_\mu\tau_h$ channels is measured in $Z/\gamma^* \rightarrow ee$ and in $Z/\gamma^* \rightarrow \mu\mu$ events. The misidentification rates depend on η. For electrons in the ECAL barrel and endcap regions, the misidentifications are at respective levels of 0.2 and 0.1%, with accuracies of 13 and 29% [75]. The misidentification rate for muons lies between less than one and several tenths of a percent, and is known to within an uncertainty of 30%. The contribution from W+jets background in the $\tau_e\tau_\mu$ and $\tau_\mu\tau_\mu$ channels is modelled using MC simulation, and is known to an accuracy of 15%. The production of SM Higgs bosons is assigned an uncertainty of 30%, reflecting the present experimental uncertainty in the $H \rightarrow \tau\tau$ rate measured at $\sqrt{s} = 13$ TeV [14].

The theoretical uncertainty in the product of signal acceptance and efficiency for the $Z/\gamma^* \rightarrow \tau\tau$ signal is $\approx 2\%$ in the $\tau_e\tau_h$, $\tau_\mu\tau_h$, $\tau_e\tau_\mu$, and $\tau_\mu\tau_\mu$ channels, and 6% in the $\tau_h\tau_h$ channel. The quoted uncertainties include the effect of missing higher-order terms in the perturbative expansion for the calculated cross section, estimated through indepen-

dent changes in the renormalization and factorization scales by factors of 2 and 1/2 relative to their nominal equal values [92,93], uncertainties in the NNPDF3.0 set of PDF, estimated following the recommendations given in Ref. [94], and the uncertainties in the modelling of parton showers (PS) and the underlying event (UE). The theoretical uncertainty is larger in the $\tau_h\tau_h$ channel, as the acceptance depends crucially on the modelling of the p_T distribution of the Z boson, which is also affected by the missing higher-order terms in the calculation.

The systematic uncertainties are summarized in Table 2. The table also quantifies the impact that each systematic uncertainty has on the measurement of the $Z/\gamma^* \to \tau\tau$ cross section, defined as the percent change in the measured cross section when individual sources are changed by one standard deviation relative to their nominal values. The impacts are computed for the values of nuisance parameters obtained in the ML fit used to extract the signal (described in Sect. 8).

The uncertainties in the integrated luminosity, in the cross section for DY production of electron and muon pairs, and in the electron, muon, and τ_h reconstruction and identification efficiencies have greatest impact on the results.

The impact of the uncertainty on the integrated luminosity amounts to 1.9%. This is smaller than the 2.3% uncertainty in the integrated luminosity measurement, because of correlations of the nuisance parameter representing the integrated luminosity with other nuisance parameters. When the integrated luminosity changes by 2.3%, the ML fit readjusts the nuisance parameters that represent the rates for background processes obtained from MC simulation, as well as identification and trigger efficiencies for e, μ, and τ_h, such that the measured $Z/\gamma^* \to \tau\tau$ cross section changes by only 1.9%. The uncertainty in the integrated luminosity is not constrained in the ML fit.

The impact of the uncertainty in the production rate of $Z/\gamma^* \to ee$ and $Z/\gamma^* \to \mu\mu$ background processes amounts to 1.8%. The impact is sizeable, because of the small statistical uncertainty in the $Z/\gamma^* \to \mu\mu$ background in the $\tau_\mu\tau_\mu$ channel, which, in the absence of uncertainties in the $Z/\gamma^* \to \mu\mu$ production rate, would constrain the efficiency for muon reconstruction and identification, as well as the integrated luminosity.

The impact of uncertainties in the efficiencies to reconstruct and identify electrons and muons amounts to 1.5 and 1.6%, respectively. Their impact is considerable, because these uncertainties are not reduced greatly in the ML fit, as they affect all channels, except the $\tau_h\tau_h$ channel, in a similar way.

The impact of the uncertainty in the efficiency to reconstruct and identify τ_h is of similar size, amounting to 1.5%, despite that the uncertainty in the τ_h ID efficiency is significantly larger than the uncertainties in the electron and muon ID efficiencies. This is because the simultaneous fit to the $m_{\tau\tau}$ distributions in all five channels reduces the uncertainties in the τ_h ID efficiency and the τ_h ES significantly, diminishing thereby the impact that these uncertainties have on the $Z/\gamma^* \to \tau\tau$ cross section. When the $Z/\gamma^* \to \tau\tau$ cross section is measured in the individual $\tau_e\tau_h$, $\tau_\mu\tau_h$, and $\tau_h\tau_h$ channels, the impact of the uncertainty on the τ_h ID efficiency increases to 6, 6, and 10%, respectively.

The uncertainty in τ_h ES becomes relevant for the $\tau_h\tau_h$ channel when the $Z/\gamma^* \to \tau\tau$ cross section is measured in this channel alone, and amounts to 9%. In the $\tau_e\tau_h$ and $\tau_\mu\tau_h$ channels, the impact of the τ_h ES uncertainty amounts to less than 1%, even when the $Z/\gamma^* \to \tau\tau$ cross section is measured just in these channels.

8 Signal extraction

The cross section $\sigma(pp \to Z/\gamma^*+X)\,\mathcal{B}(Z/\gamma^* \to \tau\tau)$ for DY production of τ pairs is obtained through a simultaneous ML fit to the observed $m_{\tau\tau}$ distributions in the five decay channels: $\tau_e\tau_h$, $\tau_\mu\tau_h$, $\tau_h\tau_h$, $\tau_e\tau_\mu$, and $\tau_\mu\tau_\mu$. The likelihood function $\mathcal{L}(\text{data}\,|\,\xi, \Theta)$ depends on the value of the cross section, denoted by the symbol ξ, which defines the parameter of interest (POI) in the fit, and it also depends on the values of nuisance parameters θ_k that represent the systematic uncertainties discussed in Sect. 7:

$$\mathcal{L}(\text{data}\,|\,\xi, \Theta) = \prod_i \mathcal{P}(n_i|\xi, \Theta) \prod_k \rho\left(\tilde{\theta}_k|\theta_k\right). \tag{7}$$

The index i refers to individual bins of the $m_{\tau\tau}$ distribution in each of the five final states. The set of all nuisance parameters θ_k is denoted by the symbol Θ. Correlations among decay channels as well as between the $Z/\gamma^* \to \tau\tau$ signal and background processes are taken into account through relationships among channels, processes, and nuisance parameters in the ML fit. The probability to observe n_i events in a given bin i, when $\nu_i(\xi, \Theta)$ events are expected in that bin is given by the Poisson distribution:

$$\mathcal{P}(n_i|\xi, \Theta) = \frac{(\nu_i(\xi, \Theta))^{n_i}}{n_i!} \exp\left(-\nu_i(\xi, \Theta)\right). \tag{8}$$

The number of events expected in each bin corresponds to the sum of the number of signal (ν_i^S) and background (ν_i^B) events: $\nu_i(\xi, \Theta) = \nu_i^S(\xi, \Theta) + \nu_i^B(\Theta)$. The estimate in the number of background events is obtained as described in Sect. 6. The number of signal events is proportional to ξ, with the coefficient of proportionality depending on the signal acceptance and on the signal selection efficiency, with both obtained from MC simulation.

The function $\rho\left(\tilde{\theta}_k|\theta_k\right)$ represents the probability to observe a value $\tilde{\theta}_k$ in an auxiliary measurement of the nui-

Table 2 Effect of experimental and theoretical uncertainties in the measurement of the $Z/\gamma^* \to \tau\tau$ cross section. The sources of systematic uncertainty are specified in the leftmost column, and apply to the processes given in the second column. The relative changes in the acceptance $\mathcal{A}$ for the $Z/\gamma^* \to \tau\tau$ signal, and in the yield from background processes that correspond to a one standard deviation change in a given source of uncertainty is given in the third column. The range in this column represents the range in signal acceptance or background yield across all decay channels and background processes. The impact that each change produces is quantified by its effect on the measured $Z/\gamma^* \to \tau\tau$ cross section, given in the rightmost column

Source	Applies to	Change in $\mathcal{A}$ or yield (%)	Impact (%)
Integrated luminosity	Simulated processes	2.3	1.9
Hadronic τ ID and trigger	Simulated processes	6–12	1.5
τ_h ES	Simulated processes	2–17	< 0.1
Rate of e misidentified as τ_h	$Z/\gamma^* \to$ ee	13–29	0.4
Rate of μ misidentified as τ_h	$Z/\gamma^* \to \mu\mu$	30	0.2
Electron ID and trigger	Simulated processes	2	1.5
e ES	Simulated processes	< 1	0.2
Muon ID and trigger	Simulated processes	2	1.6
μ ES	Simulated processes	< 1	< 0.1
E_T^{miss} response and resolution	Simulated processes	1–10	0.2
Norm. $Z/\gamma^* \to$ ee, $\mu\mu$	$Z/\gamma^* \to$ ee, $\mu\mu$	Unconstrained	1.8
Norm. and shape of false τ_h	$\tau_e\tau_h$, $\tau_\mu\tau_h$, $\tau_h\tau_h$ channels	6–16	< 0.1
Norm. and shape of multijet	$\tau_e\tau_\mu$, $\tau_\mu\tau_\mu$ channels	20	0.2
Norm. $t\bar{t}$	$t\bar{t}$	7	1.0
Shape $t\bar{t}$	$t\bar{t}$	1–6	< 0.1
Norm. SM H	SM H	30	< 0.1
Norm. single top quark	Single top quark	15	< 0.1
Norm. diboson	Diboson	15	0.2
Norm. W+jets	W+jets	15	< 0.1
PDF	Signal	1	1.0
Scale dependence	Signal	< 6	0.5
UE and PS	Signal	1	1.0

sance parameter, given that the true value is θ_k. The nuisance parameters are treated via the frequentist paradigm, as described in Refs. [95,96]. Systematic uncertainties that affect only the normalization, but not the distribution in $m_{\tau\tau}$, are represented by the Gamma function if they are statistical in origin, e.g. corresponding to the number of events observed in a control region, and otherwise by log-normal probability density functions. Systematic uncertainties that affect the distribution in $m_{\tau\tau}$ are incorporated into the ML fit via the technique detailed in Ref. [97], and represented by Gaussian probability density functions. Nuisance parameters representing systematic uncertainties of the latter type can also affect the normalization of the $Z/\gamma^* \to \tau\tau$ signal or of its backgrounds. The nuisance parameters corresponding to the cross sections for DY production of electron and muon pairs are left unconstrained in the fit.

The best fit value $\hat{\xi}$ of the POI is the value that maximizes the likelihood $\mathcal{L}(\text{data} \,|\, \xi, \Theta)$ in Eq. (7). A 68% confidence interval (CI) on the POI is obtained using the profile likelihood ratio (PLR) [95,96,98]:

$$\lambda(\xi) = \frac{\mathcal{L}\left(\text{data} \,|\, \xi, \hat{\Theta}_\xi\right)}{\mathcal{L}\left(\text{data} \,|\, \hat{\xi}, \hat{\Theta}\right)}. \tag{9}$$

The symbol $\hat{\Theta}_\xi$ denotes the values of nuisance parameters that maximize the likelihood for a given value of ξ. The combination of $\hat{\xi}$ and $\hat{\Theta}$ correspond to the values of ξ and Θ for which the likelihood function reaches its maximum. The 68% CI is defined by the values of ξ for which $-2\ln\lambda(\xi)$ increases by one unit relative to its minimum. To quantify the effects from individual statistical uncertainties, the uncertainty in the integrated luminosity, and other systematic uncertainties, we ignore some single source of uncertainties at a time, and recompute the 68% CI. The nuisance parameters θ_k corresponding to uncertainties that are ignored are fixed at the values $\hat{\theta}_k$ that yield the best fit to the data. The square root of the quadratic difference between the CI, computed for all sources of uncertainties in the fit, and for the case that some given source is ignored, reflects the estimate of the uncertainty in the POI resulting from a single source. The procedure is illustrated in Fig. 9 for the combined fit of

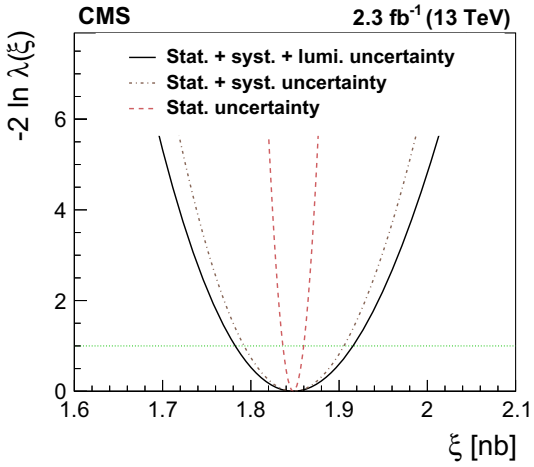

Fig. 9 Dependence of $-2\ln\lambda(\xi)$ on the cross section ξ for DY production of τ pairs. The PLR is computed for the simultaneous ML fit to the observed $m_{\tau\tau}$ distributions in the $\tau_e\tau_h$, $\tau_\mu\tau_h$, $\tau_h\tau_h$, $\tau_e\tau_\mu$, and $\tau_\mu\tau_\mu$ channels. The dashed, dash-dotted, and solid curves correspond to situations when just the statistical uncertainties are used in the fit, when the uncertainty in integrated luminosity is also included, and when all uncertainties are included in the fit. The values of nuisance parameters, corresponding to uncertainties that are ignored, are fixed at the values that yield the best fit to the data. The horizontal line represents the value of $-2\ln\lambda(\xi)$ that is used to determine the 68% CI on ξ

Table 4 Cross section $\sigma(pp \to Z/\gamma^*+X)\,\mathcal{B}(Z/\gamma^* \to \tau\tau)$ measured in individual final states

Channel	$\sigma(pp \to Z/\gamma^*+X)\,\mathcal{B}(Z/\gamma^* \to \tau\tau)$ [pb]
$\tau_e\tau_h$	1799 ± 29 (stat) ± 120 (syst) ± 34 (lumi)
$\tau_\mu\tau_h$	1784 ± 17 (stat) ± 117 (syst) ± 34 (lumi)
$\tau_h\tau_h$	1477 ± 137 (stat) ± 270 (syst) ± 30 (lumi)
$\tau_e\tau_\mu$	1851 ± 19 (stat) ± 58 (syst) ± 34 (lumi)
$\tau_\mu\tau_\mu$	1967 ± 121 (stat) ± 92 (syst) ± 37 (lumi)

all five final states. Correlations among different sources of uncertainty are estimated through this procedure.

The cross section for DY production of τ pairs is quoted within the mass window $60 < m_{\tau\tau}^{\text{true}} < 120$ GeV. The contribution from $Z/\gamma^* \to \tau\tau$ events that pass the selection criteria described in Sect. 5, but have a mass outside of this window is at the level of a few percent in the $\tau_e\tau_h$, $\tau_\mu\tau_h$, $\tau_e\tau_\mu$, and $\tau_\mu\tau_\mu$ channels. In the $\tau_h\tau_h$ channel, this contribution from outside of the mass window is $\approx 40\%$, the reason for this being so large is the high p_T threshold on the τ_h candidates required in the trigger. The $Z/\gamma^* \to \tau\tau$ events that have two τ_h with $p_T > 40$ GeV contain either a Z boson of high p_T or a τ lepton pair above the mass of the Z boson.

Table 3 Yields expected in $Z/\gamma^* \to \tau\tau$ signal events and backgrounds in the $\tau_e\tau_h$, $\tau_\mu\tau_h$, $\tau_h\tau_h$, $\tau_e\tau_\mu$, and $\tau_\mu\tau_\mu$ channels, obtained from the ML fit described in Sect. 8. The uncertainties are rounded to two significant digits, except when they are < 10, in which case they are rounded to one significant digit, and the event yields are rounded to match the precision in the uncertainties. The analysed data corresponds to an integrated luminosity of 2.3 fb^{-1}

Process	$\tau_e\tau_h$	$\tau_\mu\tau_h$	$\tau_h\tau_h$
$Z/\gamma^* \to \tau\tau$	7160 ± 130	$20{,}020 \pm 220$	415 ± 32
Jets misidentified as τ_h	5690 ± 160	$10{,}550 \pm 220$	770 ± 49
$t\bar{t}$	354 ± 26	639 ± 47	17 ± 2
$Z/\gamma^* \to$ ee, $\mu\mu$ (e or μ misidentified as τ_h)	718 ± 96	840 ± 130	–
Electroweak	93 ± 13	183 ± 28	40 ± 6
SM H	49 ± 11	103 ± 23	13 ± 3
Total expected background	6900 ± 130	$12{,}310 \pm 180$	841 ± 46
Total SM expectation	$14{,}060 \pm 120$	$32{,}340 \pm 180$	1255 ± 40
Observed data	14,063	32,350	1255

Process	$\tau_e\tau_\mu$	$\tau_\mu\tau_\mu$
$Z/\gamma^* \to \tau\tau$	$13{,}600 \pm 220$	2067 ± 34
Multijet	4620 ± 240	710 ± 110
$Z/\gamma^* \to \mu\mu$	—	8010 ± 170
$t\bar{t}$	3500 ± 140	1239 ± 79
Electroweak	1146 ± 98	293 ± 30
SM H	57 ± 12	18 ± 4
Total expected background	9300 ± 210	$10{,}270 \pm 120$
Total SM expectation	$22{,}930 \pm 130$	$12{,}340 \pm 120$
Observed data	22,930	12,327

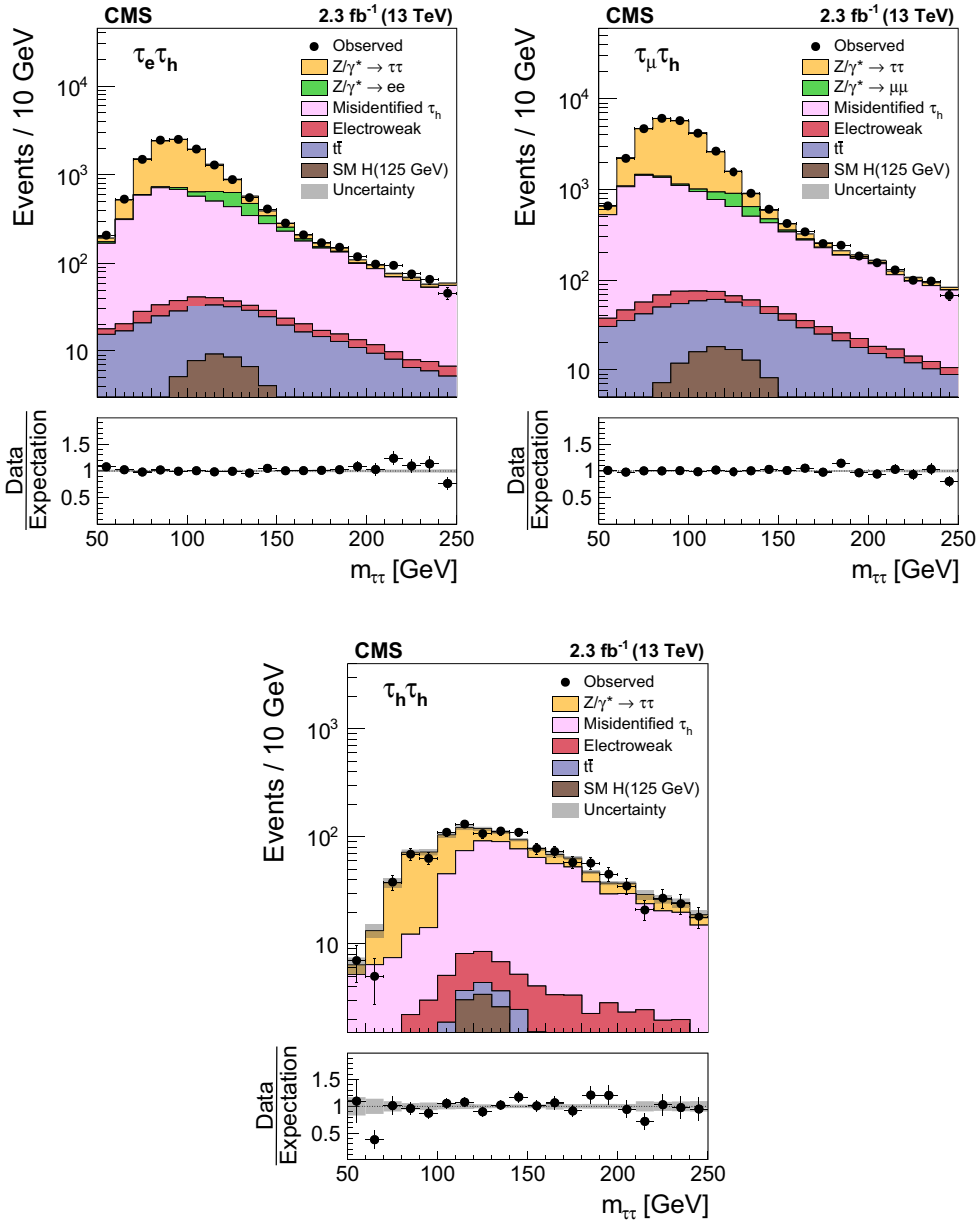

Fig. 10 Distributions in $m_{\tau\tau}$ for events selected in the (upper left) $\tau_e\tau_h$, (upper right) $\tau_\mu\tau_h$, and (lower) $\tau_h\tau_h$ channels. Signal and background contributions are shown for values of nuisance parameters obtained in the ML fit to the data

Only a small fraction of signal events pass either of these two conditions, which leads to the smallest event yield from the $Z/\gamma^* \to \tau\tau$ signal in the $\tau_h\tau_h$ channel (as shown in Table 3), and to the largest fraction of signal events containing a τ lepton pair of mass outside of the $60 < m_{\tau\tau}^{\text{true}} < 120\,\text{GeV}$ window.

The PLR depends on the τ_h ID efficiency and on the τ_h ES through its dependence on the corresponding two nuisance parameters. The τ_h ID efficiency and τ_h ES are determined by promoting these nuisance parameters to the role of POI. The cross section for DY production of τ pairs, the τ_h ID efficiency, and the τ_h ES are left unconstrained in the fit, and the PLR is minimized as a function of all three parameters.

9 Results

The yields expected in $Z/\gamma^* \to \tau\tau$ signal and in background contributions from the ML fit to the $m_{\tau\tau}$ distributions in the different decay channels are given in Table 3. The cross sections are displayed in Table 4, and the distributions in $m_{\tau\tau}$ for the selected events are shown in Figs. 10 and 11.

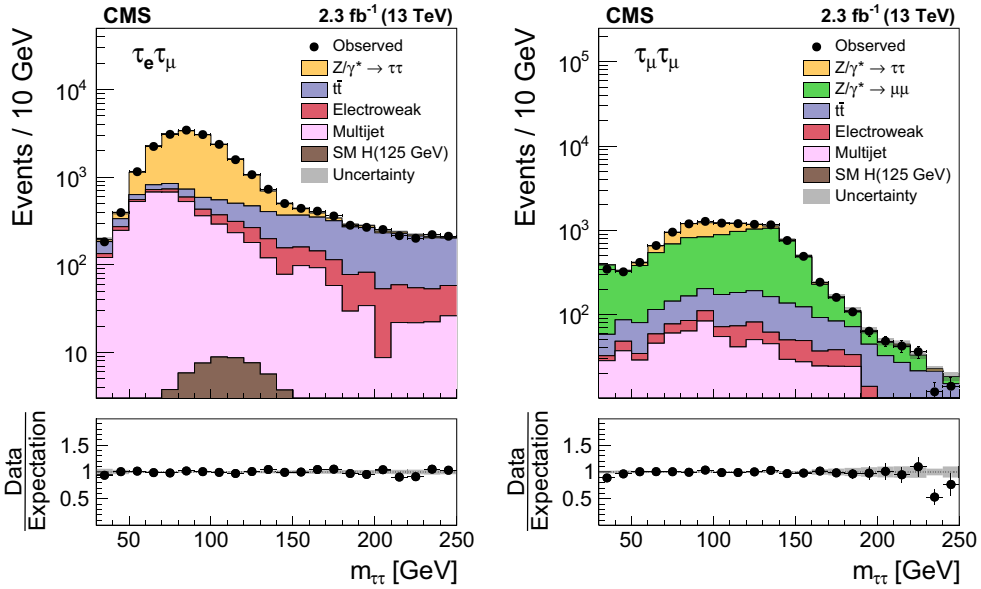

Fig. 11 Distributions in $m_{\tau\tau}$ for events selected in the (left) $\tau_e\tau_\mu$ and (right) $\tau_\mu\tau_\mu$ channels. Signal and background contributions are shown for the values of nuisance parameters obtained in the ML fit to the data

The total uncertainty in the cross section is decomposed into statistical contributions, uncertainty in the integrated luminosity of the data, and other systematic uncertainties, as described in Sect. 8. The measured values are compatible with each other. The largest deviation, amounting to a little more than one standard deviation, is observed in the $\tau_h\tau_h$ channel. A deviation of this magnitude is expected. We proceed to a simultaneous fit of the $m_{\tau\tau}$ distributions in the five final states. The value of the cross section obtained from the combined fit is:

$$\sigma(\mathrm{pp} \to \mathrm{Z}/\gamma^*\mathrm{+X})\,\mathcal{B}(\mathrm{Z}/\gamma^* \to \tau\tau) = 1848 \pm 12\,(\mathrm{stat}) \pm 57\,(\mathrm{syst}) \pm 35\,(\mathrm{lumi})\ \mathrm{pb}. \quad (10)$$

The result is compatible with the prediction of 1845^{+12}_{-6} (scale) $\pm$ 33 (PDF) pb, computed at NNLO accuracy [60] using the NNPDF3.0 PDF. The results are illustrated in Fig. 12. The inner and outer error bars represent, respectively, the statistical uncertainties, and the quadratic sum of the uncertainties in the statistical, systematic, and integrated-luminosity components. The uncertainty in $\sigma(\mathrm{pp} \to \mathrm{Z}/\gamma^*\mathrm{+X})\,\mathcal{B}(\mathrm{Z}/\gamma^* \to \tau\tau)$ arising from the uncertainty in the integrated luminosity is smaller than the uncertainty in the integrated luminosity, for the reasons discussed in Sect. 7.

As a side note, the values of the nuisance parameters that correspond to the cross sections in the $\mathrm{Z}/\gamma^* \to$ ee and $\mathrm{Z}/\gamma^* \to \mu\mu$ backgrounds, obtained from the simultaneous fit to the $m_{\tau\tau}$ distributions in the five final states in data, are also compatible with the expected values.

Two-dimensional projections of $-2\ln\lambda(\xi)$, obtained when the τ_h ID efficiency and τ_h ES are left unconstrained

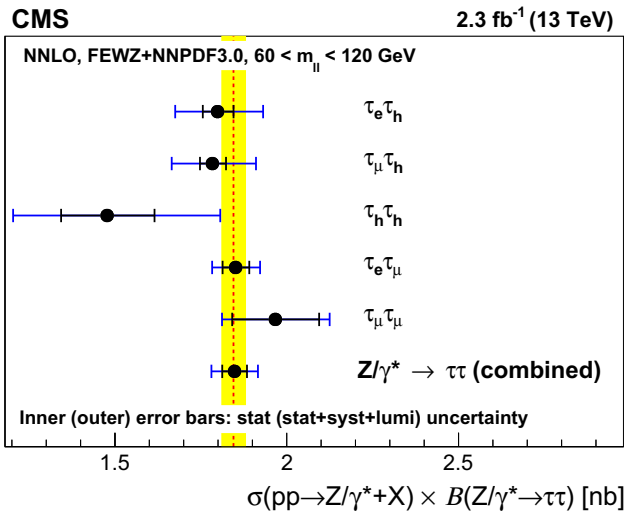

Fig. 12 The inclusive cross section $\sigma(\mathrm{pp} \to \mathrm{Z}/\gamma^*\mathrm{+X})\,\mathcal{B}(\mathrm{Z}/\gamma^* \to \tau\tau)$ measured in individual channels, and in the combination of all final states, compared to the theoretical prediction [60]

in the fit, are shown in Fig. 13. Measured values of the τ_h ID efficiency and of τ_h ES are quoted as scale factors (SF) relative to their MC expectation. The values of $\sigma(\mathrm{pp} \to \mathrm{Z}/\gamma^*\mathrm{+X})\,\mathcal{B}(\mathrm{Z}/\gamma^* \to \tau\tau)$, τ_h ID efficiency, and τ_h ES that minimize $-2\ln\lambda(\xi)$, yielding the best fit to the data, are indicated by a cross. Contours for which $-2\ln\lambda(\xi)$ exceeds its minimum value by 2.30 and 6.18 units, corresponding to coverage probabilities of 68 and 95% in the two-dimensional parameter plane, are also shown. The 68% CIs for the τ_h ID efficiency and τ_h ES are obtained as the values of the respective parameter for which $-2\ln\lambda(\xi)$ increases

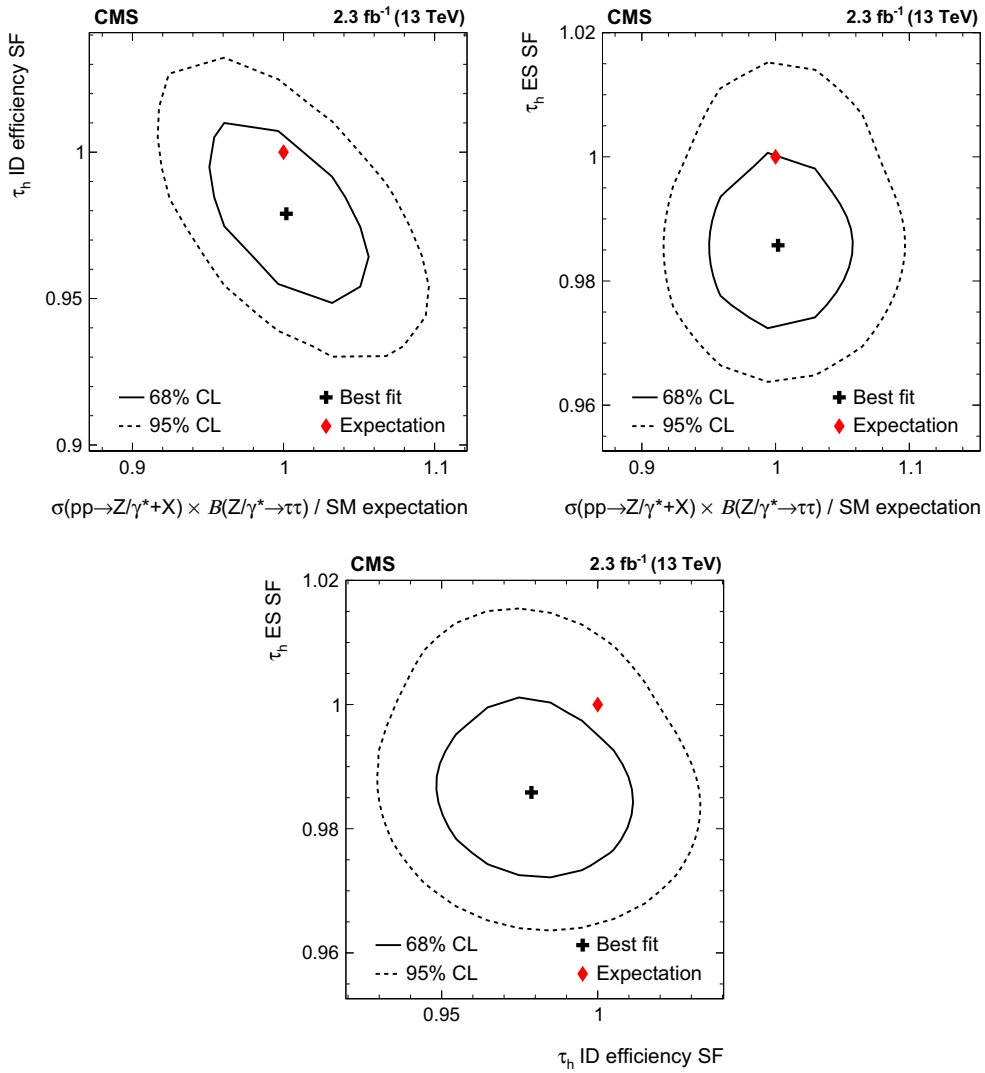

Fig. 13 Likelihood contours for the joint parameter estimation of (upper left) $\sigma(\mathrm{pp} \to \mathrm{Z}/\gamma^{*}\mathrm{+X})\,\mathcal{B}(\mathrm{Z}/\gamma^{*} \to \tau\tau)$ and the τ_h ID efficiency, (upper right) $\sigma(\mathrm{pp} \to \mathrm{Z}/\gamma^{*}\mathrm{+X})\,\mathcal{B}(\mathrm{Z}/\gamma^{*} \to \tau\tau)$ and τ_h ES, and (lower) the τ_h ES and the τ_h ID efficiency, at 68 and 95% confidence level (CL). The values of the τ_h ID efficiency and of τ_h ES are quoted in terms of scale factors (SF) relative to their standard model, MC expectation

by one unit relative to its minimum. The measured SF for the τ_h ID efficiency and for τ_h ES amount to 0.979 ± 0.022 and 0.986 ± 0.009, respectively. Both SF are compatible with unity, indicating that the measured values of the τ_h ID efficiency and of the τ_h ES are in agreement with the MC expectation. The expected τ_h ID efficiency in the LHC data is documented in Ref. [75].

10 Summary

The cross section for inclusive Drell–Yan production of τ pairs has been measured using pp collisions recorded by the CMS experiment at $\sqrt{s} = 13$ TeV at the LHC. The analysed data correspond to an integrated luminosity of 2.3 fb^{-1}. The signal yield was determined in a global fit to the mass distributions in five $\tau\tau$ decay channels: $\tau_\mathrm{e}\tau_\mathrm{h}$, $\tau_\mu\tau_\mathrm{h}$, $\tau_\mathrm{h}\tau_\mathrm{h}$, $\tau_\mathrm{e}\tau_\mu$, and $\tau_\mu\tau_\mu$. The measured cross section times branching fraction $\sigma(\mathrm{pp} \to \mathrm{Z}/\gamma^{*}\mathrm{+X})\,\mathcal{B}(\mathrm{Z}/\gamma^{*} \to \tau\tau) = 1848 \pm 12\,(\mathrm{stat}) \pm 57\,(\mathrm{syst}) \pm 35\,(\mathrm{lumi})$ pb is in agreement with the standard model expectation, computed at next-to-next-to-leading order accuracy in perturbation theory. As a byproduct of the global fit, the efficiency for reconstructing and identifying the decays of τ leptons to hadrons ($\tau \to \mathrm{hadrons} + \nu_\tau$), as well as the τ_h energy scale, have been determined. The results from data agree with Monte Carlo simulation within the uncertainties of the measurement, amounting to 2.2% relative uncertainty in the τ_h identification efficiency, and 0.9% in the energy scale.

Acknowledgements We congratulate our colleagues in the CERN accelerator departments for the excellent performance of the LHC and thank the technical and administrative staffs at CERN and at other CMS institutes for their contributions to the success of the CMS effort. In addition, we gratefully acknowledge the computing centres and personnel of the Worldwide LHC Computing Grid for delivering so effectively the computing infrastructure essential to our analyses. Finally, we acknowledge the enduring support for the construction and operation of the LHC and the CMS detector provided by the following funding agencies: the Austrian Federal Ministry of Science, Research and Economy and the Austrian Science Fund; the Belgian Fonds de la Recherche Scientifique, and Fonds voor Wetenschappelijk Onderzoek; the Brazilian Funding Agencies (CNPq, CAPES, FAPERJ, and FAPESP); the Bulgarian Ministry of Education and Science; CERN; the Chinese Academy of Sciences, Ministry of Science and Technology, and National Natural Science Foundation of China; the Colombian Funding Agency (COLCIENCIAS); the Croatian Ministry of Science, Education and Sport, and the Croatian Science Foundation; the Research Promotion Foundation, Cyprus; the Secretariat for Higher Education, Science, Technology and Innovation, Ecuador; the Ministry of Education and Research, Estonian Research Council via IUT23-4 and IUT23-6 and European Regional Development Fund, Estonia; the Academy of Finland, Finnish Ministry of Education and Culture, and Helsinki Institute of Physics; the Institut National de Physique Nucléaire et de Physique des Particules/CNRS, and Commissariat à l'Énergie Atomique et aux Énergies Alternatives/CEA, France; the Bundesministerium für Bildung und Forschung, Deutsche Forschungsgemeinschaft, and Helmholtz-Gemeinschaft Deutscher Forschungszentren, Germany; the General Secretariat for Research and Technology, Greece; the National Scientific Research Foundation, and National Innovation Office, Hungary; the Department of Atomic Energy and the Department of Science and Technology, India; the Institute for Studies in Theoretical Physics and Mathematics, Iran; the Science Foundation, Ireland; the Istituto Nazionale di Fisica Nucleare, Italy; the Ministry of Science, ICT and Future Planning, and National Research Foundation (NRF), Republic of Korea; the Lithuanian Academy of Sciences; the Ministry of Education, and University of Malaya (Malaysia); the Mexican Funding Agencies (BUAP, CINVESTAV, CONACYT, LNS, SEP, and UASLP-FAI); the Ministry of Business, Innovation and Employment, New Zealand; the Pakistan Atomic Energy Commission; the Ministry of Science and Higher Education and the National Science Centre, Poland; the Fundação para a Ciência e a Tecnologia, Portugal; JINR, Dubna; the Ministry of Education and Science of the Russian Federation, the Federal Agency of Atomic Energy of the Russian Federation, Russian Academy of Sciences, the Russian Foundation for Basic Research and the Russian Competitiveness Program of NRNU "MEPhI"; the Ministry of Education, Science and Technological Development of Serbia; the Secretaría de Estado de Investigación, Desarrollo e Innovación, Programa Consolider-Ingenio 2010, Plan de Ciencia, Tecnología e Innovación 2013–2017 del Principado de Asturias and Fondo Europeo de Desarrollo Regional, Spain; the Swiss Funding Agencies (ETH Board, ETH Zurich, PSI, SNF, UniZH, Canton Zurich, and SER); the Ministry of Science and Technology, Taipei; the Thailand Center of Excellence in Physics, the Institute for the Promotion of Teaching Science and Technology of Thailand, Special Task Force for Activating Research and the National Science and Technology Development Agency of Thailand; the Scientific and Technical Research Council of Turkey, and Turkish Atomic Energy Authority; the National Academy of Sciences of Ukraine, and State Fund for Fundamental Researches, Ukraine; the Science and Technology Facilities Council, UK; the US Department of Energy, and the US National Science Foundation. Individuals have received support from the Marie-Curie programme and the European Research Council and Horizon 2020 Grant, Contract no. 675440 (European Union); the Leventis Foundation; the A. P. Sloan Foundation; the Alexander von Humboldt Foundation; the Belgian Federal Science Policy Office; the Fonds pour la Formation à la Recherche dans l'Industrie et dans l'Agriculture (FRIA-Belgium); the Agentschap voor Innovatie door Wetenschap en Technologie (IWT-Belgium); the Ministry of Education, Youth and Sports (MEYS) of the Czech Republic; the Council of Scientific and Industrial Research, India; the HOMING PLUS programme of the Foundation for Polish Science, cofinanced from European Union, Regional Development Fund, the Mobility Plus programme of the Ministry of Science and Higher Education, the National Science Center (Poland), contracts Harmonia 2014/14/M/ST2/00428, Opus 2014/13/B/ST2/02543, 2014/15/B/ST2/03998, and 2015/19/B/ST2/02861, Sonata-bis 2012/07/E/ST2/01406; the National Priorities Research Program by Qatar National Research Fund; the Programa Severo Ochoa del Principado de Asturias; the Thalis and Aristeia programmes cofinanced by EU-ESF and the Greek NSRF; the Rachadapisek Sompot Fund for Postdoctoral Fellowship, Chulalongkorn University and the Chulalongkorn Academic into Its 2nd Century Project Advancement Project (Thailand); the Welch Foundation, contract C-1845; and the Weston Havens Foundation (USA).

A Validation of background model in event categories

The validity of the background estimation described in Sect. 6 is checked in event categories that are relevant for the SM $H \to \tau\tau$ analysis as well as in searches for new physics.

Event categories based on jet multiplicity, p_T of the τ lepton pair, and on the multiplicity of b jets are defined by the conditions given in Table 5.

The transverse momentum of the Z boson (p_T^Z) is reconstructed by adding the momentum vectors from the visible τ decay products and the reconstructed $\vec{p}_T^{\,\text{miss}}$ in the transverse plane. The observables m_{jj} and $\Delta\eta_{jj}$ are used to select signal events produced through the fusion of virtual vector bosons (VBF) in the SM $H \to \tau\tau$ analysis, and refer, respectively, to the mass and to the separation in pseudorapidity of the two jets of highest p_T in events containing two or more jets.

Background contributions arising from $Z/\gamma^* \to ee$, $Z/\gamma^* \to \mu\mu$, W+jets, $t\bar{t}$, single top quark, and diboson production to the event categories defined in Table 5 in the $\tau_e\tau_h$, $\tau_\mu\tau_h$, $\tau_h\tau_h$, and $\tau_e\tau_\mu$ channels are estimated as described above. The fractions R_p of multijet, W+jets, DY, and $t\bar{t}$ backgrounds used in Eq. (6) are calculated separately for each of the event categories.

The contribution of $Z/\gamma^* \to \tau\tau$ is determined from data, using $Z/\gamma^* \to \mu\mu$ events. Events passing the single-muon trigger are selected by the presence of two muons of opposite charge passing tight identification and isolation criteria. At least one of the muons is required to have $p_T > 20\,\text{GeV}$ and $|\eta| < 2.1$, while the other muon is required to satisfy the conditions $p_T > 10\,\text{GeV}$ and $|\eta| < 2.4$. The number

Table 5 Event categories used to study the modelling of backgrounds. Similar categories have been used in previous $H \to \tau\tau$ analyses at the LHC

Category	Selection
0-jet	No jets[1] and no b jets[2]
1-jet, low Z boson p_T	At least one jet[1], no b jets[2], $p_T^Z < 50$ GeV, excluding events selected in 2-jet VBF category
1-jet, medium Z boson p_T	At least one jet[1], no b jets[2], $50 < p_T^Z < 100$ GeV, excluding events selected in 2-jet VBF category
1-jet, high Z boson p_T	At least one jet[1], no b jets[2], $p_T^Z > 100$ GeV, excluding events selected in 2-jet VBF category
2-jet VBF	At least one pair of jets[1] satisfying $m_{jj} > 500$ GeV and $\Delta\eta_{jj} > 3.5$, no b jets[2]
1 b jet	Exactly one b jet[2]
2 b jet	Exactly two b jets[2]

[1] With $p_T > 30$ GeV and $|\eta| < 4.7$
[2] With $p_T > 20$ GeV, $|\eta| < 2.4$, and identified by the CSV algorithm as originating from the hadronization of b quarks

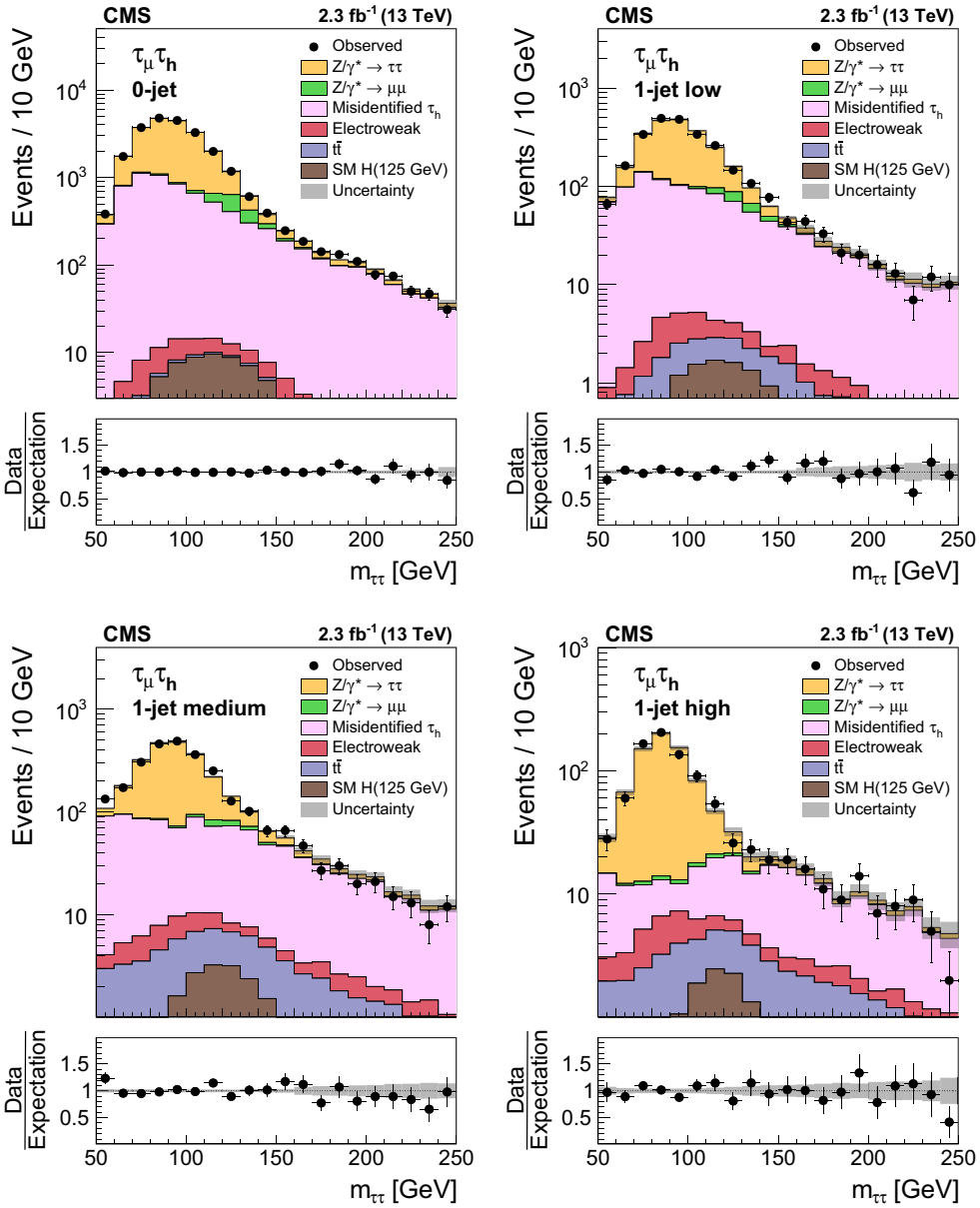

Fig. 14 Distributions in $m_{\tau\tau}$ for different categories in the $\tau_\mu\tau_h$ channel: (upper left) 0-jet, (upper right) 1-jet low, (lower left) medium, and (lower right) high Z boson p_T

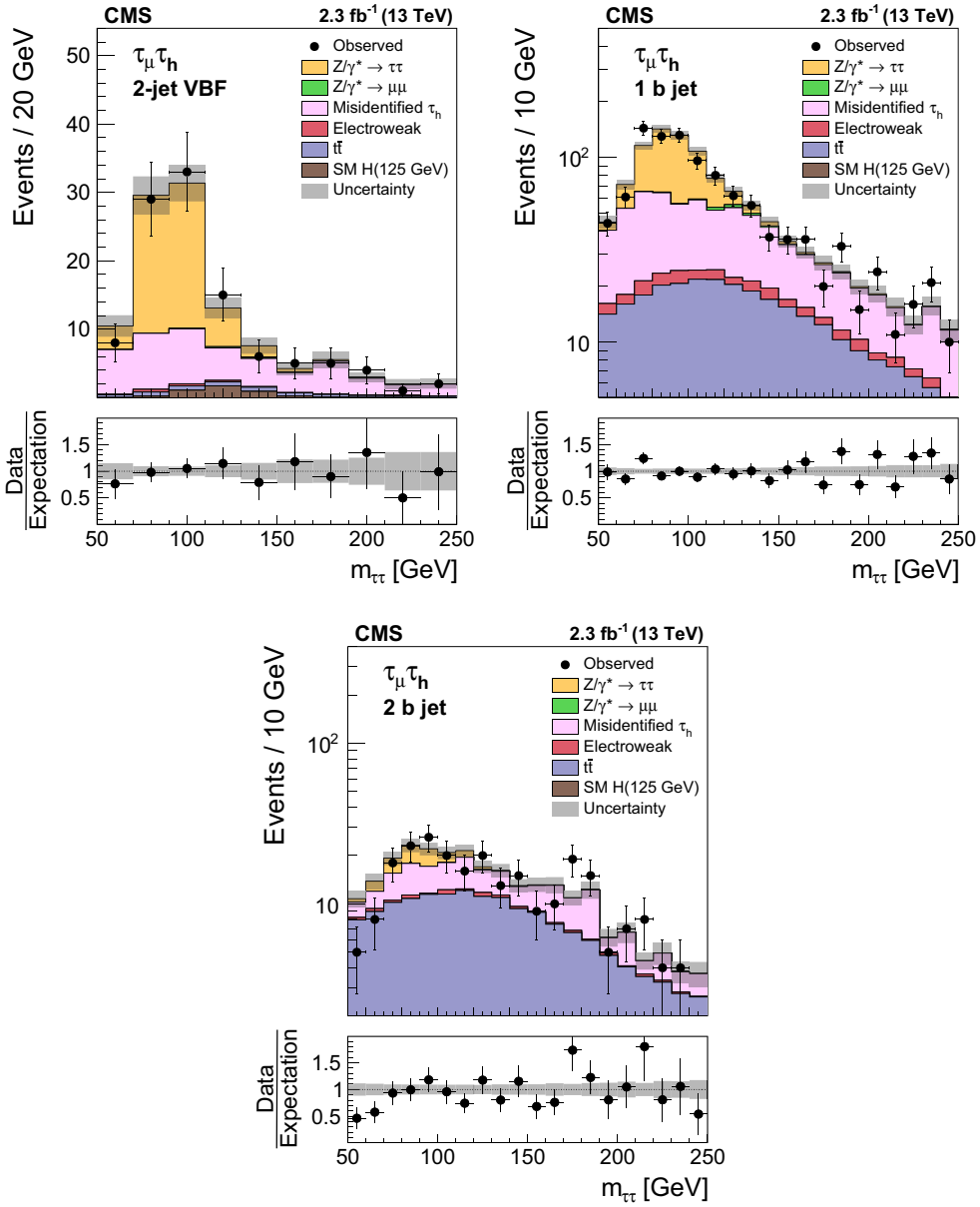

Fig. 15 Distributions in $m_{\tau\tau}$ for different categories in the $\tau_\mu\tau_h$ channel: (upper) 2-jet VBF, (lower left) 1 b jet, and (lower right) 2 b jet

of $Z/\gamma^* \to \mu\mu$ candidate events selected in the different categories in data is compared to the MC expectation for $Z/\gamma^* \to \mu\mu$ production, and their ratio is used as a scale factor to correct the MC expectation for the $Z/\gamma^* \to \tau\tau$ event yield in that category. The expected contribution of background processes, obtained from MC simulation, is subtracted from the data before taking the ratio. The selection criteria applied on muon p_T and η in $Z/\gamma^* \to \mu\mu$, and on p_T and η of the visible τ decay products in $Z/\gamma^* \to \tau\tau$ events are known to cause a bias in the p_T^Z distribution. The latter is correlated with the multiplicity of jets. The bias must be corrected, as its magnitude is very different for $Z/\gamma^* \to \mu\mu$ and $Z/\gamma^* \to \tau\tau$ events. The bias is emulated by replacing the muons reconstructed in $Z/\gamma^* \to \mu\mu$ candidate events with generator-level τ leptons. The τ leptons are decayed using TAUOLA++ 1.1.4 [99,100], and effects of τ lepton polarization in the decays are modelled through weights computed with the TAUSPINNER [101] program. A sample of 1000 random τ lepton decays is generated for each $Z/\gamma^* \to \mu\mu$ candidate event, and the weights computed in TAUSPINNER are recorded for each decay. The ratio of the sum of the weights for decays in which the visible products of both τ leptons pass selection criteria on p_T and η, to the sum of all weights computed for the 1000 decays, is applied as event weight to the $Z/\gamma^* \to \mu\mu$ candidate, which corrects for the difference in bias of p_T^Z caused by selection criteria on between

$Z/\gamma^* \to \mu\mu$ and $Z/\gamma^* \to \tau\tau$ events. The procedure is validated through MC simulation.

The contributions of background processes that are modelled in the MC simulation to the different categories are affected by uncertainties in the jet energy scale and resolution. The energy scale of jets is measured using the p_T balance of jets with Z bosons and photons in $Z/\gamma^* \to ee$ and $Z/\gamma^* \to \mu\mu$ and γ+jets events and the p_T balance between jets in dijet events as described in Ref. [79]. The uncertainty in the jet energy scale is a few percent and depends on p_T and η. The impact of jet energy scale and resolution uncertainties on the yields of background processes is evaluated by varying the jet energy scale and resolution within their uncertainties, redetermining the multiplicity of jets and b jets, and reapplying the event categorization conditions given in Table 5.

Distributions in $m_{\tau\tau}$ for events selected in different event categories are shown for the $\tau_\mu\tau_h$ channel in Figs. 14 and 15. The corresponding distributions for events selected in the $\tau_e\tau_h$, $\tau_h\tau_h$, $\tau_e\tau_\mu$, and $\tau_\mu\tau_\mu$ channels are published as supplemental material.

The distributions expected for the $Z/\gamma^* \to \tau\tau$ signal and for backgrounds are shown for the values of nuisance parameters obtained from the ML fit described in Sect. 8. The ML fit is performed independently for each category. The $m_{\tau\tau}$ distributions are shown within the range $50 < m_{\tau\tau} < 250$ GeV, indicating good agreement with background expectations over that mass range. A similar level of agreement between the data and the background prediction is observed in the $\tau_e\tau_h$, $\tau_h\tau_h$, and $\tau_\mu\tau_\mu$ channels.

The agreement confirms the reliability of the F_F method to estimate the reducible backgrounds in the $\tau_e\tau_h$, $\tau_\mu\tau_h$, and $\tau_h\tau_h$ channels in future $H \to \tau\tau$ analyses. It also validates the fact that the $Z/\gamma^* \to \tau\tau$ contribution to event categories, based on jet and b jet multiplicities, and on the pT of the τ lepton pair, can be modelled using $Z/\gamma^* \to \mu\mu$ data, without the so-called "embedding" technique [43,102] used previously to model the $Z/\gamma^* \to \tau\tau$ background in $H \to \tau\tau$ analyses of ATLAS and CMS.

References

1. ATLAS Collaboration, Observation of a new particle in the search for the Standard Model Higgs boson with the ATLAS detector at the LHC. Phys. Lett. B **716**, 1 (2012). https://doi.org/10.1016/j.physletb.2012.08.020. arXiv:1207.7214
2. CMS Collaboration, Observation of a new boson at a mass of 125 GeV with the CMS experiment at the LHC. Phys. Lett. B **716**, 30 (2012). https://doi.org/10.1016/j.physletb.2012.08.021. arXiv:1207.7235
3. CMS Collaboration, Observation of a new boson with mass near 125 GeV in pp collisions at $\sqrt{s} = 7$ and 8 TeV. JHEP **06**, 081 (2013). https://doi.org/10.1007/JHEP06(2013)081. arXiv:1303.4571
4. ATLAS and CMS Collaborations, Measurements of the Higgs boson production and decay rates and constraints on its couplings from a combined ATLAS and CMS analysis of the LHC pp collision data at $\sqrt{s} = 7$ and 8 TeV. JHEP **08**, 045 (2016). https://doi.org/10.1007/JHEP08(2016)045. arXiv:1606.02266
5. CMS Collaboration, Search for a light charged Higgs boson in top quark decays in pp collisions at $\sqrt{s} = 7$ TeV. JHEP **07**, 143 (2012). https://doi.org/10.1007/JHEP07(2012)143. arXiv:1205.5736
6. CMS Collaboration, Search for a charged Higgs boson in pp collisions at $\sqrt{s} = 8$ TeV. JHEP **11**, 018 (2015). https://doi.org/10.1007/JHEP11(2015)018. arXiv:1508.07774
7. CMS Collaboration, A search for a doubly-charged Higgs boson in pp collisions at $\sqrt{s} = 7$ TeV. Eur. Phys. J. C **72**, 2189 (2012). https://doi.org/10.1140/epjc/s10052-012-2189-5. arXiv:1207.2666
8. ATLAS Collaboration, Search for charged Higgs bosons decaying via $H^\pm \to \tau^\pm\nu$ in fully hadronic final states using pp collision data at $\sqrt{s} = 8$ TeV with the ATLAS detector. JHEP **03** (2015) 088, https://doi.org/10.1007/JHEP03(2015)088, arXiv:1412.6663
9. CMS Collaboration, Search for neutral MSSM Higgs bosons decaying to τ pairs in pp collisions at $\sqrt{s} = 7$ TeV. Phys. Rev. Lett. **106**, 231801 (2011). https://doi.org/10.1103/PhysRevLett.106.231801. arXiv:1104.1619
10. CMS Collaboration, Search for neutral Higgs bosons decaying to τ pairs in pp collisions at $\sqrt{s} = 7$ TeV. Phys. Lett. B **713**, 68 (2012). https://doi.org/10.1016/j.physletb.2012.05.028. arXiv:1202.4083
11. CMS Collaboration, Search for neutral MSSM Higgs bosons decaying to a pair of τ leptons in pp collisions. JHEP **10**, 160 (2014). https://doi.org/10.1007/JHEP10(2014)160. arXiv:1408.3316
12. CMS Collaboration, Search for a very light NMSSM Higgs boson produced in decays of the 125 GeV scalar boson and decaying into τ leptons in pp collisions at $\sqrt{s} = 8$ TeV. JHEP **01**, 079 (2016). https://doi.org/10.1007/JHEP01(2016)079. arXiv:1510.06534
13. CMS Collaboration, Search for a low-mass pseudoscalar Higgs boson produced in association with a $b\bar{b}$ pair in pp collisions at $\sqrt{s} = 8$ TeV. Phys. Lett. B **758**, 296 (2016). https://doi.org/10.1016/j.physletb.2016.05.003. arXiv:1511.03610
14. C.M.S. Collaboration, Observation of the Higgs boson decay to a pair of τ leptons with the CMS detector. Phys. Lett. B **779**, 283 (2018). https://doi.org/10.1016/j.physletb.2018.02.004. arXiv:1708.00373
15. ATLAS Collaboration, Search for neutral MSSM Higgs bosons decaying to $\tau^+\tau^-$ pairs in pp collisions at $\sqrt{s} = 7$ TeV with the ATLAS detector. Phys. Lett. B **705**, 174 (2011). https://doi.org/10.1016/j.physletb.2011.10.001. arXiv:1107.5003
16. ATLAS Collaboration, Search for neutral Higgs bosons of the minimal supersymmetric standard model in pp collisions at $\sqrt{s} = 8$ TeV with the ATLAS detector. JHEP **11**, 056 (2014). https://doi.org/10.1007/JHEP11(2014)056. arXiv:1409.6064
17. ATLAS Collaboration, Search for Higgs bosons decaying to aa in the $\mu\mu\tau\tau$ final state in pp collisions at $\sqrt{s} = 8$ TeV with the ATLAS experiment. Phys. Rev. D **92**, 052002 (2015). https://doi.org/10.1103/PhysRevD.92.052002. arXiv:1505.01609
18. CMS Collaboration, Search for lepton-flavour-violating decays of the Higgs boson. Phys. Lett. B **749**, 337 (2015). https://doi.org/10.1016/j.physletb.2015.07.053. arXiv:1502.07400
19. ATLAS Collaboration, Search for lepton-flavour-violating $H \to \mu\tau$ decays of the Higgs boson with the ATLAS detector. JHEP **11**, 211 (2015). https://doi.org/10.1007/JHEP11(2015)211. arXiv:1508.03372
20. ATLAS Collaboration, Search for a heavy neutral particle decaying to $e\mu$, $e\tau$, or $\mu\tau$ in pp collisions at $\sqrt{s} = 8$ TeV with the

ATLAS Detector. Phys. Rev. Lett. **115**, 031801 (2015). https://doi.org/10.1103/PhysRevLett.115.031801. arXiv:1503.04430
21. CMS Collaboration, Search for physics beyond the standard model in events with τ leptons, jets, and large transverse momentum imbalance in pp collisions at $\sqrt{s} = 7$ TeV. Eur. Phys. J. C **73**, 2493 (2013). https://doi.org/10.1140/epjc/s10052-013-2493-8. arXiv:1301.3792
22. CMS Collaboration, Search for anomalous production of events with three or more leptons in pp collisions at $\sqrt{s} = 8$ TeV. Phys. Rev. D **90**, 032006 (2014). https://doi.org/10.1103/PhysRevD.90.032006. arXiv:1404.5801
23. CMS. Collaboration, Search for top squarks in R-parity-violating supersymmetry using three or more leptons and b-tagged jets. Phys. Rev. Lett. **111**, 221801 (2013).https://doi.org/10.1103/PhysRevLett.111.221801. arXiv:1306.6643
24. ATLAS Collaboration, "Search for a heavy narrow resonance decaying to $e\mu$, $e\tau$, or $\mu\tau$ with the ATLAS detector in $\sqrt{s} = 7$ TeV pp collisions at the LHC". Phys. Lett. B **723**, 15 (2013). https://doi.org/10.1016/j.physletb.2013.04.035. arXiv:1212.1272
25. ATLAS Collaboration, Search for supersymmetry in events with large missing transverse momentum, jets, and at least one τ lepton in 20 fb^{-1} of $\sqrt{s} = 8$ TeV pp collision data with the ATLAS detector. JHEP **09**, 103 (2014). https://doi.org/10.1007/JHEP09(2014)103. arXiv:1407.0603
26. ATLAS Collaboration, Search for the direct production of charginos, neutralinos and staus in final states with at least two hadronically decaying taus and missing transverse momentum in pp collisions at $\sqrt{s} = 8$ TeV with the ATLAS detector. JHEP **10**, 96 (2014). https://doi.org/10.1007/JHEP10(2014)096. arXiv:1407.0350
27. ATLAS Collaboration, Search for direct production of charginos and neutralinos in events with three leptons and missing transverse momentum in $\sqrt{s} = 8$ TeV pp collisions with the ATLAS detector. JHEP **04**, 169 (2014). https://doi.org/10.1007/JHEP04(2014)169. arXiv:1402.7029
28. ATLAS Collaboration, Search for direct scalar top pair production in final states with two τ leptons in pp collisions at $\sqrt{s} = 8$ TeV with the ATLAS detector. Eur. Phys. J. C **76**, 81 (2016). https://doi.org/10.1140/epjc/s10052-016-3897-z. arXiv:1509.04976
29. CMS Collaboration, Search for pair production of third-generation leptoquarks and top squarks in pp collisions at $\sqrt{s} = 7$ TeV. Phys. Rev. Lett. **110**, 081801 (2013). https://doi.org/10.1103/PhysRevLett.110.081801. arXiv:1210.5629
30. CMS Collaboration, Search for third-generation scalar leptoquarks in the tτ channel in pp collisions at $\sqrt{s} = 8$TeV. JHEP **07**, 042 (2015). https://doi.org/10.1007/JHEP07(2015)042. arXiv:1503.09049
31. CMS Collaboration, A search for Higgs boson pair production in the bb$\tau\tau$ final state in pp collisions at $\sqrt{s} = 8$ TeV. Phys. Rev. D **96**(7), 072004 (2017). https://doi.org/10.1103/PhysRevD.96.072004. arXiv:1707.00350
32. ATLAS Collaboration, Searches for Higgs boson pair production in the hh $\rightarrow$ bb$\tau\tau$, $\gamma\gamma$WW*, $\gamma\gamma$bb, bbbb channels with the ATLAS detector". Phys. Rev. D **92**, 092004 (2015). https://doi.org/10.1103/PhysRevD.92.092004. arXiv:1509.04670
33. CMS Collaboration, Search for high mass resonances decaying into τ lepton pairs in pp collisions at $\sqrt{s} = 7$ TeV. Phys. Lett. B **716**, 82 (2012). https://doi.org/10.1016/j.physletb.2012.07.062. arXiv:1206.1725
34. CMS Collaboration, Search for W' decaying to τ lepton and neutrino in pp collisions at $\sqrt{s} = 8$ TeV. Phys. Lett. B **755**, 196 (2016). https://doi.org/10.1016/j.physletb.2016.02.002. arXiv:1508.04308
35. ATLAS Collaboration, A search for high-mass resonances decaying to $\tau^+\tau^-$ in pp collisions at $\sqrt{s} = 8$ TeV with the ATLAS detector. JHEP **07**, 157 (2015). https://doi.org/10.1007/JHEP07(2015)157. arXiv:1502.07177
36. S.D. Drell, T.M. Yan, Massive lepton pair production in hadron–hadron collisions at high energies. Phys. Rev. Lett. **25**, 316 (1970). https://doi.org/10.1103/PhysRevLett.25.316 [Erratum: https://doi.org/10.1103/PhysRevLett.25.902.2]
37. CMS Collaboration, Reconstruction and identification of τ lepton decays to hadrons and ν_τ at CMS. JINST **11**, P01019 (2016). https://doi.org/10.1088/1748-0221/11/01/P01019. arXiv:1510.07488
38. CMS Collaboration, Measurement of the inclusive Z cross section via decays to τ pairs in pp collisions at $\sqrt{s} = 7$ TeV. JHEP **08**, 117 (2011). https://doi.org/10.1007/JHEP08(2011)117. arXiv:1104.1617
39. ATLAS Collaboration, Measurement of the Z $\rightarrow \tau\tau$ cross section with the ATLAS Detector. Phys. Rev. D **84**, 112006 (2011). https://doi.org/10.1103/PhysRevD.84.112006. arXiv:1108.2016
40. CDF Collaboration, Measurement of $\sigma(p\bar{p} \rightarrow Z) \times \mathcal{B}(Z \rightarrow \tau\tau)$ in $p\bar{p}$ collisions at $\sqrt{s} = 1.96$ TeV. Phys. Rev. D **75**, 092004 (2007). https://doi.org/10.1103/PhysRevD.75.092004
41. D0 Collaboration, First measurement of $\sigma(p\bar{p} \rightarrow Z) \times \mathcal{B}(Z \rightarrow \tau\tau)$ at $\sqrt{s} = 1.96$ TeV. Phys. Rev. D **71**, 072004 (2005). https://doi.org/10.1103/PhysRevD.71.072004. arXiv:hep-ex/0412020 [Erratum: 10.1103/PhysRevD.77.039901]
42. D0 Collaboration, Measurement of $\sigma(p\bar{p} \rightarrow Z + X) \times \mathcal{B}(Z \rightarrow \tau^+\tau^-)$ at $\sqrt{s} = 1.96$ TeV. Phys. Lett. B **670**, 292 (2009). https://doi.org/10.1016/j.physletb.2008.11.010. arXiv:0808.1306
43. CMS Collaboration, Evidence for the 125 GeV Higgs boson decaying to a pair of τ leptons. JHEP **05**, 104 (2014). https://doi.org/10.1007/JHEP05(2014)104. arXiv:1401.5041
44. CMS Collaboration, Description and performance of track and primary-vertex reconstruction with the CMS tracker. JINST **9**, P10009 (2014). https://doi.org/10.1088/1748-0221/9/10/P10009. arXiv:1405.6569
45. CMS Collaboration, The CMS experiment at the CERN LHC. JINST **3**, S08004 (2008). https://doi.org/10.1088/1748-0221/3/08/S08004
46. J. Alwall, The automated computation of tree-level and next-to-leading order differential cross sections, and their matching to parton shower simulations. JHEP **07**, 079 (2014). https://doi.org/10.1007/JHEP07(2014)079. arXiv:1405.0301
47. P. Nason, A new method for combining NLO QCD with shower Monte Carlo algorithms. JHEP **11**, 040 (2004). https://doi.org/10.1088/1126-6708/2004/11/040. arXiv:hep-ph/0409146
48. S. Frixione, P. Nason, C. Oleari, Matching NLO QCD computations with parton shower simulations: the POWHEG method. JHEP **11**, 070 (2007). https://doi.org/10.1088/1126-6708/2007/11/070. arXiv:0709.2092
49. S. Alioli, P. Nason, C. Oleari, E. Re, A general framework for implementing NLO calculations in shower Monte Carlo programs: the POWHEG BOX. JHEP **06**, 043 (2010). https://doi.org/10.1007/JHEP06(2010)043. arXiv:1002.2581
50. S. Frixione, P. Nason, G. Ridolfi, A positive-weight next-to-leading-order Monte Carlo for heavy flavour hadroproduction. JHEP **09**, 126 (2007). https://doi.org/10.1088/1126-6708/2007/09/126. arXiv:0707.3088
51. S. Alioli, P. Nason, C. Oleari, E. Re, NLO single-top production matched with shower in POWHEG: s- and t-channel contributions. JHEP **09**, 111 (2009). https://doi.org/10.1088/1126-6708/2009/09/111. arXiv:0907.4076 [Erratum: https://doi.org/10.1007/JHEP02(2010)011]
52. S. Alioli, P. Nason, C. Oleari, E. Re, NLO Higgs boson production via gluon fusion matched with shower in POWHEG. JHEP **04**, 002 (2009). https://doi.org/10.1088/1126-6708/2009/04/002. arXiv:0812.0578

53. P. Nason, C. Oleari, NLO Higgs boson production via vector-boson fusion matched with shower in POWHEG. JHEP **02**, 037 (2010). https://doi.org/10.1007/JHEP02(2010)037. arXiv:0911.5299
54. NNPDF Collaboration, Parton distributions with QED corrections. Nucl. Phys. B **877**, 290 (2013). https://doi.org/10.1016/j.nuclphysb.2013.10.010, arXiv:1308.0598
55. NNPDF Collaboration, Unbiased global determination of parton distributions and their uncertainties at NNLO and at LO. Nucl. Phys. B **855**, 153 (2012). https://doi.org/10.1016/j.nuclphysb.2011.09.024. arXiv:1107.2652
56. NNPDF Collaboration, Parton distributions for the LHC Run II. JHEP **04**, 040 (2015). https://doi.org/10.1007/JHEP04(2015)040. arXiv:1410.8849
57. T. Sjöstrand, S. Mrenna, P.Z. Skands, A brief introduction to PYTHIA 8.1. Comput. Phys. Commun. **178**, 852 (2008). https://doi.org/10.1016/j.cpc.2008.01.036. arXiv:0710.3820
58. CMS Collaboration, Event generator tunes obtained from underlying event and multiparton scattering measurements. Eur. Phys. J. C **76**, 155 (2016). https://doi.org/10.1140/epjc/s10052-016-3988-x. arXiv:1512.00815
59. P. Skands, S. Carrazza, J. Rojo, Tuning PYTHIA 8.1: the Monash, tune. Eur. Phys. J. C **74**(2014), 3024 (2013). https://doi.org/10.1140/epjc/s10052-014-3024-y. arXiv:1404.5630
60. Y. Li, F. Petriello, Combining QCD and electroweak corrections to dilepton production in FEWZ. Phys. Rev. D **86**, 094034 (2012). https://doi.org/10.1103/PhysRevD.86.094034. arXiv:1208.5967
61. M. Czakon, A. Mitov, Top++: a program for the calculation of the top-pair cross section at hadron colliders. Comput. Phys. Commun. **185**, 2930 (2014). https://doi.org/10.1016/j.cpc.2014.06.021. arXiv:1112.5675
62. CMS Collaboration, Measurement of differential top-quark pair production cross sections in pp colisions at $\sqrt{s} = 7$ TeV. Eur. Phys. J. C **73**, 2339 (2013). https://doi.org/10.1140/epjc/s10052-013-2339-4. arXiv:1211.2220
63. CMS Collaboration, Measurement of the differential cross section for top quark pair production in pp collisions at $\sqrt{s} = 8$ TeV. Eur. Phys. J. C **75**, 542 (2015). https://doi.org/10.1140/epjc/s10052-015-3709-x. arXiv:1505.04480
64. P. Kant et al., HATHOR for single top-quark production: updated predictions and uncertainty estimates for single top-quark production in hadronic collisions. Comput. Phys. Commun. **191**, 74 (2015). https://doi.org/10.1016/j.cpc.2015.02.001. arXiv:1406.4403
65. M. Aliev et al., HATHOR: HAdronic Top and Heavy quarks crOss section calculatoR. Comput. Phys. Commun. **182**, 1034 (2011). https://doi.org/10.1016/j.cpc.2010.12.040. arXiv:1007.1327
66. N. Kidonakis, Two-loop soft anomalous dimensions for single top quark associated production with a W^- or H^-. Phys. Rev. D **82**, 054018 (2010). https://doi.org/10.1103/PhysRevD.82.054018. arXiv:1005.4451
67. J.M. Campbell, R.K. Ellis, C. Williams, Vector boson pair production at the LHC. JHEP **07**, 018 (2011). https://doi.org/10.1007/JHEP07(2011)018. arXiv:1105.0020
68. GEANT4 Collaboration, GEANT4—a simulation toolkit. Nucl. Instrum. Meth. A **506**, 250 (2003). https://doi.org/10.1016/S0168-9002(03)01368-8
69. C.M.S. Collaboration, Particle-flow reconstruction and global event description with the CMS detector. JINST **12**, P10003 (2017). https://doi.org/10.1088/1748-0221/12/10/P10003. arXiv:1706.04965
70. CMS Collaboration, Performance of electron reconstruction and selection with the CMS detector in pp collisions at $\sqrt{s} = 8$ TeV. JINST **10**, P06005 (2015). https://doi.org/10.1088/1748-0221/10/06/P06005. arXiv:1502.02701
71. H. Voss, A. Höcker, J. Stelzer, F. Tegenfeldt, TMVA, the toolkit for multivariate data analysis with ROOT. In: XIth International Workshop on Advanced Computing and Analysis Techniques in Physics Research (ACAT) (2007), p. 40. arXiv:physics/0703039
72. CMS Collaboration, Performance of CMS muon reconstruction in pp collision events at $\sqrt{s} = 7$ TeV. JINST **7**, P10002 (2012). https://doi.org/10.1088/1748-0221/7/10/P10002. arXiv:1206.4071
73. E. Chabanat, N. Estre, Deterministic annealing for vertex finding at CMS. In: Computing in High Energy Physics and Nuclear Physics. Proceedings, Conference, CHEP'04, Interlaken, Switzerland, September 27–October 1, 2004 (2005), p. 287
74. W. Waltenberger, R. Frühwirth, P. Vanlaer, Adaptive vertex fitting. J. Phys. G **34**, N343 (2007). https://doi.org/10.1088/0954-3899/34/12/N01
75. CMS Collaboration, Performance of reconstruction and identification of τ leptons in their decays to hadrons and ν_τ in LHC Run 2. CMS Physics Analysis Summary CMS-PAS-TAU-16-002, (2016)
76. M. Cacciari, G.P. Salam, G. Soyez, The anti-k_t jet clustering algorithm. JHEP **04**, 063 (2008). https://doi.org/10.1088/1126-6708/2008/04/063. arXiv:0802.1189
77. M. Cacciari, G.P. Salam, G. Soyez, FastJet user manual. Eur. Phys. J. C **72**, 1896 (2012). https://doi.org/10.1140/epjc/s10052-012-1896-2. arXiv:1111.6097
78. CMS Collaboration, Jet performance in pp collisions at $\sqrt{s} = 7$ TeV. CMS physics analysis summary CMS-PAS-JME-10-003 (2010)
79. CMS Collaboration, Jet energy scale and resolution in the CMS experiment in pp collisions at 8 TeV. JINST **12**, P02014 (2017). https://doi.org/10.1088/1748-0221/12/02/P02014. arXiv:1607.03663
80. M. Cacciari, G.P. Salam, G. Soyez, The catchment area of jets. JHEP **04**, 005 (2008). https://doi.org/10.1088/1126-6708/2008/04/005. arXiv:0802.1188
81. M. Cacciari, G.P. Salam, Pileup subtraction using jet areas. Phys. Lett. B **659**, 119 (2008). https://doi.org/10.1016/j.physletb.2007.09.077. arXiv:0707.1378
82. CMS Collaboration, Identification of b quark jets with the CMS experiment. JINST **8**, P04013 (2013). https://doi.org/10.1088/1748-0221/8/04/P04013. arXiv:1211.4462
83. CMS Collaboration, Performance of the CMS missing transverse momentum reconstruction in pp data at $\sqrt{s} = 8$ TeV. JINST **10**, P02006 (2015). https://doi.org/10.1088/1748-0221/10/02/P02006. arXiv:1411.0511
84. L. Bianchini, J. Conway, E.K. Friis, C. Veelken, Reconstruction of the Higgs mass in $H \to \tau\tau$ events by dynamical likelihood techniques. J. Phys. Conf. Ser. **513**, 022035 (2014). https://doi.org/10.1088/1742-6596/513/2/022035
85. CMS Collaboration, Missing transverse energy performance of the CMS detector. JINST **6**, P09001 (2011). https://doi.org/10.1088/1748-0221/6/09/P09001. arXiv:1106.5048
86. CDF Collaboration, Search for neutral MSSM Higgs bosons decaying to τ pairs in $p\bar{p}$ collisions at $\sqrt{s} = 1.96$ TeV. Phys. Rev. Lett. **96**, 011802 (2006). https://doi.org/10.1103/PhysRevLett.96.011802. arXiv:hep-ex/0508051
87. CMS Collaboration, Searches for a heavy scalar boson H decaying to a pair of 125 GeV Higgs bosons hh or for a heavy pseudoscalar boson A decaying to Zh, in the final states with $h \to \tau\tau$. Phys. Lett. B **755**, 217 (2016). https://doi.org/10.1016/j.physletb.2016.01.056. arXiv:1510.01181
88. CMS Collaboration, The CMS trigger system. JINST **12**, P01020 (2017). https://doi.org/10.1088/1748-0221/12/01/P01020. arXiv:1609.02366
89. CMS Collaboration, Measurements of inclusive W and Z cross sections in pp collisions at $\sqrt{s} = 7$ TeV. JHEP **01**, 080 (2011). https://doi.org/10.1007/JHEP01(2011)080. arXiv:1012.2466

90. CMS Collaboration, Performance of missing energy reconstruction in 13 TeV pp collision data using the CMS detector. CMS physics analysis summary CMS-PAS-JME-16-004 (2016)
91. CMS Collaboration, CMS luminosity measurement for the 2015 data-taking period. CMS physics analysis summary CMS-PAS-LUM-15-001 (2015)
92. M. Cacciari et al., The $t\bar{t}$ cross-section at 1.8 TeV and 1.96 TeV: a study of the systematics due to parton densities and scale dependence. JHEP **04**, 068 (2004). https://doi.org/10.1088/1126-6708/2004/04/068. arXiv:hep-ph/0303085
93. S. Catani, D. de Florian, M. Grazzini, P. Nason, Soft gluon resummation for Higgs boson production at hadron colliders. JHEP **07**, 028 (2003). https://doi.org/10.1088/1126-6708/2003/07/028. arXiv:hep-ph/0306211
94. J. Butterworth et al., PDF4LHC recommendations for LHC Run II. J. Phys. G **43**, 023001 (2016). https://doi.org/10.1088/0954-3899/43/2/023001. arXiv:1510.03865
95. ATLAS and CMS Collaborations and LHC Higgs Combination Group, Procedure for the LHC Higgs boson search combination in Summer 2011. Technical Report ATL-PHYS-PUB-2011-011, CMS-NOTE-2011-005 (2011)
96. CMS Collaboration, Combined results of searches for the standard model Higgs boson in pp collisions at $\sqrt{s} = 7$ TeV. Phys. Lett. B **710**, 26 (2012). https://doi.org/10.1016/j.physletb.2012.02.064. arXiv:1202.1488
97. J.S. Conway, Incorporating nuisance parameters in likelihoods for multisource spectra Proceedings of the PHYSTAT 2011 Workshop on Statistical Issues Related to Discovery Claims in Search Experiments and Unfolding, CERN, Geneva, Switzerland, 17–20 January 2011, pp. 115–120 (2011). arXiv:1103.0354
98. CMS Collaboration, Precise determination of the mass of the Higgs boson and tests of compatibility of its couplings with the standard model predictions using proton collisions at 7 and 8 TeV. Eur. Phys. J. C **75**, 212 (2015). https://doi.org/10.1140/epjc/s10052-015-3351-7. arXiv:1412.8662
99. S. Jadach, Z. Wąs, R. Decker, J.H. Kühn, The τ decay library TAUOLA, version 2.4. Comput. Phys. Commun. **76**, 361 (1993). https://doi.org/10.1016/0010-4655(93)90061-G
100. N. Davidson et al., Universal interface of TAUOLA technical and physics documentation. Comput. Phys. Commun. **183**, 821 (2012). https://doi.org/10.1016/j.cpc.2011.12.009. arXiv:1002.0543
101. Z. Czyczula, T. Przedzinski, Z. Wąs, TauSpinner program for studies on spin effect in τ production at the LHC. Eur. Phys. J. C **72**, 1988 (2012). https://doi.org/10.1140/epjc/s10052-012-1988-z. arXiv:1201.0117
102. ATLAS Collaboration, Modelling $Z \to \tau\tau$ processes in ATLAS with τ-embedded $Z \to \mu\mu$ data. JINST **10**, P09018 (2015). https://doi.org/10.1088/1748-0221/2015/9/P09018. arXiv:1506.05623

CMS Collaboration

Yerevan Physics Institute, Yerevan, Armenia
A. M. Sirunyan, A. Tumasyan

Institut für Hochenergiephysik, Wien, Austria
W. Adam, F. Ambrogi, E. Asilar, T. Bergauer, J. Brandstetter, E. Brondolin, M. Dragicevic, J. Erö, A. Escalante Del Valle, M. Flechl, M. Friedl, R. Frühwirth[1], V. M. Ghete, J. Grossmann, J. Hrubec, M. Jeitler[1], A. König, N. Krammer, I. Krätschmer, D. Liko, T. Madlener, I. Mikulec, E. Pree, N. Rad, H. Rohringer, J. Schieck[1], R. Schöfbeck, M. Spanring, D. Spitzbart, A. Taurok, W. Waltenberger, J. Wittmann, C.-E. Wulz[1], M. Zarucki

Institute for Nuclear Problems, Minsk, Belarus
V. Chekhovsky, V. Mossolov, J. Suarez Gonzalez

Universiteit Antwerpen, Antwerpen, Belgium
E. A. De Wolf, D. Di Croce, X. Janssen, J. Lauwers, M. Van De Klundert, H. Van Haevermaet, P. Van Mechelen, N. Van Remortel

Vrije Universiteit Brussel, Brussel, Belgium
S. Abu Zeid, F. Blekman, J. D'Hondt, I. De Bruyn, J. De Clercq, K. Deroover, G. Flouris, D. Lontkovskyi, S. Lowette, I. Marchesini, S. Moortgat, L. Moreels, Q. Python, K. Skovpen, S. Tavernier, W. Van Doninck, P. Van Mulders, I. Van Parijs

Université Libre de Bruxelles, Bruxelles, Belgium
D. Beghin, B. Bilin, H. Brun, B. Clerbaux, G. De Lentdecker, H. Delannoy, B. Dorney, G. Fasanella, L. Favart, R. Goldouzian, A. Grebenyuk, A. K. Kalsi, T. Lenzi, J. Luetic, T. Maerschalk, A. Marinov, T. Seva, E. Starling, C. Vander Velde, P. Vanlaer, D. Vannerom, R. Yonamine, F. Zenoni

Ghent University, Ghent, Belgium
T. Cornelis, D. Dobur, A. Fagot, M. Gul, I. Khvastunov[2], D. Poyraz, C. Roskas, S. Salva, D. Trocino, M. Tytgat, W. Verbeke, N. Zaganidis

Université Catholique de Louvain, Louvain-la-Neuve, Belgium
H. Bakhshiansohi, O. Bondu, S. Brochet, G. Bruno, C. Caputo, A. Caudron, P. David, S. De Visscher, C. Delaere, M. Delcourt, B. Francois, A. Giammanco, M. Komm, G. Krintiras, V. Lemaitre, A. Magitteri, A. Mertens, M. Musich, K. Piotrzkowski, L. Quertenmont, A. Saggio, M. Vidal Marono, S. Wertz, J. Zobec

Centro Brasileiro de Pesquisas Fisicas, Rio de Janeiro, Brazil
W. L. Aldá Júnior, F. L. Alves, G. A. Alves, L. Brito, G. Correia Silva, C. Hensel, A. Moraes, M. E. Pol, P. Rebello Teles

Universidade do Estado do Rio de Janeiro, Rio de Janeiro, Brazil
E. Belchior Batista Das Chagas, W. Carvalho, J. Chinellato[3], E. Coelho, E. M. Da Costa, G. G. Da Silveira[4], D. De Jesus Damiao, S. Fonseca De Souza, L. M. Huertas Guativa, H. Malbouisson, M. Melo De Almeida, C. Mora Herrera, L. Mundim, H. Nogima, L. J. Sanchez Rosas, A. Santoro, A. Sznajder, M. Thiel, E. J. Tonelli Manganote[3], F. Torres Da Silva De Araujo, A. Vilela Pereira

Universidade Estadual Paulista[a], Universidade Federal do ABC[b], São Paulo, Brazil
S. Ahuja[a], C. A. Bernardes[a], T. R. Fernandez Perez Tomei[a], E. M. Gregores[b], P. G. Mercadante[b], S. F. Novaes[a], Sandra S. Padula[a], D. Romero Abad[b], J. C. Ruiz Vargas[a]

Institute for Nuclear Research and Nuclear Energy, Bulgarian Academy of Sciences, Sofia, Bulgaria
A. Aleksandrov, R. Hadjiiska, P. Iaydjiev, M. Misheva, M. Rodozov, M. Shopova, G. Sultanov

University of Sofia, Sofia, Bulgaria
A. Dimitrov, L. Litov, B. Pavlov, P. Petkov

Beihang University, Beijing, China
W. Fang[5], X. Gao[5], L. Yuan

Institute of High Energy Physics, Beijing, China
M. Ahmad, J. G. Bian, G. M. Chen, H. S. Chen, M. Chen, Y. Chen, C. H. Jiang, D. Leggat, H. Liao, Z. Liu, F. Romeo, S. M. Shaheen, A. Spiezia, J. Tao, C. Wang, Z. Wang, E. Yazgan, T. Yu, H. Zhang, J. Zhao

State Key Laboratory of Nuclear Physics and Technology, Peking University, Beijing, China
Y. Ban, G. Chen, J. Li, Q. Li, S. Liu, Y. Mao, S. J. Qian, D. Wang, Z. Xu, F. Zhang[5]

Tsinghua University, Beijing, China
Y. Wang

Universidad de Los Andes, Bogota, Colombia
C. Avila, A. Cabrera, C. A. Carrillo Montoya, L. F. Chaparro Sierra, C. Florez, C. F. González Hernández, J. D. Ruiz Alvarez, M. A. Segura Delgado

Faculty of Electrical Engineering, Mechanical Engineering and Naval Architecture, University of Split, Split, Croatia
B. Courbon, N. Godinovic, D. Lelas, I. Puljak, P. M. Ribeiro Cipriano, T. Sculac

Faculty of Science, University of Split, Split, Croatia
Z. Antunovic, M. Kovac

Institute Rudjer Boskovic, Zagreb, Croatia
V. Brigljevic, D. Ferencek, K. Kadija, B. Mesic, A. Starodumov[6], T. Susa

University of Cyprus, Nicosia, Cyprus
M. W. Ather, A. Attikis, G. Mavromanolakis, J. Mousa, C. Nicolaou, F. Ptochos, P. A. Razis, H. Rykaczewski

Charles University, Prague, Czech Republic
M. Finger[7], M. Finger Jr.[7]

Universidad San Francisco de Quito, Quito, Ecuador
E. Carrera Jarrin

Academy of Scientific Research and Technology of the Arab Republic of Egypt, Egyptian Network of High Energy Physics, Cairo, Egypt
H. Abdalla[8], E. El-khateeb[9], S. Khalil[10]

National Institute of Chemical Physics and Biophysics, Tallinn, Estonia
S. Bhowmik, R. K. Dewanjee, M. Kadastik, L. Perrini, M. Raidal, A. Tiko, C. Veelken

Department of Physics, University of Helsinki, Helsinki, Finland
P. Eerola, H. Kirschenmann, J. Pekkanen, M. Voutilainen

Helsinki Institute of Physics, Helsinki, Finland
J. Havukainen, J. K. Heikkilä, T. Järvinen, V. Karimäki, R. Kinnunen, T. Lampén, K. Lassila-Perini, S. Laurila, S. Lehti, T. Lindén, P. Luukka, T. Mäenpää, H. Siikonen, E. Tuominen, J. Tuominiemi

Lappeenranta University of Technology, Lappeenranta, Finland
T. Tuuva

IRFU, CEA, Université Paris-Saclay, Gif-sur-Yvette, France
M. Besancon, F. Couderc, M. Dejardin, D. Denegri, J. L. Faure, F. Ferri, S. Ganjour, S. Ghosh, A. Givernaud, P. Gras, G. Hamel de Monchenault, P. Jarry, I. Kucher, C. Leloup, E. Locci, M. Machet, J. Malcles, G. Negro, J. Rander, A. Rosowsky, M. Ö. Sahin, M. Titov

Laboratoire Leprince-Ringuet, Ecole polytechnique, CNRS/IN2P3, Université Paris-Saclay, Palaiseau, France
A. Abdulsalam[11], C. Amendola, I. Antropov, S. Baffioni, F. Beaudette, P. Busson, L. Cadamuro, C. Charlot, R. Granier de Cassagnac, M. Jo, S. Lisniak, A. Lobanov, J. Martin Blanco, M. Nguyen, C. Ochando, G. Ortona, P. Paganini, P. Pigard, R. Salerno, J. B. Sauvan, Y. Sirois, A. G. Stahl Leiton, T. Strebler, Y. Yilmaz, A. Zabi, A. Zghiche

Université de Strasbourg, CNRS, IPHC UMR 7178, 67000 Strasbourg, France
J.-L. Agram[12], J. Andrea, D. Bloch, J.-M. Brom, M. Buttignol, E. C. Chabert, N. Chanon, C. Collard, E. Conte[12], X. Coubez, F. Drouhin[12], J.-C. Fontaine[12], D. Gelé, U. Goerlach, M. Jansová, P. Juillot, A.-C. Le Bihan, N. Tonon, P. Van Hove

Centre de Calcul de l'Institut National de Physique Nucleaire et de Physique des Particules, CNRS/IN2P3, Villeurbanne, France
S. Gadrat

Université de Lyon, Université Claude Bernard Lyon 1, CNRS-IN2P3, Institut de Physique Nucléaire de Lyon, Villeurbanne, France
S. Beauceron, C. Bernet, G. Boudoul, R. Chierici, D. Contardo, P. Depasse, H. El Mamouni, J. Fay, L. Finco, S. Gascon, M. Gouzevitch, G. Grenier, B. Ille, F. Lagarde, I. B. Laktineh, M. Lethuillier, L. Mirabito, A. L. Pequegnot, S. Perries, A. Popov[13], V. Sordini, M. Vander Donckt, S. Viret, S. Zhang

Georgian Technical University, Tbilisi, Georgia
T. Toriashvili[14]

Tbilisi State University, Tbilisi, Georgia
Z. Tsamalaidze[7]

RWTH Aachen University, I. Physikalisches Institut, Aachen, Germany
C. Autermann, L. Feld, M. K. Kiesel, K. Klein, M. Lipinski, M. Preuten, C. Schomakers, J. Schulz, M. Teroerde, B. Wittmer, V. Zhukov[13]

RWTH Aachen University, III. Physikalisches Institut A, Aachen, Germany
A. Albert, D. Duchardt, M. Endres, M. Erdmann, S. Erdweg, T. Esch, R. Fischer, A. Güth, M. Hamer, T. Hebbeker, C. Heidemann, K. Hoepfner, S. Knutzen, M. Merschmeyer, A. Meyer, P. Millet, S. Mukherjee, T. Pook, M. Radziej, H. Reithler, M. Rieger, F. Scheuch, D. Teyssier, S. Thüer

RWTH Aachen University, III. Physikalisches Institut B, Aachen, Germany
G. Flügge, B. Kargoll, T. Kress, A. Künsken, T. Müller, A. Nehrkorn, A. Nowack, C. Pistone, O. Pooth, A. Stahl[15]

Deutsches Elektronen-Synchrotron, Hamburg, Germany
M. Aldaya Martin, T. Arndt, C. Asawatangtrakuldee, K. Beernaert, O. Behnke, U. Behrens, A. Bermúdez Martínez, A. A. Bin Anuar, K. Borras[16], V. Botta, A. Campbell, P. Connor, C. Contreras-Campana, F. Costanza, C. Diez Pardos, D. Domínguez Damiani, G. Eckerlin, D. Eckstein, T. Eichhorn, E. Eren, E. Gallo[17], J. Garay Garcia, A. Geiser, J. M. Grados Luyando, A. Grohsjean, P. Gunnellini, M. Guthoff, A. Harb, J. Hauk, M. Hempel[18], H. Jung, M. Kasemann, J. Keaveney, C. Kleinwort, I. Korol, D. Krücker, W. Lange, A. Lelek, T. Lenz, J. Leonard, K. Lipka, W. Lohmann[18], R. Mankel, I.-A. Melzer-Pellmann, A. B. Meyer, M. Missiroli, G. Mittag, J. Mnich, A. Mussgiller, E. Ntomari, D. Pitzl, A. Raspereza, M. Savitskyi, P. Saxena, R. Shevchenko, N. Stefaniuk, G. P. Van Onsem, R. Walsh, Y. Wen, K. Wichmann, C. Wissing, O. Zenaiev

University of Hamburg, Hamburg, Germany
R. Aggleton, S. Bein, V. Blobel, M. Centis Vignali, T. Dreyer, E. Garutti, D. Gonzalez, J. Haller, A. Hinzmann, M. Hoffmann, A. Karavdina, R. Klanner, R. Kogler, N. Kovalchuk, S. Kurz, T. Lapsien, D. Marconi, M. Meyer, M. Niedziela, D. Nowatschin, F. Pantaleo[15], T. Peiffer, A. Perieanu, C. Scharf, P. Schleper, A. Schmidt, S. Schumann, J. Schwandt, J. Sonneveld, H. Stadie, G. Steinbrück, F. M. Stober, M. Stöver, H. Tholen, D. Troendle, E. Usai, A. Vanhoefer, B. Vormwald

Institut für Experimentelle Kernphysik, Karlsruhe, Germany
M. Akbiyik, C. Barth, M. Baselga, S. Baur, E. Butz, R. Caspart, T. Chwalek, F. Colombo, W. De Boer, A. Dierlamm, N. Faltermann, B. Freund, R. Friese, M. Giffels, M. A. Harrendorf, F. Hartmann[15], S. M. Heindl, U. Husemann, F. Kassel[15], S. Kudella, H. Mildner, M. U. Mozer, Th. Müller, M. Plagge, G. Quast, K. Rabbertz, M. Schröder, I. Shvetsov, G. Sieber, H. J. Simonis, R. Ulrich, S. Wayand, M. Weber, T. Weiler, S. Williamson, C. Wöhrmann, R. Wolf

Institute of Nuclear and Particle Physics (INPP), NCSR Demokritos, Aghia Paraskevi, Greece
G. Anagnostou, G. Daskalakis, T. Geralis, A. Kyriakis, D. Loukas, I. Topsis-Giotis

National and Kapodistrian University of Athens, Athens, Greece
G. Karathanasis, S. Kesisoglou, A. Panagiotou, N. Saoulidou

National Technical University of Athens, Athens, Greece
K. Kousouris

University of Ioánnina, Ioánnina, Greece
I. Evangelou, C. Foudas, P. Gianneios, P. Katsoulis, P. Kokkas, S. Mallios, N. Manthos, I. Papadopoulos, E. Paradas, J. Strologas, F. A. Triantis, D. Tsitsonis

MTA-ELTE Lendület CMS Particle and Nuclear Physics Group, Eötvös Loránd University, Budapest, Hungary
M. Csanad, N. Filipovic, G. Pasztor, O. Surányi, G. I. Veres[19]

Wigner Research Centre for Physics, Budapest, Hungary
G. Bencze, C. Hajdu, D. Horvath[20], Á. Hunyadi, F. Sikler, V. Veszpremi, G. Vesztergombi[19]

Institute of Nuclear Research ATOMKI, Debrecen, Hungary
N. Beni, S. Czellar, J. Karancsi[21], A. Makovec, J. Molnar, Z. Szillasi

Institute of Physics, University of Debrecen, Debrecen, Hungary
M. Bartók[19], P. Raics, Z. L. Trocsanyi, B. Ujvari

Indian Institute of Science (IISc), Bangalore, India
S. Choudhury, J. R. Komaragiri

National Institute of Science Education and Research, Bhubaneswar, India
S. Bahinipati[22], P. Mal, K. Mandal, A. Nayak[23], D. K. Sahoo[22], N. Sahoo, S. K. Swain

Panjab University, Chandigarh, India
S. Bansal, S. B. Beri, V. Bhatnagar, R. Chawla, N. Dhingra, A. Kaur, M. Kaur, S. Kaur, R. Kumar, P. Kumari, A. Mehta, J. B. Singh, G. Walia

University of Delhi, Delhi, India
A. Bhardwaj, S. Chauhan, B. C. Choudhary, R. B. Garg, S. Keshri, A. Kumar, Ashok Kumar, S. Malhotra, M. Naimuddin, K. Ranjan, Aashaq Shah, R. Sharma

Saha Institute of Nuclear Physics, HBNI, Kolkata, India
R. Bhardwaj, R. Bhattacharya, S. Bhattacharya, U. Bhawandeep, S. Dey, S. Dutt, S. Dutta, S. Ghosh, N. Majumdar, A. Modak, K. Mondal, S. Mukhopadhyay, S. Nandan, A. Purohit, A. Roy, S. Roy Chowdhury, S. Sarkar, M. Sharan, S. Thakur

Indian Institute of Technology Madras, Chennai, India
P. K. Behera

Bhabha Atomic Research Centre, Mumbai, India
R. Chudasama, D. Dutta, V. Jha, V. Kumar, A. K. Mohanty[15], P. K. Netrakanti, L. M. Pant, P. Shukla, A. Topkar

Tata Institute of Fundamental Research-A, Mumbai, India
T. Aziz, S. Dugad, B. Mahakud, S. Mitra, G. B. Mohanty, N. Sur, B. Sutar

Tata Institute of Fundamental Research-B, Mumbai, India
S. Banerjee, S. Bhattacharya, S. Chatterjee, P. Das, M. Guchait, Sa. Jain, S. Kumar, M. Maity[24], G. Majumder, K. Mazumdar, T. Sarkar[24], N. Wickramage[23]

Indian Institute of Science Education and Research (IISER), Pune, India
S. Chauhan, S. Dube, V. Hegde, A. Kapoor, K. Kothekar, S. Pandey, A. Rane, S. Sharma

Institute for Research in Fundamental Sciences (IPM), Tehran, Iran
S. Chenarani[26], E. Eskandari Tadavani, S. M. Etesami[26], M. Khakzad, M. Mohammadi Najafabadi, M. Naseri, S. Paktinat Mehdiabadi[27], F. Rezaei Hosseinabadi, B. Safarzadeh[28], M. Zeinali

University College Dublin, Dublin, Ireland
M. Felcini, M. Grunewald

INFN Sezione di Bari[a], Università di Bari[b], Politecnico di Bari[c], Bari, Italy
M. Abbrescia[a,b], C. Calabria[a,b], A. Colaleo[a], D. Creanza[a,c], L. Cristella[a,b], N. De Filippis[a,c], M. De Palma[a,b], F. Errico[a,b], L. Fiore[a], G. Iaselli[a,c], S. Lezki[a,b], G. Maggi[a,c], M. Maggi[a], G. Miniello[a,b], S. My[a,b], S. Nuzzo[a,b], A. Pompili[a,b], G. Pugliese[a,c], R. Radogna[a], A. Ranieri[a], G. Selvaggi[a,b], A. Sharma[a], L. Silvestris[a,15], R. Venditti[a], P. Verwilligen[a]

INFN Sezione di Bologna[a], Università di Bologna[b], Bologna, Italy
G. Abbiendi[a], C. Battilana[a,b], D. Bonacorsi[a,b], L. Borgonovi[a,b], S. Braibant-Giacomelli[a,b], R. Campanini[a,b], P. Capiluppi[a,b], A. Castro[a,b], F. R. Cavallo[a], S. S. Chhibra[a,b], G. Codispoti[a,b], M. Cuffiani[a,b], G. M. Dallavalle[a], F. Fabbri[a], A. Fanfani[a], D. Fasanella[a,b], P. Giacomelli[a], C. Grandi[a], L. Guiducci[a,b], S. Marcellini[a], G. Masetti[a], A. Montanari[a], F. L. Navarria[a,b], A. Perrotta[a], A. M. Rossi[a,b], T. Rovelli[a,b], G. P. Siroli[a,b], N. Tosi[a]

INFN Sezione di Catania[a], Università di Catania[b], Catania, Italy
S. Albergo[a,b], S. Costa[a,b], A. Di Mattia[a], F. Giordano[a,b], R. Potenza[a,b], A. Tricomi[a,b], C. Tuve[a,b]

INFN Sezione di Firenze[a], Università di Firenze[b], Firenze, Italy
G. Barbagli[a], K. Chatterjee[a,b], V. Ciulli[a,b], C. Civinini[a], R. D'Alessandro[a,b], E. Focardi[a,b], P. Lenzi[a,b], M. Meschini[a], S. Paoletti[a], L. Russo[a,29], G. Sguazzoni[a], D. Strom[a], L. Viliani[a]

INFN Laboratori Nazionali di Frascati, Frascati, Italy
L. Benussi, S. Bianco, F. Fabbri, D. Piccolo, F. Primavera[15]

INFN Sezione di Genova[a], Università di Genova[b], Genova, Italy
V. Calvelli[a,b], F. Ferro[a], F. Ravera[a,b], E. Robutti[a], S. Tosi[a,b]

INFN Sezione di Milano-Bicocca[a], Università di Milano-Bicocca[b], Milano, Italy
A. Benaglia[a], A. Beschi[b], L. Brianza[a,b], F. Brivio[a,b], V. Ciriolo[a,b,15], M. E. Dinardo[a,b], S. Fiorendi[a,b], S. Gennai[a], A. Ghezzi[a,b], P. Govoni[a,b], M. Malberti[a,b], S. Malvezzi[a], R. A. Manzoni[a,b], D. Menasce[a], L. Moroni[a], M. Paganoni[a,b], K. Pauwels[a,b], D. Pedrini[a], S. Pigazzini[a,b,30], S. Ragazzi[a,b], T. Tabarelli de Fatis[a,b]

INFN Sezione di Napoli[a], Università di Napoli 'Federico II' [b], Napoli, Italy, Università della Basilicata[c], Potenza, Italy, Università G. Marconi[d], Roma, Italy
S. Buontempo[a], N. Cavallo[a,c], S. Di Guida[a,d,15], F. Fabozzi[a,c], F. Fienga[a,b], A. O. M. Iorio[a,b], W. A. Khan[a], L. Lista[a], S. Meola[a,d,15], P. Paolucci[a,15], C. Sciacca[a,b], F. Thyssen[a]

INFN Sezione di Padova[a], Università di Padova[b], Padova, Italy, Università di Trento[c], Trento, Italy
P. Azzi[a], N. Bacchetta[a], M. Bellato[a], L. Benato[a,b], D. Bisello[a,b], A. Boletti[a,b], A. Carvalho Antunes De Oliveira[a,b], P. Checchia[a], M. Dall'Osso[a,b], P. De Castro Manzano[a], T. Dorigo[a], U. Dosselli[a], F. Gasparini[a,b], U. Gasparini[a,b], S. Lacaprara[a], P. Lujan, M. Margoni[a,b], A. T. Meneguzzo[a,b], N. Pozzobon[a,b], P. Ronchese[a,b], R. Rossin[a,b], F. Simonetto[a,b], E. Torassa[a], M. Zanetti[a,b], P. Zotto[a,b], G. Zumerle[a,b]

INFN Sezione di Pavia[a], Università di Pavia[b], Pavia, Italy
A. Braghieri[a], A. Magnani[a], P. Montagna[a,b], S. P. Ratti[a,b], V. Re[a], M. Ressegotti[a,b], C. Riccardi[a,b], P. Salvini[a], I. Vai[a,b], P. Vitulo[a,b]

INFN Sezione di Perugia[a], Università di Perugia[b], Perugia, Italy
L. Alunni Solestizi[a,b], M. Biasini[a,b], G. M. Bilei[a], C. Cecchi[a,b], D. Ciangottini[a,b], L. Fanò[a,b], P. Lariccia[a,b], R. Leonardi[a,b], E. Manoni[a], G. Mantovani[a,b], V. Mariani[a,b], M. Menichelli[a], A. Rossi[a,b], A. Santocchia[a,b], D. Spiga[a]

INFN Sezione di Pisa[a], Università di Pisa[b], Scuola Normale Superiore di Pisa[c], Pisa, Italy
K. Androsov[a], P. Azzurri[a,15], G. Bagliesi[a], T. Boccali[a], L. Borrello, R. Castaldi[a], M. A. Ciocci[a,b], R. Dell'Orso[a], G. Fedi[a], L. Giannini[a,c], A. Giassi[a], M. T. Grippo[a,29], F. Ligabue[a,c], T. Lomtadze[a], E. Manca[a,c], G. Mandorli[a,c], A. Messineo[a,b], F. Palla[a], A. Rizzi[a,b], A. Savoy-Navarro[a,31], P. Spagnolo[a], R. Tenchini[a], G. Tonelli[a,b], A. Venturi[a], P. G. Verdini[a]

INFN Sezione di Roma[a], Sapienza Università di Roma[b], Rome, Italy
L. Barone[a,b], F. Cavallari[a], M. Cipriani[a,b], N. Daci[a], D. Del Re[a,b], E. Di Marco[a,b], M. Diemoz[a], S. Gelli[a,b], E. Longo[a,b], F. Margaroli[a,b], B. Marzocchi[a,b], P. Meridiani[a], G. Organtini[a,b], R. Paramatti[a,b], F. Preiato[a,b], S. Rahatlou[a,b], C. Rovelli[a], F. Santanastasio[a,b]

INFN Sezione di Torino[a], Università di Torino[b], Torino, Italy, Università del Piemonte Orientale[c], Novara, Italy
N. Amapane[a,b], R. Arcidiacono[a,c], S. Argiro[a,b], M. Arneodo[a,c], N. Bartosik[a], R. Bellan[a,b], C. Biino[a], N. Cartiglia[a], F. Cenna[a,b], M. Costa[a,b], R. Covarelli[a,b], A. Degano[a,b], N. Demaria[a], B. Kiani[a,b], C. Mariotti[a], S. Maselli[a], E. Migliore[a,b], V. Monaco[a,b], E. Monteil[a,b], M. Monteno[a], M. M. Obertino[a,b], L. Pacher[a,b], N. Pastrone[a], M. Pelliccioni[a], G. L. Pinna Angioni[a,b], A. Romero[a,b], M. Ruspa[a,c], R. Sacchi[a,b], K. Shchelina[a,b], V. Sola[a], A. Solano[a,b], A. Staiano[a], P. Traczyk[a,b]

INFN Sezione di Trieste[a], Università di Trieste[b], Trieste, Italy
S. Belforte[a], M. Casarsa[a], F. Cossutti[a], G. Della Ricca[a,b], A. Zanetti[a]

Kyungpook National University, Daegu, Korea
D. H. Kim, G. N. Kim, M. S. Kim, J. Lee, S. Lee, S. W. Lee, C. S. Moon, Y. D. Oh, S. Sekmen, D. C. Son, Y. C. Yang

Chonnam National University, Institute for Universe and Elementary Particles, Kwangju, Korea
H. Kim, D. H. Moon, G. Oh

Hanyang University, Seoul, Korea
J. A. Brochero Cifuentes, J. Goh, T. J. Kim

Korea University, Seoul, Korea
S. Cho, S. Choi, Y. Go, D. Gyun, S. Ha, B. Hong, Y. Jo, Y. Kim, K. Lee, K. S. Lee, S. Lee, J. Lim, S. K. Park, Y. Roh

Seoul National University, Seoul, Korea
J. Almond, J. Kim, J. S. Kim, H. Lee, K. Lee, K. Nam, S. B. Oh, B. C. Radburn-Smith, S. h. Seo, U. K. Yang, H. D. Yoo, G. B. Yu

University of Seoul, Seoul, Korea
H. Kim, J. H. Kim, J. S. H. Lee, I. C. Park

Sungkyunkwan University, Suwon, Korea
Y. Choi, C. Hwang, J. Lee, I. Yu

Vilnius University, Vilnius, Lithuania
V. Dudenas, A. Juodagalvis, J. Vaitkus

National Centre for Particle Physics, Universiti Malaya, Kuala Lumpur, Malaysia
I. Ahmed, Z. A. Ibrahim, M. A. B. Md Ali[32], F. Mohamad Idris[33], W. A. T. Wan Abdullah, M. N. Yusli, Z. Zolkapli

Centro de Investigacion y de Estudios Avanzados del IPN, Mexico City, Mexico
M. C. Duran-Osuna, H. Castilla-Valdez, E. De La Cruz-Burelo, G. Ramirez-Sanchez, I. Heredia-De La Cruz[34], R. I. Rabadan-Trejo, R. Lopez-Fernandez, J. Mejia Guisao, R Reyes-Almanza, A. Sanchez-Hernandez

Universidad Iberoamericana, Mexico City, Mexico
S. Carrillo Moreno, C. Oropeza Barrera, F. Vazquez Valencia

Benemerita Universidad Autonoma de Puebla, Puebla, Mexico
J. Eysermans, I. Pedraza, H. A. Salazar Ibarguen, C. Uribe Estrada

Universidad Autónoma de San Luis Potosí, San Luis Potosí, Mexico
A. Morelos Pineda

University of Auckland, Auckland, New Zealand
D. Krofcheck

University of Canterbury, Christchurch, New Zealand
P. H. Butler

National Centre for Physics, Quaid-I-Azam University, Islamabad, Pakistan
A. Ahmad, M. Ahmad, Q. Hassan, H. R. Hoorani, A. Saddique, M. A. Shah, M. Shoaib, M. Waqas

National Centre for Nuclear Research, Swierk, Poland
H. Bialkowska, M. Bluj, B. Boimska, T. Frueboes, M. Górski, M. Kazana, K. Nawrocki, M. Szleper, P. Zalewski

Institute of Experimental Physics, Faculty of Physics, University of Warsaw, Warsaw, Poland
K. Bunkowski, A. Byszuk[35], K. Doroba, A. Kalinowski, M. Konecki, J. Krolikowski, M. Misiura, M. Olszewski, A. Pyskir, M. Walczak

Laboratório de Instrumentação e Física Experimental de Partículas, Lisboa, Portugal
P. Bargassa, C. Beirão Da Cruz E Silva, A. Di Francesco, P. Faccioli, B. Galinhas, M. Gallinaro, J. Hollar, N. Leonardo, L. Lloret Iglesias, M. V. Nemallapudi, J. Seixas, G. Strong, O. Toldaiev, D. Vadruccio, J. Varela

Joint Institute for Nuclear Research, Dubna, Russia
V. Alexakhin, A. Golunov, I. Golutvin, N. Gorbounov, A. Kamenev, V. Karjavin, A. Lanev, A. Malakhov, V. Matveev[36,37], P. Moisenz, V. Palichik, V. Perelygin, M. Savina, S. Shmatov, S. Shulha, N. Skatchkov, V. Smirnov, N. Voytishin, A. Zarubin

Petersburg Nuclear Physics Institute, Gatchina (St. Petersburg), Russia
Y. Ivanov, V. Kim[38], E. Kuznetsova[39], P. Levchenko, V. Murzin, V. Oreshkin, I. Smirnov, D. Sosnov, V. Sulimov, L. Uvarov, S. Vavilov, A. Vorobyev

Institute for Nuclear Research, Moscow, Russia
Yu. Andreev, A. Dermenev, S. Gninenko, N. Golubev, A. Karneyeu, M. Kirsanov, N. Krasnikov, A. Pashenkov, D. Tlisov, A. Toropin

Institute for Theoretical and Experimental Physics, Moscow, Russia
V. Epshteyn, V. Gavrilov, N. Lychkovskaya, V. Popov, I. Pozdnyakov, G. Safronov, A. Spiridonov, A. Stepennov, V. Stolin, M. Toms, E. Vlasov, A. Zhokin

Moscow Institute of Physics and Technology, Moscow, Russia
T. Aushev, A. Bylinkin[37]

National Research Nuclear University 'Moscow Engineering Physics Institute' (MEPhI), Moscow, Russia
M. Chadeeva[40], O. Markin, P. Parygin, D. Philippov, S. Polikarpov, V. Rusinov

P.N. Lebedev Physical Institute, Moscow, Russia
V. Andreev, M. Azarkin[37], I. Dremin[37], M. Kirakosyan[37], S. V. Rusakov, A. Terkulov

Skobeltsyn Institute of Nuclear Physics, Lomonosov Moscow State University, Moscow, Russia
A. Baskakov, A. Belyaev, E. Boos, V. Bunichev, M. Dubinin[41], L. Dudko, A. Gribushin, V. Klyukhin, O. Kodolova, I. Lokhtin, I. Miagkov, S. Obraztsov, M. Perfilov, S. Petrushanko, V. Savrin

Novosibirsk State University (NSU), Novosibirsk, Russia
V. Blinov[42], D. Shtol[42], Y. Skovpen[42]

State Research Center of Russian Federation, Institute for High Energy Physics of NRC, "Kurchatov Institute", Protvino, Russia
I. Azhgirey, I. Bayshev, S. Bitioukov, D. Elumakhov, A. Godizov, V. Kachanov, A. Kalinin, D. Konstantinov, P. Mandrik, V. Petrov, R. Ryutin, A. Sobol, S. Troshin, N. Tyurin, A. Uzunian, A. Volkov

University of Belgrade, Faculty of Physics and Vinca Institute of Nuclear Sciences, Belgrade, Serbia
P. Adzic[43], P. Cirkovic, D. Devetak, M. Dordevic, J. Milosevic, V. Rekovic

Centro de Investigaciones Energéticas Medioambientales y Tecnológicas (CIEMAT), Madrid, Spain
J. Alcaraz Maestre, A. Álvarez Fernández, I. Bachiller, M. Barrio Luna, M. Cerrada, N. Colino, B. De La Cruz, A. Delgado Peris, C. Fernandez Bedoya, J. P. Fernández Ramos, J. Flix, M. C. Fouz, O. Gonzalez Lopez, S. Goy Lopez, J. M. Hernandez, M. I. Josa, D. Moran, A. Pérez-Calero Yzquierdo, J. Puerta Pelayo, I. Redondo, L. Romero, M. S. Soares, A. Triossi

Universidad Autónoma de Madrid, Madrid, Spain
C. Albajar, J. F. de Trocóniz

Universidad de Oviedo, Oviedo, Spain
J. Cuevas, C. Erice, J. Fernandez Menendez, I. Gonzalez Caballero, J. R. González Fernández, E. Palencia Cortezon, S. Sanchez Cruz, P. Vischia, J. M. Vizan Garcia

Instituto de Física de Cantabria (IFCA), CSIC-Universidad de Cantabria, Santander, Spain
I. J. Cabrillo, A. Calderon, B. Chazin Quero, E. Curras, J. Duarte Campderros, M. Fernandez, J. Garcia-Ferrero, G. Gomez, A. Lopez Virto, J. Marco, C. Martinez Rivero, P. Martinez Ruiz del Arbol, F. Matorras, J. Piedra Gomez, T. Rodrigo, A. Ruiz-Jimeno, L. Scodellaro, N. Trevisani, I. Vila, R. Vilar Cortabitarte

CERN, European Organization for Nuclear Research, Geneva, Switzerland
D. Abbaneo, B. Akgun, E. Auffray, P. Baillon, A. H. Ball, D. Barney, J. Bendavid, M. Bianco, P. Bloch, A. Bocci, C. Botta, T. Camporesi, R. Castello, M. Cepeda, G. Cerminara, E. Chapon, Y. Chen, D. d'Enterria, A. Dabrowski, V. Daponte, A. David, M. De Gruttola, A. De Roeck, N. Deelen, M. Dobson, T. du Pree, M. Dünser, N. Dupont, A. Elliott-Peisert, P. Everaerts, F. Fallavollita, G. Franzoni, J. Fulcher, W. Funk, D. Gigi, A. Gilbert, K. Gill, F. Glege, D. Gulhan, P. Harris, J. Hegeman, V. Innocente, A. Jafari, P. Janot, O. Karacheban[18], J. Kieseler, V. Knünz, A. Kornmayer, M. J. Kortelainen, M. Krammer[1], C. Lange, P. Lecoq, C. Lourenço, M. T. Lucchini, L. Malgeri, M. Mannelli, A. Martelli, F. Meijers, J. A. Merlin, S. Mersi, E. Meschi, P. Milenovic[44], F. Moortgat, M. Mulders, H. Neugebauer, J. Ngadiuba, S. Orfanelli, L. Orsini, L. Pape, E. Perez, M. Peruzzi, A. Petrilli, G. Petrucciani, A. Pfeiffer, M. Pierini, D. Rabady, A. Racz, T. Reis, G. Rolandi[45], M. Rovere, H. Sakulin, C. Schäfer, C. Schwick, M. Seidel, M. Selvaggi, A. Sharma, P. Silva, P. Sphicas[46], A. Stakia, J. Steggemann, M. Stoye, M. Tosi, D. Treille, A. Tsirou, V. Veckalns[47], M. Verweij, W. D. Zeuner

Paul Scherrer Institut, Villigen, Switzerland
W. Bertl[†], L. Caminada[48], K. Deiters, W. Erdmann, R. Horisberger, Q. Ingram, H. C. Kaestli, D. Kotlinski, U. Langenegger, T. Rohe, S. A. Wiederkehr

ETH Zurich-Institute for Particle Physics and Astrophysics (IPA), Zurich, Switzerland
M. Backhaus, L. Bäni, P. Berger, L. Bianchini, B. Casal, G. Dissertori, M. Dittmar, M. Donegà, C. Dorfer, C. Grab, C. Heidegger, D. Hits, J. Hoss, G. Kasieczka, T. Klijnsma, W. Lustermann, B. Mangano, M. Marionneau, M. T. Meinhard, D. Meister, F. Micheli, P. Musella, F. Nessi-Tedaldi, F. Pandolfi, J. Pata, F. Pauss, G. Perrin, L. Perrozzi, M. Quittnat, M. Reichmann, D. A. Sanz Becerra, M. Schönenberger, L. Shchutska, V. R. Tavolaro, K. Theofilatos, M. L. Vesterbacka Olsson, R. Wallny, D. H. Zhu

Universität Zürich, Zurich, Switzerland
T. K. Aarrestad, C. Amsler[49], D. Brzhechko, M. F. Canelli, A. De Cosa, R. Del Burgo, S. Donato, C. Galloni, T. Hreus, B. Kilminster, D. Pinna, G. Rauco, P. Robmann, D. Salerno, K. Schweiger, C. Seitz, Y. Takahashi, A. Zucchetta

National Central University, Chung-Li, Taiwan
V. Candelise, Y. H. Chang, K. y. Cheng, T. H. Doan, Sh. Jain, R. Khurana, C. M. Kuo, W. Lin, A. Pozdnyakov, S. S. Yu

National Taiwan University (NTU), Taipei, Taiwan
P. Chang, Y. Chao, K. F. Chen, P. H. Chen, F. Fiori, W.-S. Hou, Y. Hsiung, Arun Kumar, Y. F. Liu, R.-S. Lu, E. Paganis, A. Psallidas, A. Steen, J. f. Tsai

Department of Physics, Faculty of Science, Chulalongkorn University, Bangkok, Thailand
B. Asavapibhop, K. Kovitanggoon, G. Singh, N. Srimanobhas

Physics Department, Science and Art Faculty, Çukurova University, Adana, Turkey
A. Bat, F. Boran, S. Cerci[50], S. Damarseckin, Z. S. Demiroglu, C. Dozen, I. Dumanoglu, S. Girgis, G. Gokbulut, Y. Guler, I. Hos[51], E. E. Kangal[52], O. Kara, A. Kayis Topaksu, U. Kiminsu, M. Oglakci, G. Onengut[53], K. Ozdemir[54], D. Sunar Cerci[50], B. Tali[50], U. G. Tok, S. Turkcapar, I. S. Zorbakir, C. Zorbilmez

Physics Department, Middle East Technical University, Ankara, Turkey
G. Karapinar[55], K. Ocalan[56], M. Yalvac, M. Zeyrek

Bogazici University, Istanbul, Turkey
E. Gülmez, M. Kaya[57], O. Kaya[58], S. Tekten, E. A. Yetkin[59]

Istanbul Technical University, Istanbul, Turkey
M. N. Agaras, S. Atay, A. Cakir, K. Cankocak, Y. Komurcu

Institute for Scintillation Materials of National Academy of Science of Ukraine, Kharkov, Ukraine
B. Grynyov

National Scientific Center, Kharkov Institute of Physics and Technology, Kharkov, Ukraine
L. Levchuk

University of Bristol, Bristol, UK
F. Ball, L. Beck, J. J. Brooke, D. Burns, E. Clement, D. Cussans, O. Davignon, H. Flacher, J. Goldstein, G. P. Heath, H. F. Heath, L. Kreczko, D. M. Newbold[60], S. Paramesvaran, T. Sakuma, S. Seif El Nasr-storey, D. Smith, V. J. Smith

Rutherford Appleton Laboratory, Didcot, UK
K. W. Bell, A. Belyaev[61], C. Brew, R. M. Brown, L. Calligaris, D. Cieri, D. J. A. Cockerill, J. A. Coughlan, K. Harder, S. Harper, J. Linacre, E. Olaiya, D. Petyt, C. H. Shepherd-Themistocleous, A. Thea, I. R. Tomalin, T. Williams, W. J. Womersley

Imperial College, London, UK
G. Auzinger, R. Bainbridge, J. Borg, S. Breeze, O. Buchmuller, A. Bundock, S. Casasso, M. Citron, D. Colling, L. Corpe, P. Dauncey, G. Davies, A. De Wit, M. Della Negra, R. Di Maria, A. Elwood, Y. Haddad, G. Hall, G. Iles, T. James, C. Laner, L. Lyons, A.-M. Magnan, S. Malik, L. Mastrolorenzo, T. Matsushita, J. Nash, A. Nikitenko[6], V. Palladino, M. Pesaresi, D. M. Raymond, A. Richards, A. Rose, E. Scott, C. Seez, A. Shtipliyski, S. Summers, A. Tapper, K. Uchida, M. Vazquez Acosta[62], T. Virdee[15], N. Wardle, D. Winterbottom, J. Wright, S. C. Zenz

Brunel University, Uxbridge, UK
J. E. Cole, P. R. Hobson, A. Khan, P. Kyberd, I. D. Reid, L. Teodorescu, S. Zahid

Baylor University, Waco, USA
A. Borzou, K. Call, J. Dittmann, K. Hatakeyama, H. Liu, N. Pastika, C. Smith

Catholic University of America, Washington, DC, USA
R. Bartek, A. Dominguez

The University of Alabama, Tuscaloosa, USA
A. Buccilli, S. I. Cooper, C. Henderson, P. Rumerio, C. West

Boston University, Boston, USA
D. Arcaro, A. Avetisyan, T. Bose, D. Gastler, D. Rankin, C. Richardson, J. Rohlf, L. Sulak, D. Zou

Brown University, Providence, USA
G. Benelli, D. Cutts, M. Hadley, J. Hakala, U. Heintz, J. M. Hogan, K. H. M. Kwok, E. Laird, G. Landsberg, J. Lee, Z. Mao, M. Narain, J. Pazzini, S. Piperov, S. Sagir, R. Syarif, D. Yu

University of California, Davis, Davis, USA
R. Band, C. Brainerd, R. Breedon, D. Burns, M. Calderon De La Barca Sanchez, M. Chertok, J. Conway, R. Conway, P. T. Cox, R. Erbacher, C. Flores, G. Funk, W. Ko, O. Kukral, R. Lander, C. Mclean, M. Mulhearn, D. Pellett, J. Pilot, S. Shalhout, M. Shi, J. Smith, D. Stolp, K. Tos, M. Tripathi, Z. Wang

University of California, Los Angeles, Los Angeles, USA
M. Bachtis, C. Bravo, R. Cousins, A. Dasgupta, A. Florent, J. Hauser, M. Ignatenko, N. Mccoll, S. Regnard, D. Saltzberg, C. Schnaible, V. Valuev

University of California, Riverside, Riverside, USA
E. Bouvier, K. Burt, R. Clare, J. Ellison, J. W. Gary, S. M. A. Ghiasi Shirazi, G. Hanson, J. Heilman, G. Karapostoli, E. Kennedy, F. Lacroix, O. R. Long, M. Olmedo Negrete, M. I. Paneva, W. Si, L. Wang, H. Wei, S. Wimpenny, B. R. Yates

University of California, San Diego, La Jolla, USA
J. G. Branson, S. Cittolin, M. Derdzinski, R. Gerosa, D. Gilbert, B. Hashemi, A. Holzner, D. Klein, G. Kole, V. Krutelyov, J. Letts, M. Masciovecchio, D. Olivito, S. Padhi, M. Pieri, M. Sani, V. Sharma, S. Simon, M. Tadel, A. Vartak, S. Wasserbaech[63], J. Wood, F. Würthwein, A. Yagil, G. Zevi Della Porta

Department of Physics, University of California, Santa Barbara, Santa Barbara, USA
N. Amin, R. Bhandari, J. Bradmiller-Feld, C. Campagnari, A. Dishaw, V. Dutta, M. Franco Sevilla, L. Gouskos, R. Heller, J. Incandela, A. Ovcharova, H. Qu, J. Richman, D. Stuart, I. Suarez, J. Yoo

California Institute of Technology, Pasadena, USA
D. Anderson, A. Bornheim, J. Bunn, J. M. Lawhorn, H. B. Newman, T. Q. Nguyen, C. Pena, M. Spiropulu, J. R. Vlimant, R. Wilkinson, S. Xie, Z. Zhang, R. Y. Zhu

Carnegie Mellon University, Pittsburgh, USA
M. B. Andrews, T. Ferguson, T. Mudholkar, M. Paulini, J. Russ, M. Sun, H. Vogel, I. Vorobiev, M. Weinberg

University of Colorado Boulder, Boulder, USA
J. P. Cumalat, W. T. Ford, F. Jensen, A. Johnson, M. Krohn, S. Leontsinis, T. Mulholland, K. Stenson, K. A. Ulmer, S. R. Wagner

Cornell University, Ithaca, USA
J. Alexander, J. Chaves, J. Chu, S. Dittmer, K. Mcdermott, N. Mirman, J. R. Patterson, D. Quach, A. Rinkevicius, A. Ryd, L. Skinnari, L. Soffi, S. M. Tan, Z. Tao, J. Thom, J. Tucker, P. Wittich, M. Zientek

Fermi National Accelerator Laboratory, Batavia, USA
S. Abdullin, M. Albrow, M. Alyari, G. Apollinari, A. Apresyan, A. Apyan, S. Banerjee, L. A. T. Bauerdick, A. Beretvas, J. Berryhill, P. C. Bhat, G. Bolla[†], K. Burkett, J. N. Butler, A. Canepa, G. B. Cerati, H. W. K. Cheung, F. Chlebana, M. Cremonesi, J. Duarte, V. D. Elvira, J. Freeman, Z. Gecse, E. Gottschalk, L. Gray, D. Green, S. Grünendahl, O. Gutsche, J. Hanlon, R. M. Harris, S. Hasegawa, J. Hirschauer, Z. Hu, B. Jayatilaka, S. Jindariani, M. Johnson, U. Joshi, B. Klima, B. Kreis, S. Lammel, D. Lincoln, R. Lipton, M. Liu, T. Liu, R. Lopes De Sá, J. Lykken, K. Maeshima, N. Magini, J. M. Marraffino, D. Mason, P. McBride, P. Merkel, S. Mrenna, S. Nahn, V. O'Dell, K. Pedro, O. Prokofyev, G. Rakness, L. Ristori, B. Schneider, E. Sexton-Kennedy, A. Soha, W. J. Spalding, L. Spiegel, S. Stoynev, J. Strait, N. Strobbe, L. Taylor, S. Tkaczyk, N. V. Tran, L. Uplegger, E. W. Vaandering, C. Vernieri, M. Verzocchi, R. Vidal, M. Wang, H. A. Weber, A. Whitbeck, W. Wu

University of Florida, Gainesville, USA
D. Acosta, P. Avery, P. Bortignon, D. Bourilkov, A. Brinkerhoff, A. Carnes, M. Carver, D. Curry, R. D. Field, I. K. Furic, S. V. Gleyzer, B. M. Joshi, J. Konigsberg, A. Korytov, K. Kotov, P. Ma, K. Matchev, H. Mei, G. Mitselmakher, K. Shi, D. Sperka, N. Terentyev, L. Thomas, J. Wang, S. Wang, J. Yelton

Florida International University, Miami, USA
Y. R. Joshi, S. Linn, P. Markowitz, J. L. Rodriguez

Florida State University, Tallahassee, USA
A. Ackert, T. Adams, A. Askew, S. Hagopian, V. Hagopian, K. F. Johnson, T. Kolberg, G. Martinez, T. Perry, H. Prosper, A. Saha, A. Santra, V. Sharma, R. Yohay

Florida Institute of Technology, Melbourne, USA
M. M. Baarmand, V. Bhopatkar, S. Colafranceschi, M. Hohlmann, D. Noonan, T. Roy, F. Yumiceva

University of Illinois at Chicago (UIC), Chicago, USA
M. R. Adams, L. Apanasevich, D. Berry, R. R. Betts, R. Cavanaugh, X. Chen, O. Evdokimov, C. E. Gerber, D. A. Hangal, D. J. Hofman, K. Jung, J. Kamin, I. D. Sandoval Gonzalez, M. B. Tonjes, H. Trauger, N. Varelas, H. Wang, Z. Wu, J. Zhang

The University of Iowa, Iowa City, USA
B. Bilki[64], W. Clarida, K. Dilsiz[65], S. Durgut, R. P. Gandrajula, M. Haytmyradov, V. Khristenko, J.-P. Merlo, H. Mermerkaya[66], A. Mestvirishvili, A. Moeller, J. Nachtman, H. Ogul[67], Y. Onel, F. Ozok[68], A. Penzo, C. Snyder, E. Tiras, J. Wetzel, K. Yi

Johns Hopkins University, Baltimore, USA
B. Blumenfeld, A. Cocoros, N. Eminizer, D. Fehling, L. Feng, A. V. Gritsan, P. Maksimovic, J. Roskes, U. Sarica, M. Swartz, M. Xiao, C. You

The University of Kansas, Lawrence, USA
A. Al-bataineh, P. Baringer, A. Bean, S. Boren, J. Bowen, J. Castle, S. Khalil, A. Kropivnitskaya, D. Majumder, W. Mcbrayer, M. Murray, C. Rogan, C. Royon, S. Sanders, E. Schmitz, J. D. Tapia Takaki, Q. Wang

Kansas State University, Manhattan, USA
A. Ivanov, K. Kaadze, Y. Maravin, A. Mohammadi, L. K. Saini, N. Skhirtladze

Lawrence Livermore National Laboratory, Livermore, USA
F. Rebassoo, D. Wright

University of Maryland, College Park, USA
A. Baden, O. Baron, A. Belloni, S. C. Eno, Y. Feng, C. Ferraioli, N. J. Hadley, S. Jabeen, G. Y. Jeng, R. G. Kellogg, J. Kunkle, A. C. Mignerey, F. Ricci-Tam, Y. H. Shin, A. Skuja, S. C. Tonwar

Massachusetts Institute of Technology, Cambridge, USA
D. Abercrombie, B. Allen, V. Azzolini, R. Barbieri, A. Baty, G. Bauer, R. Bi, S. Brandt, W. Busza, I. A. Cali, M. D'Alfonso, Z. Demiragli, G. Gomez Ceballos, M. Goncharov, D. Hsu, M. Hu, Y. Iiyama, G. M. Innocenti, M. Klute, D. Kovalskyi, Y.-J. Lee, A. Levin, P. D. Luckey, B. Maier, A. C. Marini, C. Mcginn, C. Mironov, S. Narayanan, X. Niu, C. Paus, C. Roland, G. Roland, J. Salfeld-Nebgen, G. S. F. Stephans, K. Sumorok, K. Tatar, D. Velicanu, J. Wang, T. W. Wang, B. Wyslouch

University of Minnesota, Minneapolis, USA
A. C. Benvenuti, R. M. Chatterjee, A. Evans, P. Hansen, J. Hiltbrand, S. Kalafut, Y. Kubota, Z. Lesko, J. Mans, S. Nourbakhsh, N. Ruckstuhl, R. Rusack, J. Turkewitz, M. A. Wadud

University of Mississippi, Oxford, USA
J. G. Acosta, S. Oliveros

University of Nebraska-Lincoln, Lincoln, USA
E. Avdeeva, K. Bloom, D. R. Claes, C. Fangmeier, F. Golf, R. Gonzalez Suarez, R. Kamalieddin, I. Kravchenko, J. Monroy, J. E. Siado, G. R. Snow, B. Stieger

State University of New York at Buffalo, Buffalo, USA
J. Dolen, A. Godshalk, C. Harrington, I. Iashvili, D. Nguyen, A. Parker, S. Rappoccio, B. Roozbahani

Northeastern University, Boston, USA
G. Alverson, E. Barberis, C. Freer, A. Hortiangtham, A. Massironi, D. M. Morse, T. Orimoto, R. Teixeira De Lima, T. Wamorkar, B. Wang, A. Wisecarver, D. Wood

Northwestern University, Evanston, USA
S. Bhattacharya, O. Charaf, K. A. Hahn, N. Mucia, N. Odell, M. H. Schmitt, K. Sung, M. Trovato, M. Velasco

University of Notre Dame, Notre Dame, USA
R. Bucci, N. Dev, M. Hildreth, K. Hurtado Anampa, C. Jessop, D. J. Karmgard, N. Kellams, K. Lannon, W. Li, N. Loukas, N. Marinelli, F. Meng, C. Mueller, Y. Musienko[36], M. Planer, A. Reinsvold, R. Ruchti, P. Siddireddy, G. Smith, S. Taroni, M. Wayne, A. Wightman, M. Wolf, A. Woodard

The Ohio State University, Columbus, USA
J. Alimena, L. Antonelli, B. Bylsma, L. S. Durkin, S. Flowers, B. Francis, A. Hart, C. Hill, W. Ji, T. Y. Ling, B. Liu, W. Luo, B. L. Winer, H. W. Wulsin

Princeton University, Princeton, USA
S. Cooperstein, O. Driga, P. Elmer, J. Hardenbrook, P. Hebda, S. Higginbotham, A. Kalogeropoulos, D. Lange, J. Luo, D. Marlow, K. Mei, I. Ojalvo, J. Olsen, C. Palmer, P. Piroué, D. Stickland, C. Tully

University of Puerto Rico, Mayaguez, USA
S. Malik, S. Norberg

Purdue University, West Lafayette, USA
A. Barker, V. E. Barnes, S. Das, S. Folgueras, L. Gutay, M. Jones, A. W. Jung, A. Khatiwada, D. H. Miller, N. Neumeister, C. C. Peng, H. Qiu, J. F. Schulte, J. Sun, F. Wang, R. Xiao, W. Xie

Purdue University Northwest, Hammond, USA
T. Cheng, N. Parashar, J. Stupak

Rice University, Houston, USA
Z. Chen, K. M. Ecklund, S. Freed, F. J. M. Geurts, M. Guilbaud, M. Kilpatrick, W. Li, B. Michlin, B. P. Padley, J. Roberts, J. Rorie, W. Shi, Z. Tu, J. Zabel, A. Zhang

University of Rochester, Rochester, USA
A. Bodek, P. de Barbaro, R. Demina, Y. t. Duh, T. Ferbel, M. Galanti, A. Garcia-Bellido, J. Han, O. Hindrichs, A. Khukhunaishvili, K. H. Lo, P. Tan, M. Verzetti

The Rockefeller University, New York, USA
R. Ciesielski, K. Goulianos, C. Mesropian

Rutgers, The State University of New Jersey, Piscataway, USA
A. Agapitos, J. P. Chou, Y. Gershtein, T. A. Gómez Espinosa, E. Halkiadakis, M. Heindl, E. Hughes, S. Kaplan, R. Kunnawalkam Elayavalli, S. Kyriacou, A. Lath, R. Montalvo, K. Nash, M. Osherson, H. Saka, S. Salur, S. Schnetzer, D. Sheffield, S. Somalwar, R. Stone, S. Thomas, P. Thomassen, M. Walker

University of Tennessee, Knoxville, USA
A. G. Delannoy, J. Heideman, G. Riley, K. Rose, S. Spanier, K. Thapa

Texas A&M University, College Station, USA
O. Bouhali[69], A. Castaneda Hernandez[69], A. Celik, M. Dalchenko, M. De Mattia, A. Delgado, S. Dildick, R. Eusebi, J. Gilmore, T. Huang, T. Kamon[70], R. Mueller, Y. Pakhotin, R. Patel, A. Perloff, L. Perniè, D. Rathjens, A. Safonov, A. Tatarinov

Texas Tech University, Lubbock, USA
N. Akchurin, J. Damgov, F. De Guio, P. R. Dudero, J. Faulkner, E. Gurpinar, S. Kunori, K. Lamichhane, S. W. Lee, T. Libeiro, T. Mengke, S. Muthumuni, T. Peltola, S. Undleeb, I. Volobouev, Z. Wang

Vanderbilt University, Nashville, USA
S. Greene, A. Gurrola, R. Janjam, W. Johns, C. Maguire, A. Melo, H. Ni, K. Padeken, P. Sheldon, S. Tuo, J. Velkovska, Q. Xu

University of Virginia, Charlottesville, USA
M. W. Arenton, P. Barria, B. Cox, R. Hirosky, M. Joyce, A. Ledovskoy, H. Li, C. Neu, T. Sinthuprasith, Y. Wang, E. Wolfe, F. Xia

Wayne State University, Detroit, USA
R. Harr, P. E. Karchin, N. Poudyal, J. Sturdy, P. Thapa, S. Zaleski

University of Wisconsin-Madison, Madison, WI, USA
M. Brodski, J. Buchanan, C. Caillol, D. Carlsmith, S. Dasu, L. Dodd, S. Duric, B. Gomber, M. Grothe, M. Herndon, A. Hervé, U. Hussain, P. Klabbers, A. Lanaro, A. Levine, K. Long, R. Loveless, T. Ruggles, A. Savin, N. Smith, W. H. Smith, D. Taylor, N. Woods

† **Deceased**

1: Also at Vienna University of Technology, Vienna, Austria
2: Also at IRFU; CEA; Université Paris-Saclay, Gif-sur-Yvette, France
3: Also at Universidade Estadual de Campinas, Campinas, Brazil
4: Also at Federal University of Rio Grande do Sul, Porto Alegre, Brazil

5: Also at Université Libre de Bruxelles, Bruxelles, Belgium
6: Also at Institute for Theoretical and Experimental Physics, Moscow, Russia
7: Also at Joint Institute for Nuclear Research, Dubna, Russia
8: Also at Cairo University, Cairo, Egypt
9: Now at Ain Shams University, Cairo, Egypt
10: Also at Zewail City of Science and Technology, Zewail, Egypt
11: Also at Department of Physics; King Abdulaziz University, Jeddah, Saudi Arabia
12: Also at Université de Haute Alsace, Mulhouse, France
13: Also at Skobeltsyn Institute of Nuclear Physics; Lomonosov Moscow State University, Moscow, Russia
14: Also at Tbilisi State University, Tbilisi, Georgia
15: Also at CERN; European Organization for Nuclear Research, Geneva, Switzerland
16: Also at RWTH Aachen University; III. Physikalisches Institut A, Aachen, Germany
17: Also at University of Hamburg, Hamburg, Germany
18: Also at Brandenburg University of Technology, Cottbus, Germany
19: Also at MTA-ELTE Lendület CMS Particle and Nuclear Physics Group; Eötvös Loránd University, Budapest, Hungary
20: Also at Institute of Nuclear Research ATOMKI, Debrecen, Hungary
21: Also at Institute of Physics; University of Debrecen, Debrecen, Hungary
22: Also at Indian Institute of Technology Bhubaneswar, Bhubaneswar, India
23: Also at Institute of Physics, Bhubaneswar, India
24: Also at University of Visva-Bharati, Santiniketan, India
25: Also at University of Ruhuna, Matara, Sri Lanka
26: Also at Isfahan University of Technology, Isfahan, Iran
27: Also at Yazd University, Yazd, Iran
28: Also at Plasma Physics Research Center; Science and Research Branch; Islamic Azad University, Tehran, Iran
29: Also at Università degli Studi di Siena, Siena, Italy
30: Also at INFN Sezione di Milano-Bicocca; Università di Milano-Bicocca, Milano, Italy
31: Also at Purdue University, West Lafayette, USA
32: Also at International Islamic University of Malaysia, Kuala Lumpur, Malaysia
33: Also at Malaysian Nuclear Agency; MOSTI, Kajang, Malaysia
34: Also at Consejo Nacional de Ciencia y Tecnología, Mexico city, Mexico
35: Also at Warsaw University of Technology; Institute of Electronic Systems, Warsaw, Poland
36: Also at Institute for Nuclear Research, Moscow, Russia
37: Now at National Research Nuclear University 'Moscow Engineering Physics Institute' (MEPhI), Moscow, Russia
38: Also at St. Petersburg State Polytechnical University, St. Petersburg, Russia
39: Also at University of Florida, Gainesville, USA
40: Also at P.N. Lebedev Physical Institute, Moscow, Russia
41: Also at California Institute of Technology, Pasadena, USA
42: Also at Budker Institute of Nuclear Physics, Novosibirsk, Russia
43: Also at Faculty of Physics; University of Belgrade, Belgrade, Serbia
44: Also at University of Belgrade; Faculty of Physics and Vinca Institute of Nuclear Sciences, Belgrade, Serbia
45: Also at Scuola Normale e Sezione dell'INFN, Pisa, Italy
46: Also at National and Kapodistrian University of Athens, Athens, Greece
47: Also at Riga Technical University, Riga, Latvia
48: Also at Universität Zürich, Zurich, Switzerland
49: Also at Stefan Meyer Institute for Subatomic Physics (SMI), Vienna, Austria
50: Also at Adiyaman University, Adiyaman, Turkey
51: Also at Istanbul Aydin University, Istanbul, Turkey
52: Also at Mersin University, Mersin, Turkey
53: Also at Cag University, Mersin, Turkey
54: Also at Piri Reis University, Istanbul, Turkey
55: Also at Izmir Institute of Technology, Izmir, Turkey
56: Also at Necmettin Erbakan University, Konya, Turkey
57: Also at Marmara University, Istanbul, Turkey

58: Also at Kafkas University, Kars, Turkey
59: Also at Istanbul Bilgi University, Istanbul, Turkey
60: Also at Rutherford Appleton Laboratory, Didcot, UK
61: Also at School of Physics and Astronomy; University of Southampton, Southampton, UK
62: Also at Instituto de Astrofísica de Canarias, La Laguna, Spain
63: Also at Utah Valley University, Orem, USA
64: Also at Beykent University, Istanbul, Turkey
65: Also at Bingol University, Bingol, Turkey
66: Also at Erzincan University, Erzincan, Turkey
67: Also at Sinop University, Sinop, Turkey
68: Also at Mimar Sinan University; Istanbul, Istanbul, Turkey
69: Also at Texas A&M University at Qatar, Doha, Qatar
70: Also at Kyungpook National University, Daegu, Korea